CHEMICAL REVIEWS

Review

Cite This: *Chem. Rev.* XXXX, XXX, XXX–XXX

pubs.acs.org/CR

Tuning the Luminescence of Layered Halide Perovskites

Matthew D. Smith,[†] Bridget A. Connor,[†] and Hemamala I. Karunadasa*

Department of Chemistry, Stanford University, Stanford, California 94305, United States

ABSTRACT: Layered halide perovskites offer a versatile platform for manipulating light through synthetic design. Although most layered perovskites absorb strongly in the ultraviolet (UV) or near-UV region, their emission can range from the UV to the infrared region of the electromagnetic spectrum. This emission can be very narrow, displaying high color purity, or it can be extremely broad, spanning the entire visible spectrum and providing high color rendition (or accurately reproducing illuminated colors). The origin of the photoluminescence can vary enormously. Strongly correlated electron–hole pairs, permanent lattice defects, transient light-induced defects, and ligand-field transitions in the inorganic layers and molecular chromophores in the organic layers can be involved in the emission mechanism. In this review, we highlight the different types of photoluminescence that may be attained from layered halide perovskites, with an emphasis on how the emission may be systematically tuned through changes to the bulk crystalline lattice: changes in composition, structure, and dimensionality.

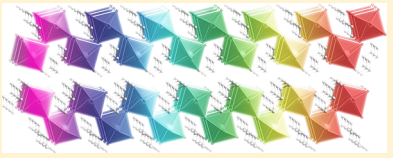

CONTENTS

Special Issue: Perovskites

Received: July 28, 2018

DOI: 10.1021/acs.chemrev.8b00477
Chem. Rev. XXXX, XXX, XXX–XXX

1. INTRODUCTION

1.1. Background

Layered halide perovskites are crystalline solids that comprise anionic metal halide sheets partitioned by arrays of cations. Often, these cations are organic molecules, giving rise to a diverse family of organic–inorganic hybrid materials (Figure 1). Layered halide perovskites are related to the perovskite (or calcium titanate) structure type through dimensional reduction: the conceptual slicing of a three-dimensional (3D) lattice along a certain index to yield a two-dimensional (2D) lattice (Figure 2).

Photoluminescence, the emission of photons following light absorption, from layered halide perovskites encompasses a striking diversity. The emission covers a range of energies/colors—near-UV, purple, blue, green, orange, red, white, and near-IR (Table 1)—and a range of widths—from narrow blue emission with high color purity to broadband white-light emission with high color rendition. The luminescence may originate from either the inorganic or the organic layers. Within the inorganic layers, radiative recombination of excitons (excited electron–hole pairs) that migrate freely in the lattice (free excitons), interact with lattice defects (bound excitons), or create transient lattice deformations (self-trapped excitons) have been invoked while describing the emission mechanism. The emission from the inorganic layers can also arise from localized transitions within the ligand-field manifold of a single metal incorporated either stoichiometrically or as a dopant. In the organic layers, the emission may originate from chromophores that are excited either directly by light or indirectly through energy transfer from the inorganic layers. These various emission pathways may also mix, with the photoluminescence showing signatures of both free and trapped excitons, self-trapped excitons that interact with lattice defects or that evolve into lattice defects, and excitation transfer between the lattice and dopants and between the organic and inorganic components.

In this article we review the substantial research on studying, understanding, and then synthetically tuning the various radiative recombination pathways in layered halide perovskites. Although the focus here is on 2D perovskites (and their close relatives), we note that many of the mechanistic insights gained from the photophysical studies of these materials are broadly applicable to other low-dimensional inorganic lattices. Importantly, the high degree of crystallinity of halide perovskites, coupled with the precise tunability of the constituent organic molecules, affords a very large phase space of compounds for careful study (Figure 1). Over the past century, these materials have evolved from scientific curiosities[1] and model compounds[2] to functional materials whose applications span technologies including photovoltaics,[3] light-emitting diodes,[4−9] and phosphors.[10,11] Indeed, early interest in the photophysics of halide perovskites rested primarily with the layered or 2D materials. However, the exemplary performance of 3D lead halide perovskites as solar-cell absorbers[12,13] motivates a timely return to their 2D congeners. We restrict our discussion to how the luminescence of the bulk material can be tuned through synthetic design and refer the interested reader to other articles for the effects of nanostructuring.[14,15]

1.1.1. Further Literature. With over a century of research behind halide perovskites,[1,16,17] there are a large number of reviews that stand alongside the development of the layered perovskites, covering a number of specialized topics in detail. In particular, we refer the interested reader to early reviews of synthesis and crystal growth,[18] the optical properties of 2D Pb–I perovskites,[19] the seminal introduction[20] to layered perovskites and a more recent review,[21] the electronic structure and its optoelectronic consequences,[22] and layered perovskites' postsynthetic transformations,[23] high-pressure properties,[24] and white-light emission,[25] as well as a general introduction to the material family.[26]

1.2. History

1.2.1. Three-Dimensional Halide Perovskites. The history of the 3D halide perovskites is contemporaneous with their layered congeners, and both classes of materials have similarly experienced peaks and troughs in study (Figure 3). The early 3D halide perovskites, with the formula $A^{I}B^{II}X_3$ (see section 2.1), which were structurally characterized by X-ray diffraction, include $KMgF_3$[27] in 1925 and $CsBCl_3$ (B^{II} = Cd^{II},

DOI: 10.1021/acs.chemrev.8b00477
Chem. Rev. XXXX, XXX, XXX–XXX

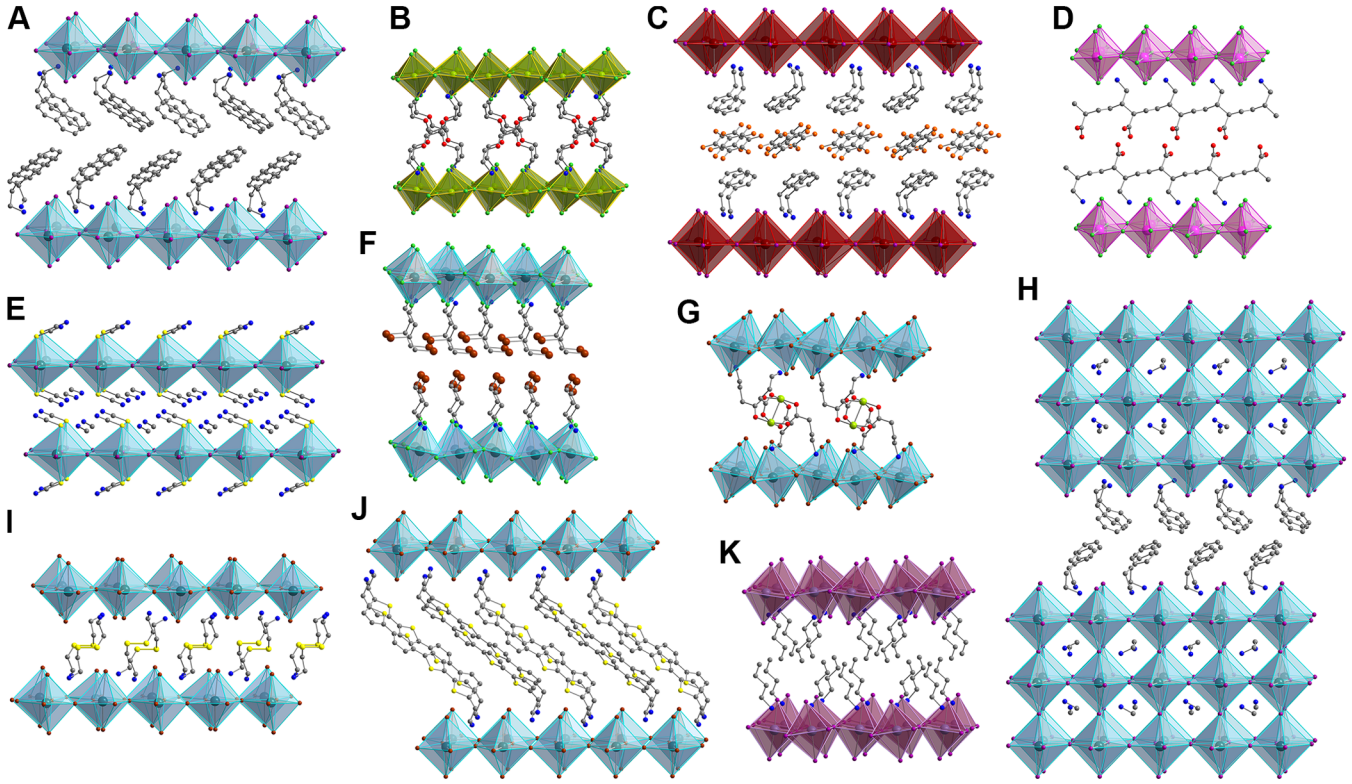

Figure 1. Diversity of (001) hybrid perovskites represented by the crystal structures for (A) $(NEA)_2PbI_4$ (NEA = 2-naphthylethylammonium),[107] (B) (EDBE)$CuCl_4$ (EDBE = 2,2′-(ethylenedioxy)bis(ethylammonium)),[114] (C) $(PEA)_2SnI_4{\cdot}C_6F_6$ (PEA = phenethylammonium),[265] (D) $(P\text{-}DEA)_{2/m}CdCl_4$ (P-DEA = poly(2*E*,4*E*)-6-ammoniohexa-2,4-dienoic acid),[266] (E) $(MA)_2PbI_2(SCN)_2$ (MA = methylammonium),[122] (F) $(BEA\text{-}Br_2)_2PbCl_4$ (BEA-Br_2= $H_2BrC{-}CBrH(CH_2)_2NH_3$),[267] (G) $Cu(GABA)_2PbBr_4$ (GABA = γ-aminobutyric acid),[81] (H) $(PEA)_2(MA)_2Pb_3I_{10}$,[3] (I) $(NH_3(CH_2)_2SS(CH_2)_2NH_3)PbBr_4$,[84] (J) (AEQT)$PbBr_4$ (AEQT = 5,5‴-bis(ethylammonium)-2,2′:5′,2″:5″,2‴-quaterthiophene),[61] and (K) $(BA)_2GeI_4$ (BA = butylammonium).[55] Turquoise, dark red, lime, pink, purple, brown, green, orange, yellow, red, blue, and gray spheres represent Pb, Sn, Cu, Cd, I, Br, Cl, F, S, O, N, and C atoms, respectively. Disordered atoms and hydrogen atoms omitted for clarity.

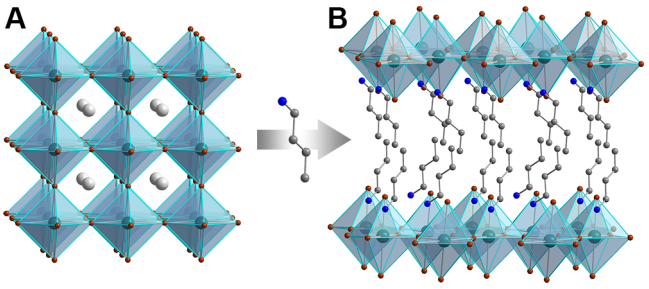

Figure 2. Crystal structures of (A) cubic 3D perovskite $CsPbBr_3$[35] and (B) 2D hybrid perovskite $(C_4H_9NH_3)_2PbBr_4$.[14,55] Turquoise, white, brown, blue, and gray spheres represent Pb, Cs, Br, N, and C atoms, respectively. Disordered atoms and hydrogen atoms omitted for clarity. Reproduced with permission from ref 26. Copyright 2018 Annual Reviews.

Table 1. Photoluminescence Colors for Representative 2D Perovskites at Room Temperature[a]

perovskite	emission color	ref
$(PEA)_2PbBr_4$	purple	257
(*N*-MPDA)$PbBr_4$	blue	11
$(BA)_2EuI_4$	blue	117
(AEQT)$PbCl_4$	green	6
$(PEA)_2PbI_4$	green	71
$(PEA)_2(MA)Pb_2I_7$	orange	4
$(BA)_2PbBr_4{:}Mn^{2+}$	orange	238
$(BA)_2SnI_4$	red	55
$(PEA)_2(MA)_2Pb_3I_{10}$	red	3
$(MA)_2Pb(SCN)_2I_2$	near-IR	151
(EDBE)$PbBr_4$	warm white	89
(EDBE)$PbCl_4$	cool white	89

[a]PEA = phenethylammonium, *N*-MPDA = N^1-methylpropane-1,3-diammonium, BA = butylammonium, AEQT = 5,5‴-bis-(ethylammonium)-2,2′:5′,2″:5″,2‴-quaterthiophene, MA = methylammonium, EDBE = 2,2′-(ethylenedioxy)bis(ethylammonium).

Hg^{II})[28] in 1928. Syntheses[29] and structure determinations[30] of the halide double perovskites, $CsAg^{I}Au^{III}Cl_6$ and $CsAu^{I}Au^{III}Cl_6$, and the mineral elpasolite,[31−33] K_2NaAlF_6, followed shortly thereafter.

The now-familiar group 14 halide perovskites $CsPbX_3$ (X = Cl, Br, I) were described by Møller in the 1950s, who reported their crystal structures, phase transitions, and, perhaps most importantly, their photoconductivity.[34,35] Notably, the syntheses of these materials occurred well before these reports.[17] In 1893, work by Wells[17] not only reports salts with the formula $CsPbX_3$ (X = Cl, Br, I), but also the mixed-halide derivatives $CsPbCl_{3-x}Br_x$ ($x \approx 0.08{-}0.2$), anticipating recent research efforts in these materials[36] by well over a century. In contrast, the first hybrid (organic−inorganic) 3D lead-halide perovskite, methylammonium lead iodide $(CH_3NH_3)PbI_3$, was not reported until 1978 by Weber.[37]

1.2.2. Two-Dimensional Halide Perovskites. The layered hybrid halide perovskites predate the 3D hybrids by

DOI: 10.1021/acs.chemrev.8b00477
Chem. Rev. XXXX, XXX, XXX−XXX

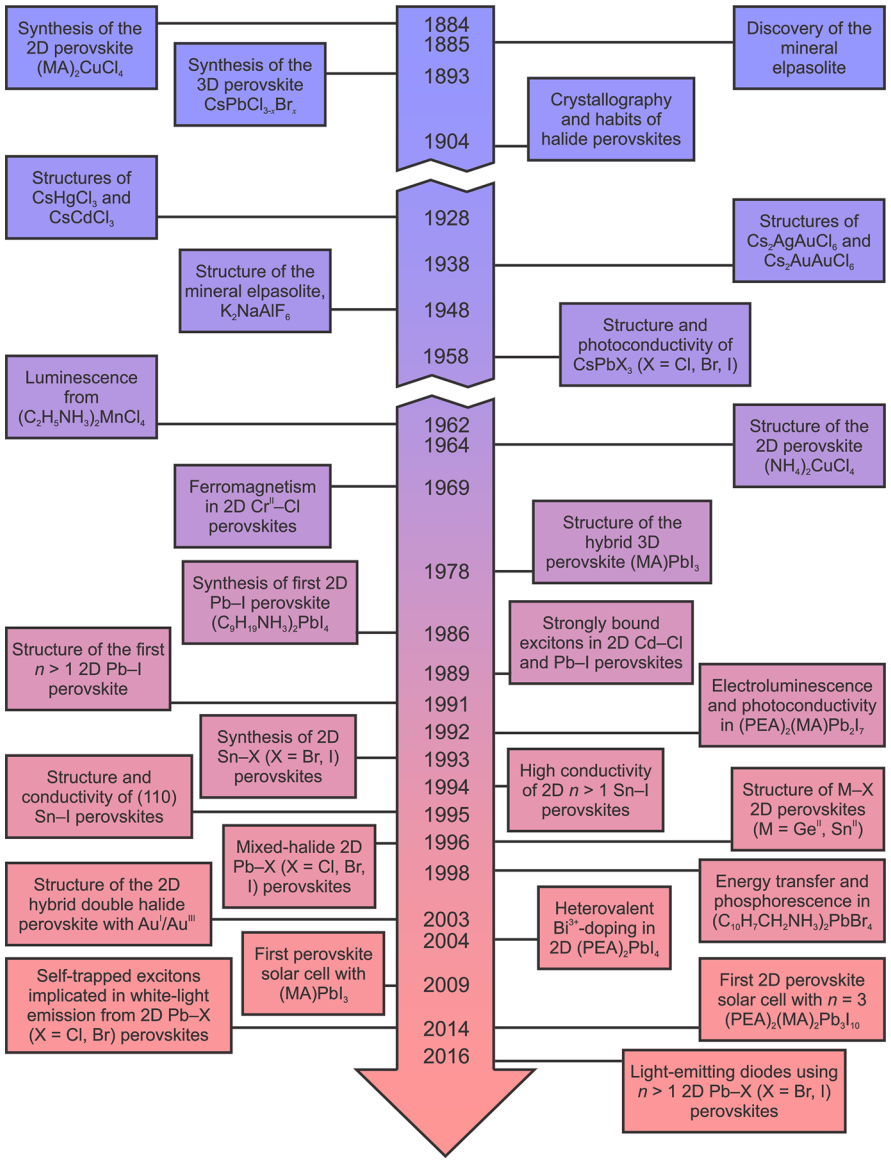

Figure 3. History of some significant developments in halide perovskites (MA = $CH_3NH_3^+$; PEA = $C_6H_5(CH_2)_2NH_3^+$).

nearly a century,[18] and their syntheses represent some of the first reports of halide perovskites (Figure 3).[1,38] Assigning a definitive date to the birth of this field is difficult, as these initial studies occurred prior to Röntgen's pioneering work on X-rays;[39] thus their atomic arrangements were unknown. Arend and colleagues[18] cataloged much of this history in an early review on the synthesis and crystal growth of the layered transition-metal hybrid perovskites. More modern examples of systematic studies on crystal structures and optical properties include Willett's studies of $(NH_4)_2CuCl_4$,[40] $(CH_3NH_3)_2CuCl_4$,[41] and $(C_2H_5NH_3)_2CuCl_4$[41] in the 1960s. Other transition-metal-based perovskites, such as the $(RNH_3)_2CrCl_4$ (R = CH_3, C_2H_5, C_8H_{17}, $C_{10}H_{21}$) hybrids, followed in the 1970s.[42,43] Much of the interest at this time in the Cu^{II}- and Cr^{II}-based perovskites focused on their magnetic properties, as they behave as 2D ferromagnets below ~10 and ~60 K, respectively.[43−45] Other divalent transition metals that form layered halide perovskites included Mn, Fe, Cd, and Pd, templated by alkylammonium or alkyldiammonium cations.[18] Notably, in 1962, red or pink photoluminescence in layered hybrid perovskites was observed in $(RNH_3)_2MnCl_4$ (R = CH_3 or C_2H_5).[46]

The layered group 14 hybrids were relative latecomers to the halide perovskite family, with the first report of $(C_9H_{19}NH_3)_2PbI_4$ in 1986 by Maruyama and colleagues.[47,48] They studied the ability of this perovskite to intercalate hexanes owing to the paraffinic nature of the nonylammonium bilayer. Following this, Ishihara and colleagues observed strong, room-temperature luminescence from the Pb−I perovskites,[49] which they attributed to excitonic recombination (section 6.1), spurring the further growth of this class of materials. The first Sn−I and Ge−I 2D perovskites were synthesized by Papavassiliou and Mitzi starting in 1993[50−55] and 1996,[55] respectively, templated by a number of different organic cations. Similarly, the structure and optoelectronic properties of the first mixed-halide 2D lead perovskites underwent extensive study by Kitazawa between 1996 and 1997 and provided a glimpse at the wide tunability of these materials.[56,57]

During the 1990s, the group 14 perovskites developed along primarily two fronts. New structural archetypes, including

DOI: 10.1021/acs.chemrev.8b00477
Chem. Rev. XXXX, XXX, XXX−XXX

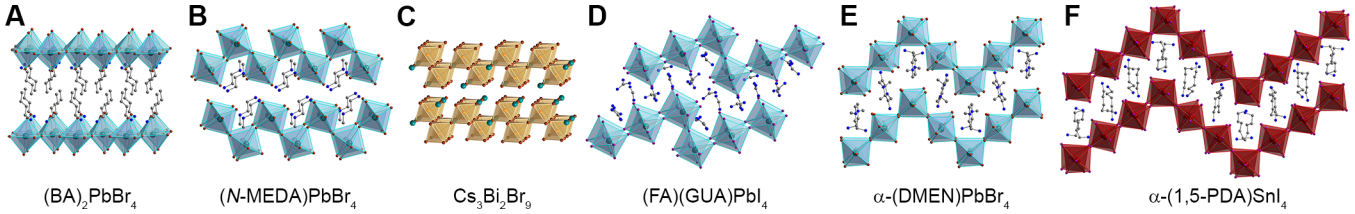

Figure 4. Crystal structures of (A) (001) perovskite $(BA)_2PbBr_4$ (BA = $C_4H_9NH_3^+$),[14] (B) (110) perovskite (*N*-MEDA)$PbBr_4$ (*N*-MEDA = N^1-methylethane-1,2-diammonium),[11] (C) (111) perovskite $Cs_3Bi_2Br_9$,[111] (D) (FA)(GUA)PbI_4 (FA = $CH(NH_2)_2^+$; GUA = $C(NH_2)_3^+$),[101] (E) *α*-(DMEN)$PbBr_4$ (DMEN = N^1,N^1-dimethylethane-1,2-diammonium),[100] and (F) *α*-(1,5-PDA)SnI_4 (1,5-PDA = 1,5-pentanediammonium).[99] Turquiose, orange, dark red, teal, purple, brown, red, blue, and gray spheres represent Pb, Bi, Sn, Cs, I, Br, O, N, and C atoms, respectively. Disordered atoms and hydrogen atoms omitted for clarity.

those with thicker inorganic layers[58] (section 2.2.3) as well as inorganic layers with new connectivities[59] (section 2.2.1), expanded the phase space to new inorganic topologies. In particular, Mitzi and colleagues showed that the Sn–I perovskites with thicker inorganic layers exhibited high electrical conductivities,[52,59] making them potentially attractive candidates for thin-film transistors that could be deposited from solution.[60] The set of possible organic cations underwent a simultaneous expansion, with significant contributions made by Mitzi and colleagues[61−63] and Papavassiliou and colleagues.[51,54,64−67] The understanding of the optoelectronic properties of 2D perovskites advanced in step. Ishihara and colleagues made major contributions to understanding the photophysics of layered Pb–I perovskites, elucidating their excitonic nature, as well as demonstrating the effects of the organic cations on the optical properties.[19,68−70] Electroluminescence from 2D Pb–I perovskite crystals, simply painted with silver contacts,[4] occurred in 1992, with reports of light-emitting diodes following as early as in 1994.[5,6,71]

Advances in the layered hybrid perovskites only accelerated in the 21st century, including studies in structure–function relationships,[63,72] crystallography and temperature-dependent phase transitions,[73−79] optical properties,[80−85] photovoltaics,[3,86,87] light-emitting diodes,[4−9] and white-light photoluminescence.[11,25,88−90]

2. STRUCTURE

2.1. Three-Dimensional Perovskites

Three-dimensional (3D) halide perovskites, which have the general formula $A^IB^{II}X_3$, consist of a simple cubic arrangement of divalent B-site cations, bridged by halide anions (X = F^-, Cl^-, Br^-, I^-), creating a 3D anionic network of corner-sharing octahedra. Small monovalent A-site cations occupy cuboctahedral cavities in the B–X sublattice and provide charge balance (Figure 2A). The metal halide octahedra may rotate or tilt with respect to each other, similar to the case for oxide perovskites, where nomenclature has been established to describe the resulting lattices.[91,92] While 3D perovskites containing Pb^{2+} at the B site have received widespread attention in recent years due to their remarkable optoelectronic properties, other B-site metals have been incorporated into the lattice, including Sn^{2+},[93,94] Ge^{2+},[95] Cd^{2+},[28] Hg^{2+},[28] and Mn^{2+}.[27] The double perovskite lattice greatly increases substitutional flexibility at the B site. Here, mono- and trivalent cations or tetravalent cations and vacancies are combined in an ordered arrangement at the B sites, maintaining an average 2+ charge.[29−31,33] The A site of 3D perovskites is frequently occupied by a small alkali metal cation such as K^+, Rb^+, or Cs^+, but in some cases, small organic cations, such as methylammonium[37] or formamidinium,[96] can be incorporated, yielding a hybrid organic–inorganic structure.[37]

2.2. Two-Dimensional Perovskites

In 3D perovskites, the A-site cation is confined to the small cuboctahedral cavity in the B–X sublattice and, therefore, cannot exceed a critical size.[62,97] Moving to larger A-site cations yields lower-dimensional 2D, one-dimensional (1D), or zero-dimensional (0D) derivatives. Typically, long, relatively narrow A-site cations, which can pack efficiently, template 2D layers of corner-sharing metal halide octahedra (Figure 2B). As in the 3D materials, the 2D perovskite structure allows for substitutions at the B and X sites, while a much greater diversity of A-site cations can be accommodated between the inorganic layers yielding a richer platform for chemical tuning.

2.2.1. Connectivity of the Inorganic Layer. The vast majority of 2D perovskites have flat sheets of corner-sharing metal halide octahedra, which can be abstractly derived from the (001) crystallographic plane of their 3D congeners (Figure 4A).[21] A smaller subset of 2D perovskites contain corrugated inorganic layers, similarly derived from the (110)[59] (Figure 4B) or (111)[98] (Figure 4C) crystallographic planes. More complex corrugation patterns yield closely related lattices whose inorganic layers cannot be simply defined by the above formalism (Figure 4D–F).[99−101] This wide array of structure types can be prepared by similar solution-state self-assembly methods with the only significant difference being the organic cation employed. This highlights the key role of the A-site cation in templating the structure of the extended inorganic lattice. Importantly, the various structure types can have dramatically different optical properties as highlighted by the discussions of (001) and (110) Pb–Br perovskites in sections 6.1 and 7.1.1, respectively.

2.2.2. Structural Distortions of the Inorganic Layer. Frequently, the inorganic sheets of 2D perovskites show significant structural distortions relative to the ideal cubic 3D perovskite lattice. Common distortions include deviations of the coordination environment about the B-site cation from ideal octahedral symmetry (unequal bond lengths or X–B–X bond angles deviating from 90 or 180°) and tilting between metal halide octahedra (Figure 5A–C). The severity of these distortions can vary widely across a series of perovskites prepared with the same B- and X-site occupants but with different A-site cations. Mitzi and colleagues found a significant variation of the Sn–I–Sn bond angle in the structures of several 2D perovskites containing different constitutional isomers of fluorophenethylammonium (e.g., the 4-fluoro (4-FPEA) and 3-fluoro (3-FPEA) isomers). These changes were linked to differences in the packing arrangements adopted by these molecules within the organic bilayer (Figure 5D), thus

DOI: 10.1021/acs.chemrev.8b00477
Chem. Rev. XXXX, XXX, XXX–XXX

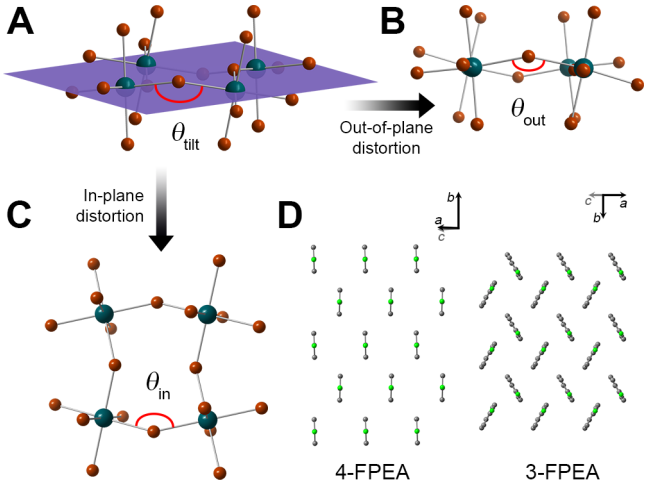

Figure 5. (A) Illustration of interoctahedral tilting in a (001) metal halide (M−X) perovskite. The M−X−M angle (θ_{tilt}) can be decomposed into (B) out-of-plane (θ_{out}) and (C) in-plane (θ_{in}) components. Turquoise and brown spheres represent the metal and halide atoms, respectively. (D) Different packing arrangements adopted by 4-fluorophenethylammonium (4-FPEA) and 3-fluorophenethylammonium (3-FPEA) within the organic bilayers of two Sn−I perovskites. These distinct packing arrangements template different θ_{tilt} values in the inorganic sheets. Gray and green spheres represent C and F atoms, respectively. Hydrogen atoms and disordered atoms are omitted for clarity. (A−C) Reproduced with permission from ref 88. Copyright 2017 Royal Society of Chemistry. (D) Adapted from ref 60. Copyright 2001 American Chemical Society.

highlighting the importance of the organic cation in templating the inorganic lattice.[60] Other studies have emphasized the importance of factors including the steric demands of the organic cation,[72] hydrogen-bonding influences,[60,102−105] and the charge density of the alkylammonium head[63,106] as well as its proximity to the plane of the inorganic sheets[107] in templating the inorganic lattice.

2.2.3. Thickness of the Inorganic Layer. In the prototypical (001) perovskites, the inorganic slabs are the thickness of a single metal halide octahedron (Figure 4A). However, between this structure and the 3D perovskite structure, there exists an entire series of intermediate structures with inorganic layers of varying thicknesses that can be prepared by using both small and large A-site cations (Figure 1H).[58] For (001) perovskites, structures with thicker inorganic layers have the general formula $A'_2A_{n-1}B_nX_{3n+1}$, where the small (A) cations occupy the cavities between octahedra within the inorganic slabs while the larger (A′) cations partition the inorganic layers. By varying the ratio of small to large cations, the thickness of the inorganic sheets can be tuned. This thickness is quantified as "*n*", the number (*n*) of octahedral layers that make up a single slab (Figure 6C). Similarly, thicker inorganic layers with both (110)[59] and (111)[108] inorganic sheets can be synthesized (Figure 6D). With increasing *n*, the optical properties of 2D perovskites approach those of the parent 3D perovskite[86,109] (the $n = \infty$ structure), although important distinctions remain and phase-pure materials are difficult to isolate (sections 5.2.2 and 6.2.2).

2.2.4. The A Site. In most 2D halide perovskites, organoammonium cations occupy the A site with terminal ammonium groups forming hydrogen bonds with the halides of the inorganic sublattice. Bilayers of monoammonium cations (RNH_3^+; R = aliphatic or aromatic group; Figure 1A) or monolayers of diammonium cations ($^+H_3N{-}R{-}NH_3^+$; R = aliphatic or aromatic group; Figure 1B) are typically found in the organic layers. There are also examples of perovskites with alkali metal cations residing between the inorganic sheets.[110−112] The choice of A-site cation plays an important role in templating the structure of the inorganic sublattice and, therefore, can greatly influence the luminescence properties of the material. The organic and inorganic layers should be considered as mutual templates. For example, packing interactions between oligothiophene chains in the organic layer have afforded $(AEQT)Bi_{2/3}\square_{1/3}I_4$ (AEQT = 5,5‴-bis(ethylammonium)-2,2′:5′,2″:5″,2‴-quaterthiophene, □ = Bi^{3+} vacancy) perovskites with trivalent Bi^{3+} cations in two-thirds of the B sites—an inorganic layer that has not been stabilized through simple alkyl ammonium cations.[113] Similarly, the inorganic layers may template unusual organic architectures, such as the criss-crossed network of polyether chains found in $(EDBE)CuCl_4$ (EDBE = 2,2′-(ethylenedioxy)-bis(ethylammonium); Figure 1B).[114]

2.2.5. The B Site. The choice of B-site cation largely determines the electronic structure of the 2D perovskite (see section 4) and, hence, its emissive properties (Table 2). A wide range of divalent B-site cations have been incorporated into 2D halide perovskites including Pb^{2+},[47] Sn^{2+},[51] Ge^{2+},[55] Cu^{2+},[40] Mn^{2+},[115] Fe^{2+},[116] and Eu^{2+} (Figure 1).[117] Additionally, by leveraging the templating effect of the organic cation, Mitzi successfully prepared a 2D perovskite containing Bi^{3+}, where the excess positive charge is balanced by B-site vacancies.[113] The double perovskite framework provides another avenue to expand the range of B-site cations that can be incorporated into 2D perovskites. Guloy and colleagues used this strategy to incorporate Au^+ and Au^{3+} into a (001) hybrid perovskite,[118] and Karunadasa and co-workers recently reported $n = 1$ and 2 (001) hybrid perovskites with Ag^+ and Bi^{3+} B-site metals

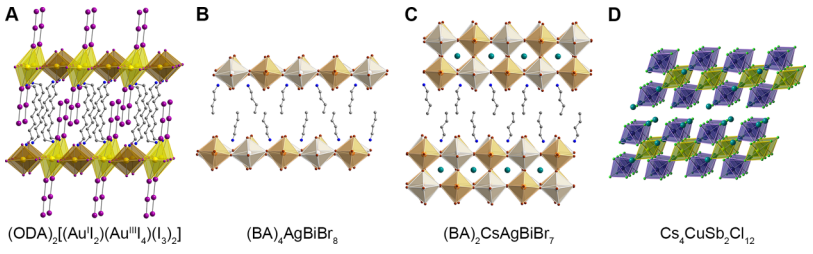

Figure 6. Crystal structures of layered double perovskite archetypes. (A) $(ODA)_2[(Au^II_2)(Au^{III}I_4)(I_3)_2]$ (ODA = 1,8-octanediammonium),[118] (B) $n = 1$ $(BA)_4AgBiBr_8$ (BA = butylammonium),[119] (C) $n = 2$ $(BA)_2CsAgBiBr_7$,[119] and (D) $Cs_4CuSb_2Cl_{12}$.[108] Yellow, dark yellow, orange, white, indigo, lime, teal, purple, brown, green, blue, and gray spheres represent Au^{III}, Au^I, Bi, Ag, Sb, Cu, Cs, I, Br, Cl, N, and C atoms, respectively. Disordered atoms and hydrogen atoms omitted for clarity. (B, C) Adapted from ref 119. Copyright 2018 American Chemical Society.

DOI: 10.1021/acs.chemrev.8b00477
Chem. Rev. XXXX, XXX, XXX−XXX

Table 2. Photoluminescence Peak Position (λ_{max}) and Width (fwhm) for a Range of 2D Butylammonium-Based Halide Perovskites Prepared with Different B-Site Cations[a]

perovskite	λ_{max} (nm)	fwhm[b] (nm)	ref
$(BA)_2GeI_4$	690	180	55
$(BA)_2PbI_4$	525	22	55
$(BA)_2SnI_4$	625	38	55
$(BA)_2EuI_4$	460	24	117
$(BA)_2PbBr_4$	420	20	238
$(BA)_2PbBr_4:Mn^{2+}$	600	80	238
$(BA)_4AgBiBr_8$[c]	470	47	119

[a]BA = butylammonium. [b]fwhm = full width at half-maximum. [c]Data collected at 25 K.

(Figure 6B,C).[119] The family of (111) layered perovskites also contains trivalent metal cations.[21] Solis-Ibarra and co-workers recently expanded this family to include double perovskites, featuring Cu^{2+} and Sb^{3+} (Figure 6D).[108]

2.2.6. The X Site. The layered hybrid perovskites typically comprise Cl^-, Br^-, or I^- anions although some inorganic 2D perovskites such as K_2MgF_4 contain F^- anions. The choice of halide has a significant impact on the band gap with the mixed-halide compositions enabling smooth variation of photoluminescence energy across the visible region (section 6.1.1).[56,57,120] However, it is important to note that some B-site cations cannot form perovskite structures with every halide, determined by the steric requirements of accommodating six halides around the B-site cation. For example, to our knowledge, there are no examples of first-row transition-metal-based layered perovskites containing iodides. Redox potentials also play a role in the stability of a proposed perovskite.[121] For example, there are no reports of Cu^{II}–I perovskites forming through aqueous self-assembly reactions as the Cu^{II} oxidizes the iodide to iodine. There are also several examples of 2D halide perovskites containing pseudohalides such as SCN^-[122] (Figure 1E) and I_3^- (Figure 6A).[118]

3. SYNTHESIS

Hybrid halide perovskites typically form through solution-state self-assembly reactions where the metal halide salt and the neutral organic amine are combined in aqueous acidic solution or the halide salt of the ammonium cation is added to an organic solvent containing the metal halide salt. In order for the desired perovskite to crystallize instead of the multiple competing side phases, the precursor stoichiometry, solution pH, temperature, and solvent(s) are varied. Standard crystallization methods employed for small molecules work well for crystallizing halide perovskites from solution:[18,20] e.g., slowly cooling a hot, saturated precursor solution, allowing a solvent in which the perovskite is not soluble to diffuse into the precursor solution, allowing the solvent to evaporate and concentrate the precursor solution or layering the precursors such that they slowly meet at the interface. Rapid crystallization affords polycrystalline powders, whereas slowing the crystallization often produces crystals of sufficient quality for single-crystal X-ray diffraction. In some cases, even larger (centimeter-scale) single crystals can be formed for other spectroscopic studies[49,69] or device fabrication.[4,123] Importantly, uniform oriented films of 2D halide perovskites can be formed on a variety of substrates through a number of different methods such as spin-coating, drop-casting, dip-coating, and single- and dual-source vapor deposition, enabling both spectroscopic studies and device fabrication.[124] Solid-state pulverization of the precursor powders and subsequent annealing also affords halide perovskites, a particularly useful method for less-soluble metal salts or metal ions (such as the lanthanides) which are strongly coordinated by solvent molecules.[20,117]

Each of the A, B, and X components may also be mixed by varying the ratio of the precursors. For example, mixed-halide perovskites (see section 6.1.1) crystallize from solutions containing a ratio of halides.[17,56] However, the stoichiometry of the halides in the resulting perovskites isolated as powders, crystals, or even spin-coated films may vary from that in the precursor solution.[89] Therefore, the halide ratio of the perovskite is best determined after the product is isolated using a bulk elemental analysis method such as inductively coupled plasma mass spectrometry. Different A-site cations can similarly be introduced to the structure,[125,126] where mixing small and large A-site cations affords layered perovskites with thicker inorganic layers (see section 2.2.3).[58] The B site can also accommodate a mixture of different cations, where a mismatch in charge allows them to form ordered double perovskite lattices.[108,118,119,127] The composition and connectivity of 2D perovskites can also be changed post synthetically, where the layered perovskite structure is preserved in the product, while new bonds are formed or atoms/molecules/ions are exchanged or inserted.[23]

4. ELECTRONIC STRUCTURE

4.1. Transition-Metal-Based 2D Perovskites

Layered perovskites of Cu^{2+}, Mn^{2+}, Cr^{2+}, and Fe^{2+} can exhibit interesting magnetic properties, providing the early impetus for their systematic study.[41,43−45] More recently, the well-studied ferromagnetic ordering of 2D Cu^{2+} perovskites was found to coexist with spontaneous ferroelectric order.[128] In general, these Mott/charge-transfer insulators[129−131] and their spectroscopic features can be well described by their molecular analogues. The d^9 electronic configuration of Cu^{2+} and the high-spin d^4 configuration of Cr^{2+} result in substantial Jahn−Teller distortions. Thus, the octahedral ligand field of Cl atoms in the perovskite lattice is distorted to a ligand field of D_{4h} symmetry, where one axis of the octahedron is elongated. These elongated axes lie along the inorganic sheets and are oriented perpendicular to one another in an antiferrodistortive alignment (Figure 7A). This arrangement leads to the partially filled orbitals on each metal center ($d_{x^2-y^2}$ in the case of Cu^{2+}) being orthogonal to one another, and hence the optical properties of these extended solids bear a strong resemblance to molecular systems.[41] Indeed, in the absorption spectrum of 2D Cu−Cl perovskites, all of the observed bands can be assigned to transitions expected for an isolated square-planar $CuCl_4^{2-}$ molecule (Figure 7B,C).[41,130,132,133]

4.2. Semiconducting 2D Perovskites

Changing the B-site cations from transition metals to the p-block metals yields semiconducting perovskites. The group 14 2D perovskites are direct-gap semiconductors, with the valence band maximum comprised of halide *n*p and metal *n*s orbitals, whereas the conduction band minimum consists primarily of metal *n*p orbitals (Figure 8B).[20,134] Typically, the organic cations do not contribute to the band extrema[20] except in cases where relatively close overlap between energetic levels enables either charge transfer between organic and inorganic components or the highest occupied molecular orbital

DOI: 10.1021/acs.chemrev.8b00477
Chem. Rev. XXXX, XXX, XXX−XXX

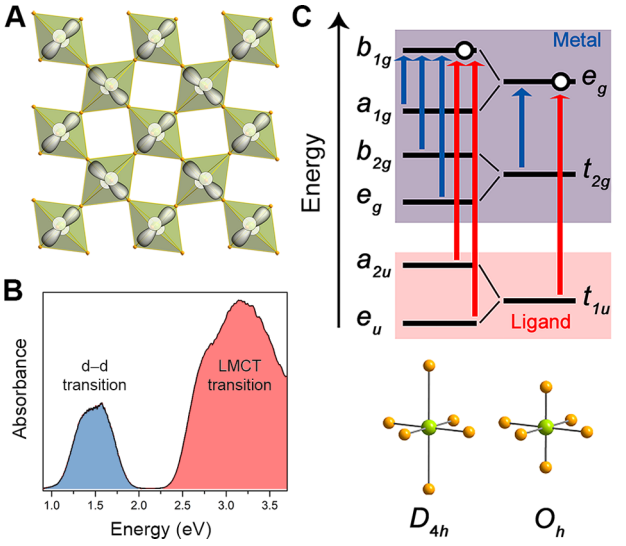

Figure 7. (A) Single inorganic layer of a Cu^{II}–Cl perovskite, viewed perpendicular to the plane of the layer, displaying the antiferrodistortive alignment of the elongated Jahn–Teller axes. Schematic $d_{x^2-y^2}$ orbitals are overlaid to illustrate their orthogonality. (B) Prototypical room-temperature absorption spectrum of a Cu–Cl perovskite. (C) Orbital energy diagrams of Cu–Cl octahedra with D_{4h} or O_h symmetry showing possible d–d (blue arrows) and ligand-to-metal charge-transfer (LMCT; red arrows) transitions, obtained from ref 133. (A, B) Adapted from ref 130. Copyright 2015 American Chemical Society. (C) Adapted with permission from ref 133. Copyright 1999 American Physical Society.

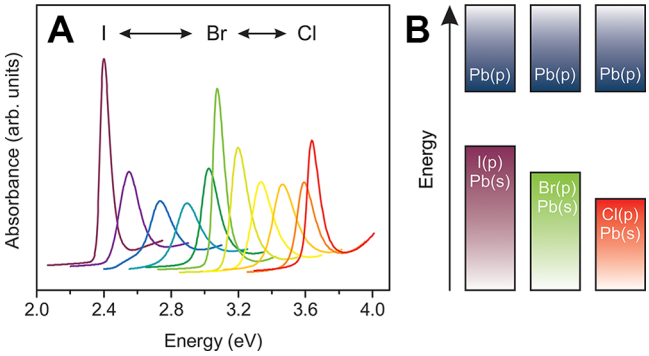

Figure 8. (A) Optical absorbance spectra of 2D mixed-halide Pb–X perovskites (X = Cl, Br, I).[166] (B) Schematic block band diagram of Pb–X (X = Cl, Br, I) 2D perovskites highlighting their change in band gap and the orbitals that contribute most to the band extrema. (A) Adapted from ref 166. Copyright 2014 American Chemical Society. (B) Reproduced with permission from ref 26. Copyright 2018 Annual Reviews.

(HOMO)–lowest unoccupied molecular orbital (LUMO) gap is smaller than the band gap of the inorganic component[61] (section 8). Instead, the organic component exerts a primarily indirect influence on the electronic structure through structural templating effects (section 2.2.2),[63,88] modulating the material's dielectric profile (section 5.2.1),[70] and through vibrational coupling in the excited state (section 6.1.3).[135,136] Much work has emphasized the important role the filled 6s shell of Pb^{2+} plays in the outstanding optoelectronic properties of the Pb-based perovskites.[137,138] Non-group 14 ions with ns^2np^0 configurations can be incorporated by using the double perovskite structure. Thus, trivalent Bi^{3+} was incorporated into n = 1 and 2 (001) double perovskites[119] (Figure 6B,C) and Sb^{3+} was incorporated into a (111) double perovskite (Figure 6D).[108] Notably, the band-gap transition in group 14 metal halide perovskites involves charge transfer from the filled s orbitals to the empty p orbitals of the same metal. In contrast, the band-gap transition of double perovskites with two different B-site metals shows considerable metal-to-metal charge-transfer character.[119] In both cases, there is also halide character at the band edges, particularly in the valence band. While the band-edge orbital compositions of the 3D and 2D congeners for group 14 metal perovskites (e.g., Pb or Sn) are similar, dimensional reduction can change the symmetry of the band extrema in double perovskites. For example, calculations reveal that the indirect band gap of the 3D ($n = \infty$) double perovskite $Cs_2AgBiBr_6$ is maintained until the inorganic layers are two octahedra thick (n = 2) and then transitions to a direct band gap at the n = 1 limit in $(C_4H_9NH_3)_4AgBiBr_8$.[119]

5. ELECTRONIC CONFINEMENT

The dimensionality of the inorganic layers strongly influences the observed electronic structure. The width of the inorganic layer in the n = 1 (001) perovskites is less than 1 nm thick.[70] Decreasing dimensionality reduces the dispersion[134] of valence and conduction bands, manifesting as an increase in the band gap, rising from 1.65 eV in $(CH_3NH_3)PbI_3$[139] to 2.58 eV in $(C_6H_5(CH_2)_2NH_3)_2PbI_4$.[69] With their periodic arrangement of thin inorganic layers, the 2D perovskites seem analogous to multiple quantum well heterostructures, a similarity that did not go unnoticed in early studies.[19] In fact, quantum wells and semiconducting layered perovskites are qualitatively similar, featuring strongly bound excitons and often, enhanced luminescence relative to their 3D analogues.[19] However, the layered perovskites do not behave as true quantum wells, as several approximations and models for those systems fail to describe the photophysics of 2D perovskites.[140] The consequences of this quantum-well-like structure manifest primarily in the excitonic behavior of the layered lead halide perovskites.

5.1. Excitons

Excited electrons and holes can experience an energetically stabilizing Coulombic attraction, forming an electrostatically neutral quasiparticle, called an exciton.[141,142] Excitons are stabilized relative to their free carrier constituents by the exciton binding energy (E_b), a quantity whose magnitude describes the energy needed to separate the Coulombically bound charges.[142] In canonical direct band gap semiconductors, such as GaAs,[143] $E_b \ll k_BT$ at 298 K (25.7 meV), so the excitons are ionized to free carriers at room temperature. Similarly, free carriers predominate in the 3D perovskite $(CH_3NH_3)PbI_3$, which also exhibits a small E_b estimated at ca. 2 meV.[144] In contrast, strong excitonic absorption and luminescence features are observed at room temperature in layered lead halide perovskites,[19] with E_b values of ca. 300 meV for typical n = 1 Pb–I[70] materials.

5.2. Electronic Confinement Effects

The strong excitonic character of the group 14 2D perovskites compared to their 3D congeners results from the cooperative effects of quantum and dielectric confinement (Table 3).[19] Despite the differences between the layered perovskites and true quantum-well systems,[140] these two effects, which apply to quantum wells, qualitatively explain 2D perovskites' greatly enhanced E_b.[19,70] In an electronically 3D material, such as $(CH_3NH_3)PbI_3$, the excitonic wave functions are similar to the

DOI: 10.1021/acs.chemrev.8b00477
Chem. Rev. XXXX, XXX, XXX–XXX

Table 3. Band Gaps (E_g) and Exciton Binding Energies (E_b) for an Array of 2D Perovskites[a]

perovskite	E_g (eV)	E_b (meV)	ref
$(DA)_2PbI_4$	2.88	320	68, 69
$(PEA)_2PbI_4$	2.58	220	69
$(PEA)_2(MA)Pb_2I_7$	2.34	170	4, 69
$(BA)_2PbBr_4$	3.42	393	150
$(PEA)_2PbBr_4$	3.40	356	150
$(IC_6)_2PbI_4$	2.56	230	149
$(IC_6)_2PbI_4{\cdot}2I_2$	2.49	180	149

[a]DA = decylammonium, PEA = phenethylammoniuim, BA = butylammonium, IC_6 = 6-iodohexylammonium.

3D hydrogenic wave functions of the Bohr model.[142] In 2D systems, dimensional confinement of the wave function leads to a 4-fold enhancement of E_b relative to its 3D congener through quantum confinement.[19,145] Dielectric confinement results from relatively poor screening of the Coulombic attraction between the electron and hole[146−148] by the organic layers, which are significantly less polarizable than the inorganic layers.[70]

5.2.1. Tuning E_b through the Organic Layer. The dielectric mismatch between organic and inorganic layers may be reduced by including polarizable groups in the organic layer. Ishihara and co-workers demonstrated this effect by synthesizing two n = 1 perovskites using amines with very different dielectric constants (decylamine, $\varepsilon \sim 2.44$; and phenethylamine, $\varepsilon \sim 3.32$), finding from absorption spectra that E_b = 320 meV for $(C_{10}H_{21}NH_3)_2PbI_4$ and E_b = 220 meV for $(C_6H_5(CH_2)_2NH_3)_2PbI_4$.[69] In both perovskites, the luminescence efficiency is essentially constant at low temperature but drops precipitously upon warming past a certain threshold (unique to each material). From this temperature dependence, an activation energy, corresponding to E_b, can be extracted. In both cases, this value of E_b agrees well with that measured from absorption spectra.[69] The polarizability of the organic layer may also be increased by adding iodoalkanes in the organic layer, which can further decrease E_b by stabilizing I_2 intercalation in the organic layers through I···I interactions. Iodine intercalation yielded a very low E_b of 180 meV in the perovskite $(IC_6H_{12}NH_3)_2PbI_4{\cdot}2I_2$, although the I_2-intercalated perovskite was transiently generated.[149]

5.2.2. Tuning E_b through the Inorganic Layer. The polarizability of the halide appears to affect E_b, as lead iodide perovskites display lower E_b values than lead bromide perovskites (Table 3).[4,68,69,150] The layered perovskite $(CH_3NH_3)_2PbI_2(SCN)_2$, with pseudohalides as the terminal ligands exhibits an E_b of 200 mV, which is particularly low for an n = 1 perovskite without polarizable groups in the organic layers.[151] Further reduction of both E_b (by reducing both dielectric and quantum confinement) and the band gap (E_g) can be achieved by increasing the thickness of the inorganic layers. Perovskites with $1 < n < \infty$ show intermediate properties between those of n = 1 and $n = \infty$ perovskites. The n = 1 member of the $(C_6H_5(CH_2)_2NH_3)_2(CH_3NH_3)_{n-1}Pb_nI_{3n+1}$ family has E_g and E_b values of 2.58 and 0.220 eV, respectively, while the n = 2 perovskite has corresponding values of 2.34 and 0.170 eV, respectively,[4,69] with these values dropping further for the n = 3 member.[3] These effects are also clearly observed for higher-n members of the series $(C_4H_9NH_3)_2(CH_3NH_3)_{n-1}Pb_nI_{3n+1}$ and lead to a similar red shifting of the luminescence with n, which converges toward the emission energy of the $n = \infty$ perovskite $(CH_3NH_3)PbI_3$ at 1.60 eV.[109]

5.3. Trapped Excitons

In the layered lead halide perovskites, there are several distinct, yet related types of excitons that radiatively decay, including free, bound, and self-trapped excitons.

5.3.1. Bound Excitons. The free exciton is the neutral electron−hole quasiparticle that is free to migrate in the material and is essentially unaffected by defects or impurities in the lattice.[142] However, excitons can interact with defects, localizing to the impurity to become bound excitons, as is the case in the Bi^{3+}-doped perovskite $(C_6H_5(CH_2)_2NH_3)_2PbI_4$.[152] These bound excitons are stabilized energetically relative to the free excitons, leading to an increase in Stokes shift of the resulting photoluminescence (section 7.6.2).

5.3.2. Self-Trapped Excitons. Excitons can localize even in the absence of lattice defects, through the creation of transient lattice defects, in a process termed "self-trapping". In a material with significant coupling between the exciton and the lattice, the exciton generates a lattice distortion and becomes (self)-trapped by the distortion it induced.[153] Self-trapped excitons are thus similar to small polarons (charge carriers that induce local lattice distortions owing to strong carrier−phonon coupling), although excitons are neutral quasiparticles and are thus uncharged. Restated, self-trapped excitons (STEs) can be considered as excited-state defects, as they exist only upon excitation, and the lattice distortion disappears following decay to the ground state. Exciton self-trapping is commonly observed across a wide variety of insulators, such as condensed rare gases, polycyclic aromatic hydrocarbons, alkali metal halides, and lead(II) halides.[153,154] Owing to the large-amplitude structural distortions and energetic stabilization that accompanies exciton self-trapping, the resulting luminescence is often broad and has a large Stokes shift (discussed further in section 7.2).[153] White-light photoluminescence in 2D Pb-based perovskites upon UV excitation has been attributed to exciton self-trapping (section 7.1).[11]

The large structural distortions that occur upon exciton self-trapping can be interpreted as changes in bonding and local coordination. In $PbBr_2$, whose band extrema are similar in orbital composition to those of layered Pb−Br perovskites,[20,155] the excited electron localizes on a Pb^{2+} ion, which dimerizes with another Pb^{2+} to form a Pb_2^{3+} species. Similarly, holes localize on adjacent Br^- ions, which form Br_2^- dimers in the excited state.[154,156]

Self-trapped excitons can be further classified as intrinsic or extrinsic depending on the nature of their interaction with the lattice (Figure 9). In cases of extrinsic self-trapping, materials defects are required to nucleate the self-trapped site. In $TlCl_{1-x}Br_x$, both TlCl and TlBr end-members exhibit narrow, free-excitonic photoluminescence with minimal Stokes shift. However, bromide doping of a chloride host lattice yields broad, Stokes shifted luminescence whose intensity depends linearly on the concentration of Br^- impurity ions, yet the absorption spectrum has no signature of the dopant ion impurities, indicating extrinsic self-trapping.[157] While intrinsic self-trapping, by definition, does not require lattice defects, they are closely interrelated. For example, in NaCl, photoexcitation yields intrinsic self-trapped excitons that nonradiatively relax on picosecond time scales to form permanent lattice defects (F−H defect pairs).[158]

DOI: 10.1021/acs.chemrev.8b00477
Chem. Rev. XXXX, XXX, XXX−XXX

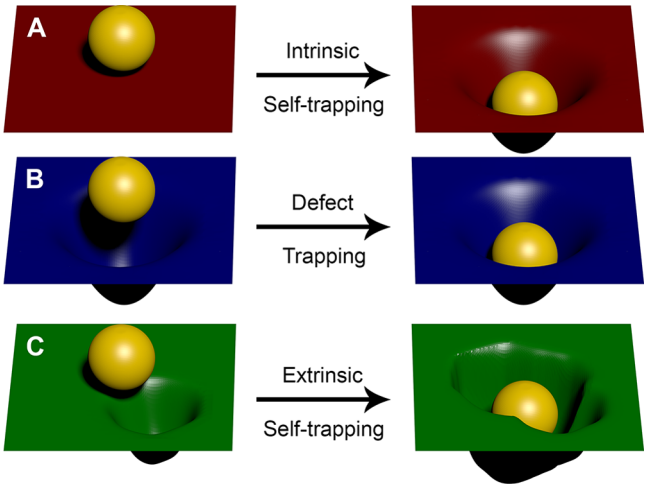

Figure 9. Exciton self-trapping and trapping at permanent defects represented by balls deforming a rubber sheet. Reprinted from ref 25. Copyright 2018 American Chemical Society.

5.3.3. An Analogy for Intrinsic and Extrinsic Self-Trapping. Intrinsic self-trapping is similar to a soccer ball that is kicked into the goal deforming the loosely held net. Prior to contact with the ball, the net may be perfectly uniform. Similarly, intrinsic self-trapping creates transient defects in the excited state even in a perfect lattice. Real lattices, however, are never perfect and contain various densities and distributions of defects (e.g., lattice vacancies, interstitials). Extending the analogy of the soccer ball and the net, extrinsic self-trapping corresponds to a net that already contains deformations (e.g., holes in the fabric, irregularities in the weave). Although the soccer ball still deforms the net, the nonuniformity of the net will affect the extent to which the ball sinks and the distortion it creates. Intrinsic self-trapping leads to homogeneous emission broadening, where the emission width depends on the extent of the distortion of the excited state with respect to the ground state (given by the Huang–Rhys parameter, S).[159] Extrinsic self-trapping creates heterogeneity in the excited state, thus adding an inhomogeneous component to the emission broadening. Both intrinsic and extrinsic self-trapping are thought to contribute to white-light emission from layered perovskites.[25,89,90]

5.4. Determining the Band Gap (E_g) and Exciton Binding Energy (E_b)

The ability to deposit halide perovskites as thin films through simple methods such as spin-coating or drop-casting[20] enables the acquisition of optical absorption spectra with characteristic resonances. The transition-metal-based 2D perovskites, such as $(C_2H_5NH_3)_2CuCl_4$,[2] feature well-resolved d–d transitions in the visible region of the electromagnetic spectrum, as well as ligand-to-metal charge-transfer bands[133] at higher energies (Figure 7B,C).

The layered group 14 perovskites exhibit strong absorption at energies above their direct band gaps, as expected. However, their most striking feature is the intense, narrow free-excitonic resonance located below the band-gap energy (E_g) (Figure 10A), corresponding to the direct creation of excitons in the inorganic layers. The large extinction of this peak results from the high oscillator strength and tightly bound nature of excitons in these layered perovskites.[68] As these materials have a 2D density of states near the band extrema, E_g manifests as a step-like onset above the excitonic absorption.[68,160] At room temperature, it is difficult to accurately determine E_g (and hence E_b) in 2D perovskites from transmission optical spectra, owing to thermal broadening effects that obscure this step. However, both E_g and E_b can be directly determined from the absorption spectra acquired at liquid helium temperatures (4 K), which yields a clear step-like feature corresponding to the band-gap onset (Figure 10A).[25,149] Then, E_b is determined as E_g − (the exciton peak energy) Figure 10B). A common method for the determination of optical band gaps of semiconductors is the Tauc method.[161] However, this method was developed to analyze amorphous and electronically 3D materials[162] in the absence of excitonic effects,[139] and therefore should not be used for the crystalline, electronically 2D, highly excitonic group 14 layered perovskites.

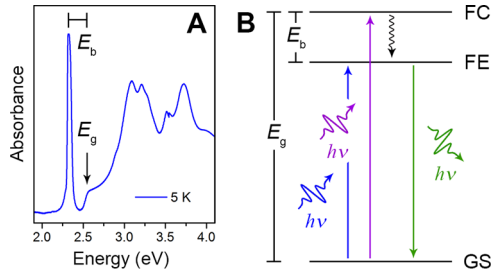

Figure 10. (A) Optical absorption spectrum of a 2D Pb–I perovskite[149] (E_g = band-gap energy; E_b = exciton binding energy). (B) Energy-level diagram of the typical excitonic and band-to-band transitions of 2D lead halide perovskites (FC = free carriers; FE = free excitons; GS = ground state. Colored arrows indicate absorption or photoluminescence, and the black arrow represents nonradiative relaxation. (A) Adapted with permission from ref 149. Copyright 2017 Royal Society of Chemistry. (B) Reprinted from ref 25. Copyright 2018 American Chemical Society.

6. NARROW EMISSION

The room-temperature photoluminescence originating from the inorganic layers of 2D perovskites can range from extremely narrow (full width at half-maximum (fwhm) ca. 100 meV)[49,55,163] to extremely broad (fwhm ca. 1 eV),[11,55,89] depending on the A-, B-, and X-site occupants (Table 4). In this section, we focus on narrow emission observed primarily in Pb- and Sn-based perovskites. Broad emission from these materials, including the Pb- and Ge-based perovskites, is discussed in section 7.

Table 4. Values of Emission Maximum (λ_{max}) and Width (fwhm) for Representative 2D Perovskites with Different Attributed Emission Mechanisms[a]

perovskite	λ_{max} (nm)	fwhm (nm)	emission mechanism	ref
(*N*-MPDA)$PbBr_4$	433	24	free excitons	11
(*N*-MEDA)$PbBr_4$	558	165	self-trapped excitons	11
(AEQT)$PbCl_4$	530	80	π^*–π transition	6
$(BA)_2EuI_4$	460	24	$4f^6 5d^1 \rightarrow 4f^7$ transition	117
$(BA)_2PbBr_4$:Mn^{2+}	600	80	Mn^{2+}:$^4T_1 \rightarrow {}^6A_1$ transition	238
$(BA)_4AgBiBr_8$	470[b]	47[b]	defect-assisted emission	119

[a] *N*-MPDA = N^1-methylpropane-1,3-diammonium, *N*-MEDA = N^1-methylethane-1,2-diammonium, AEQT = 5,5‴-bis(ethylammonium)-2,2′:5′,2″:5″,2‴-quaterthiophene, BA = butylammonium. [b] Data collected at 25 K.

DOI: 10.1021/acs.chemrev.8b00477
Chem. Rev. XXXX, XXX, XXX–XXX

6.1. Group 14 Perovskites with Thin (n = 1) Inorganic Layers

Although some layered halide perovskites containing transition metals exhibit photoluminescence (see sections 7.4 and 7.6.1),[46,119] the group 14 perovskites comprise the bulk of the luminescent perovskites.[20] In these perovskites, of which the Pb-based materials are the most closely studied,[20] the tightly bound excitons typically yield strong and sharp photoluminescence, which is minimally Stokes shifted, characteristic of free-excitonic recombination (Figure 11).[19]

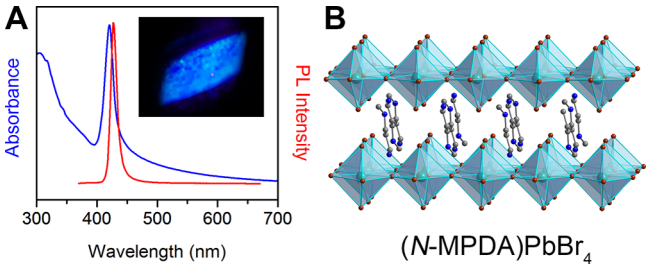

Figure 11. (A) Absorbance (blue) and photoluminescence (PL; red) spectra and (B) crystal structure of the (001) perovskite (*N*-MPDA)$PbBr_4$.[11,90] (inset) Photograph of (*N*-MPDA)$PbBr_4$ powder emitting blue light under ultraviolet illumination. Turquoise, brown, blue, and gray spheres represent Pb, Br, N, and C atoms, respectively. Disordered atoms and hydrogen atoms omitted for clarity. (A) Adapted from ref 90. Copyright 2016 American Chemical Society. (inset of A, B) Adapted from ref 11. Copyright 2014 American Chemical Society.

The free-excitonic luminescence of n = 1 Pb−I perovskites has been studied since the late 1980s. Ishihara and colleagues reported strong narrow emission with a very small Stokes shift at room temperature, which becomes stronger and sharper upon cooling to cryogenic temperatures.[49] Similar excitonic photoluminescence is also observed for the analogous Pb−Br perovskites.[164] Narrow excitonic emission has also been reported for Sn-based perovskites, although here the emission is somewhat weaker, broader, and more Stokes shifted.[55,163] In the sections below, we highlight several approaches by which this narrow excitonic emission can be tuned.

6.1.1. Halide Substitution. The halide composition of Pb halide layered perovskites offers a simple method for tuning their excitonic emission. Chloride perovskites have the widest band gap due to the lower energy of the Cl 3p orbitals, which hybridize with Pb 6s orbitals to form the valence band. In the iodide perovskites, the higher-energy iodide 5p orbitals result in a higher-lying valence band and hence a smaller band gap (Figure 8B).[134,165] Work by Kitazawa first showed that the band gap and the excitonic emission of 2D Pb halide perovskites can be continuously tuned by preparing materials with mixed-halide compositions.[56,57,120] Notably, in the series of perovskites with the general formula $(PEA)_2PbBr_xI_{4-x}$ (PEA = phenethylammonium), the fwhm of the emission is significantly larger for the mixed-halide compositions (ca. 400 meV for x = 3) than for the pure end-members (ca. 70 meV for x = 0 and ca. 80 meV for x = 4). This emission broadening has been attributed to the random distribution of different halides in the inorganic layer, which leads to variation in the local environment felt by excitons.[120] This same phenomenon leads to broadening of the excitonic absorption feature (Figure 8A).[56,166] Similar results were found for the series of tin-based perovskites $(PEA)_2Sn(Br_xI_{4-x})$.[167] In the mixed Br/Cl perovskites, the emission undergoes a different evolution than in the Br/I perovskites. Rather than causing a continuous blue shift of the emission, chloride alloying introduces a broad, highly red-shifted emission.[57,168,169] This broad feature is similar to the emission observed from many pure layered Pb−Cl perovskites.[89,168,170]

6.1.2. Structural Distortion. Beyond elemental composition and connectivity, the photoluminescence of 2D halide perovskites is highly sensitive to subtle structural distortions of the inorganic lattice. These structural distortions are primarily dictated by the organic cation.[60,72,106] Mitzi and co-workers have investigated the effect of octahedral tilting and bond length variation on the optical properties of 2D perovskites by analyzing how these parameters affect their band structures (see section 4.2).[63] Octahedral tilting decreases the orbital overlap of antibonding Sn 5s and I 5p orbitals in the valence band (VB), energetically stabilizing the valence band maximum. At the same time, the previously nonbonding Sn 5p states at the conduction band minimum should be destabilized due to antibonding character introduced by mixing with I orbitals due to the structure's lower symmetry (Figure 12A,B). Significant octahedral tilting, therefore,

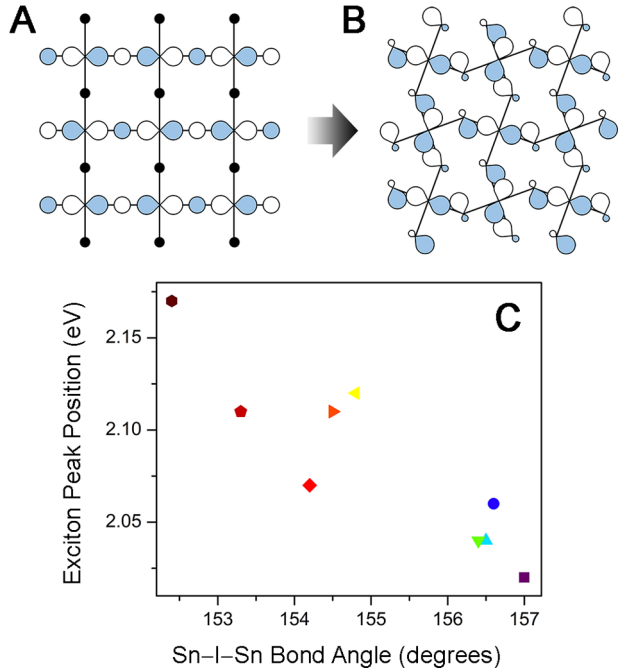

Figure 12. (A, B) Changes in orbital overlap resulting from distortion of the Sn−I−Sn in-plane bond angle. These changes introduce additional antibonding interactions at the conduction band minimum. (C) Exciton peak position as a function of Sn−I−Sn bond angle for a series of 2D Sn−I perovskites with organic layers consisting of phenethylammonium derivatives.[63] Adapted from ref 63. Copyright 2005 American Chemical Society.

increases the band gap of 2D Sn−X perovskites due to these combined effects. Variation of the in-plane Sn−I bond lengths is also expected to affect the band structure, with shorter bonds destabilizing the valence band maximum and decreasing the band gap.[63] Experimental band-gap estimates (assuming constant exciton binding energy and thus using the excitonic absorption energy as a proxy for the band gap) for a series of 2D Sn−I perovskites show a strong correlation between octahedral tilting and E_g, with increased tilting leading to a

DOI: 10.1021/acs.chemrev.8b00477
Chem. Rev. XXXX, XXX, XXX−XXX

band-gap blue shift (Figure 12C). Similarly, longer Sn−I equatorial bond lengths lead to a larger band gap, although here the changes in band gap are much smaller than those induced by octahedral tilting.[63] Prakash and co-workers performed a related study on 2D Pb−I perovskites, demonstrating how structural distortions of the inorganic lattice tune the emission wavelength of the material.[171]

Structural distortions of the inorganic lattice have also been proposed to influence the efficiency of excitonic emission in 2D lead halide perovskites. Asai and co-workers compared the photoluminescence quantum efficiencies (PLQEs) of the excitonic photoluminescence of three 2D Pb−Br perovskites, $(PEA)PbBr_4$, $(C_6H_5CH_2NH_3)_2PbBr_4$, and $(BA)_2PbBr_4$ (PEA = $C_6H_5(CH_2)_2NH_3^+$ and BA = $C_4H_9NH_3^+$). Among the materials measured, the perovskite $(PEA)_2PbBr_4$ has the highest PLQE of 22%.[172] They calculated similar nonradiative decay rates but substantially different radiative decay rates for the three perovskites, with faster radiative decay yielding more efficient emission. The authors rationalize these observations by examining structural distortions within the inorganic lattices. All three structures show significant octahedral tilting leading to deviations of the Pb−Br−Pb bond angles from linearity (151 and 152° for $(PEA)_2PbBr_4$, 150° for $(C_6H_5CH_2NH_3)_2PbBr_4$, and 155° for $(BA)_2PbBr_4$). In addition, the Pb−Br coordination sphere in $(PEA)_2PbBr_4$ shows significant deviations from ideal octahedral geometry while the octahedra in $(C_6H_5CH_2NH_3)_2PbBr_4$ and $(BA)_2PbBr_4$ are essentially undistorted.[172] As Mitzi and others have demonstrated, distortions such as these decrease orbital overlap, decreasing band dispersion in the distorted structures.[63,134] This decreased dispersion should yield a higher exciton effective mass, leading to a smaller exciton Bohr radius and a faster radiative decay rate in highly distorted structures.[172] Considering both octahedral tilting and octahedral distortion, $(PEA)_2PbBr_4$ is the most distorted of the three structures, while $(BA)_2PbBr_4$ is the least distorted. Thus, the differences in radiative decay rate and photoluminescence quantum efficiencies observed in this series of perovskites are consistent with structural distortions of the inorganic lattice induced by variation of the organic cation.[172]

6.1.3. Excited-State Coupling. Recent work has sought to understand how vibrational coupling in the excited state influences the optical properties of layered perovskites. At room temperature, the free-excitonic photoluminescence from typical 2D Pb−I perovskites, such as members of the $(C_nH_{2n+1}NH_3)_2PbI_4$ family or $(PEA)_2PbI_4$ (PEA = $C_6H_5(CH_2)_2NH_3^+$), appears as a single resonance, with some asymmetry owing to a low-energy tail.[10,69,135,136] At low temperatures, however, this resonance clearly splits into different components,[160] which have been varyingly attributed to the coexistence of free and bound excitons with phonon replicas, and free excitons and free biexcitons.[152] However, other work[10,135] more clearly implicates phonon replicas in the low-temperature peak splitting. At 10 K, Deleporte and colleagues observed two excitonic photoluminescence lines with a splitting of 14 meV (113 cm^{-1}), comparable to the longitudinal optical (LO) phonon energy of 13.7 meV (110 cm^{-1}) in the parent material PbI_2.[10] Kagan and colleagues observed a similar structuring of both the excitonic absorption and narrow photoluminescence in $(PEA)_2PbI_4$ accompanied by further peak splitting (Figure 13). They identify both the same 12−14 meV phonon replica and a higher-energy series with a splitting of ca. 40−43 meV (323−347 cm^{-1}), ascribed

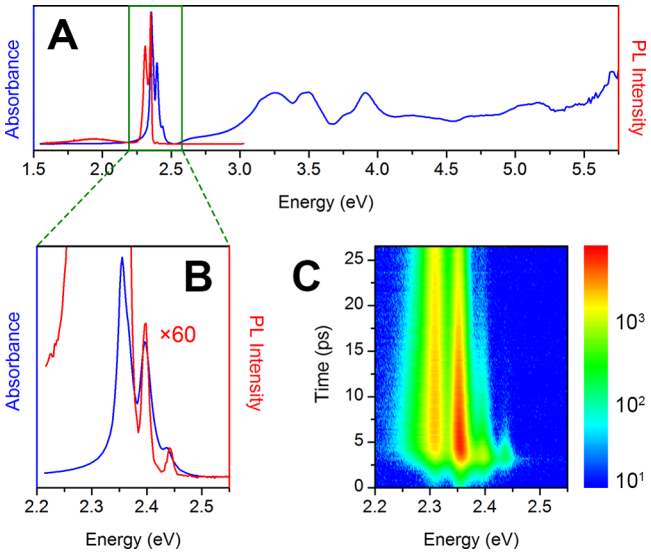

Figure 13. (A) Low-temperature (15 K) absorbance (blue) and photoluminescence (red) from a thin film of $(PEA)_2PbI_4$ (PEA = phenethylammonium). (B) Magnified view of the free-excitonic region of the absorbance and photoluminescence. The photoluminescence intensity is multiplied by 60 relative to (A) to highlight the fine structure. (C) Time-resolved excitonic photoluminescence in $(PEA)_2PbI_4$. Adapted from ref 135. Copyright 2016 American Chemical Society.

to phononic contributions from the phenethylammonium cation.[135] In a very different experiment, Rao and colleagues identify similar coupling of the excited state with vibrational modes using femtosecond time-resolved transient absorption spectroscopy.[136] They observe small-amplitude oscillations of photoinduced absorption and ground-state bleaching signals, whose Fourier transforms yield the energies of the coupled phonons, with major contributions arising from low-energy (<25 meV; <202 cm^{-1}) modes. These vibrational contributions will be important for understanding the relaxation pathways in these materials with the eventual goal of modulating the radiative recombination pathways by coupling excitations in the inorganic layers to vibrations in both the inorganic and organic layers.

6.2. Group 14 Perovskites with Thick ($1 < n < \infty$) Inorganic Layers

The value of n in the formula of layered perovskites counts the number of metal halide sheets per inorganic layer. For example, the formula for (001) perovskites is $A'_2A_{n-1}B_nX_{3n+1}$. The first reports[58] of the structures of layered lead halide perovskites with $n > 1$ by Thorn and co-workers coincided with the general rise of the group 14 layered perovskites in the 1990s. Despite the very early reports on their free-excitonic photo- and electroluminescence, as well as photoconductivity,[4] interest in the $n > 1$ layered Pb−I perovskites remained primarily academic until recently. Five years following the initial report of solar cells employing the 3D Pb−I perovskite $(CH_3NH_3)PbI_3$ as the absorber by Miyasaka and colleagues,[12] Karunadasa and colleagues reported the first solar cell based on a 2D perovskite absorber: $(C_6H_5(CH_2)_2NH_3)_2(CH_3NH_3)_2Pb_3I_{10}$ ($n = 3$).[3] Solar cells incorporating this absorber exhibited a power conversion efficiency of 4.7%. Importantly, this perovskite showed significantly enhanced moisture stability relative to the $n = \infty$ $(CH_3NH_3)PbI_3$, likely aided by the greater hydrophobicity of the phenethylammonium cations relative to

DOI: 10.1021/acs.chemrev.8b00477
Chem. Rev. XXXX, XXX, XXX−XXX

methylammonium and the higher-quality films of the 2D perovskite.[3,173] Although, unlike the single crystals, the films showed indications of several n values (see section 6.2.2), the higher-energy photoluminescence and higher open-circuit voltages obtained from the 2D perovskite cell (compared to devices with the 3D perovskite) showed the photovoltaic potential of 2D perovskite absorbers.[3] This spurred renewed interest and further development of these materials, with new understanding of their luminescence and utility for optoelectronic applications such as solar-cell absorbers, and light-emitting diodes (section 9.2) emerging over the past several years.

6.2.1. Luminescence. As the thickness of the lead halide inorganic layers in the $n > 1$ layered perovskites exerts control over both E_g and E_b, n also affects the observed photoluminescence. Despite lacking single-crystal structures, Thorn and colleagues observed excitonic absorption peaks at 430 and 450 nm of the putative $n = 2$ and $n = 3$ members of the $(C_9H_{19}NH_3)_2(CH_3NH_3)_{n-1}Pb_nBr_{3n+1}$ family, lower in energy than the peak at 393 nm observed for the pure $n = 1$ perovskite.[58] In the $(C_4H_9NH_3)_2(CH_3NH_3)_{n-1}Pb_nI_{3n+1}$ family, photoluminescence from single crystals red shifts with increasing n value, decreasing from 2.35 to 1.83 eV in the $n = 1$ and $n = 5$ members, respectively, with the emission from the $n = 5$ perovskite close to that of the $n = \infty$ $(CH_3NH_3)PbI_3$ at 1.60 eV (Figure 14).[86,109] Similar to their $n = 1$ homologues

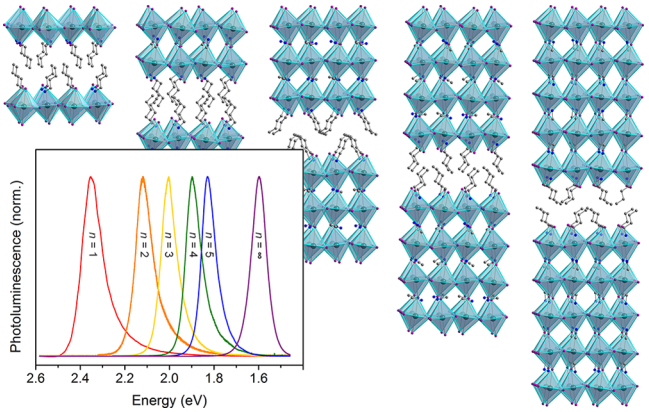

Figure 14. (left to right) Crystal structures of the $n = 1-5$ members of the $(C_4H_9NH_3)_2(CH_3NH_3)_{n-1}Pb_nI_{3n+1}$ perovskite family.[14,55,86,109] (inset) Photoluminescence obtained from single crystals of the $n = 1-5$ and ∞ members. Turquoise, purple, blue, and gray spheres represent Pb, I, N, and C atoms, respectively. Disordered atoms and hydrogen atoms omitted for clarity. (inset) Adapted with permission from ref 109. Copyright 2017 Cell Press.

(section 6.1.1), using more electronegative halides increases the band gap of $n > 1$ perovskites as well. In the mixed-halide $n = 3$ perovskite $(C_2H_5NH_3)_2(C_2H_5NH_3)_2Pb_3Cl_xBr_{10-x}$, increasing chloride content blue shifts the absorption onset energy from 2.75 to 3.45 eV. However, narrow light-blue photoluminescence is observed only in $(C_2H_5NH_3)_2(C_2H_5NH_3)_2Pb_3Br_{10}$, as chloride incorporation significantly broadens the emission (section 6.1.1).

6.2.2. Compositional Heterogeneity in Films. The first report of photo- and electroluminescence from single crystals of the $n = 2$ perovskite $(C_6H_5(CH_2)_2NH_3)_2(CH_3NH_3)Pb_2I_7$ by Ishihara and co-workers found that the luminescence was minimally Stokes shifted from the excitonic absorbance peak (E_{Stokes} < 20 meV, calculated from ref 4), suggesting free-excitonic recombination.[4] However, in thin films with the nominal composition and powder X-ray diffraction (PXRD) patterns corresponding to the $n = 3$ perovskite $(C_6H_5(CH_2)_2NH_3)_2(CH_3NH_3)_2Pb_3I_{10}$, the photoluminescence is significantly red-shifted with an estimated Stokes shift of ca. 0.4 eV.[3] Similar behavior was observed for thin films of $n > 1$ perovskites in the $(C_4H_9NH_3)_2(CH_3NH_3)_{n-1}Pb_nX_{3n+1}$ family as early as 1991,[58] contrasting sharply with the luminescence of single crystals.[174] Notably, this low-energy photoluminescence observed in films is still blue-shifted relative to the $n = \infty$ end-member (Figure 15), suggesting it does not arise from domains of pure $(CH_3NH_3)PbI_3$.[3] This relative blue shift (with respect to the 3D perovskite) holds for photo- and electroluminescence for thin films of layered perovskites with $n \geq 3$.[8]

In the first study of $n > 1$ layered lead halide perovskites, Thorn and co-workers remark on the difficulty of preparing phase-pure thin films of the $n = 2$ perovskite $(C_9H_{19}NH_3)_2(CH_3NH_3)Pb_2Br_7$. Transmission optical measurements of these films contain weak absorbance features at 390 and 530 nm, corresponding to the absorption onsets in $n = 1$ $(C_9H_{19}NH_3)_2PbBr_4$ and $n = \infty$ $(CH_3NH_3)PbBr_3$, respectively, which they ascribe to "imperfect self-assembly".[58] Optical measurements of thin films of the $n > 1$ layered Pb−I perovskites mimic this behavior, with the excitonic signatures of both higher and lower n values present in absorption spectra of films of $n = 3$ $(C_6H_5(CH_2)_2NH_3)_2(CH_3NH_3)_2Pb_3I_{10}$ (Figure 15A). The intensity of the excitonic absorption band increases with decreasing n owing to the higher oscillator strength of the excitonic transition in the lower n values. Karunadasa and colleagues attributed these additional features to "defect" layers, or local deviations from the nominal n value (deduced from the PXRD pattern) in films formed rapidly under kinetic control.[3] These features are reflected in the external quantum efficiency spectrum of a solar cell employing the $n = 3$ perovskite as an absorber, indicating that all these n-valued regions absorb light and contribute to photocurrent production (Figure 15A). The main photoluminescence peak from films of the $n = 3$ perovskite is red-shifted from its expected energy, indicating that carriers/excitons are funneling to regions with lower band gaps (attributed to higher n values) in the film.[3] A careful inspection of the photoluminescence spectra of the $n > 1$ films of layered Pb−I perovskites reveals this heterogeneity. In $(C_6H_5(CH_2)_2NH_3)_2(CH_3NH_3)_2Pb_3I_{10}$, a semilogarithmic plot of the photoluminescence intensity reveals weak features at higher energies, corresponding to luminescence from lower n values of the layered perovskite, suggesting that not all carriers migrate to the lower-band-gap regions with higher n values.[3]

An alternative explanation for the low-energy photoluminescence in $n > 1$ layered perovskite films was recently proposed by Mohite, Crochet, and colleagues, who examined the photoluminescence of exfoliated single crystals and thin films.[174] Most photoluminescence from exfoliated flakes of 2D Pb−I crystals appears narrow and free-excitonic (section 6.1). However, the edges of $n > 2$ layered perovskite flakes produce low-energy photoluminescence in confocal microphotoluminescence experiments that appears very similar to the low-energy feature that dominates the emission spectra of thin films. They attribute the low-energy feature to "layer-edge states", which they posit to be common in a thin film comprised of many small grains. The photoluminescence excitation (PLE) spectrum of the low-energy emission in an n

DOI: 10.1021/acs.chemrev.8b00477
Chem. Rev. XXXX, XXX, XXX−XXX

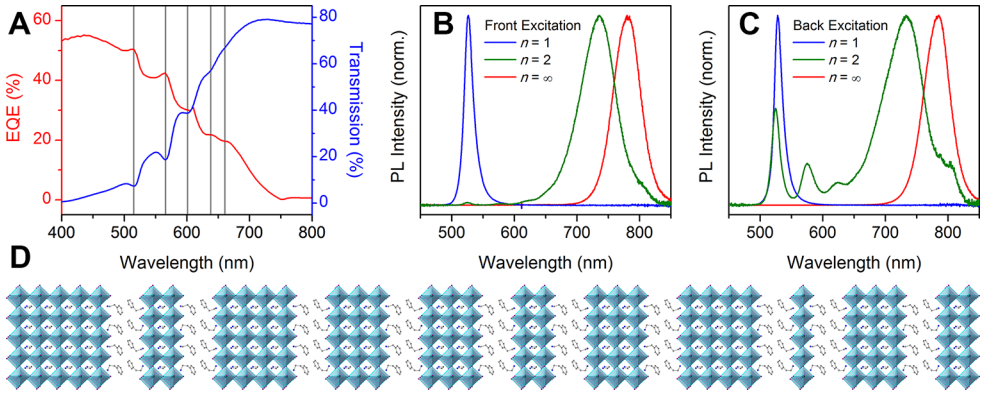

Figure 15. (A) External quantum efficiency (EQE; red) for a solar cell and transmission (blue) for a thin film containing the nominal n = 3 perovskite $(C_6H_5(CH_2)_2NH_3)_2(CH_3NH_3)_2Pb_3I_{10}$.[3] Gray lines highlight excitonic contributions from the n = 3 perovskite as well as "defect layers" with both higher and lower n values. Photoluminescence from thin films of the nominal n = 2 perovskite $(C_6H_5(CH_2)_2NH_3)_2(CH_3NH_3)Pb_2I_7$ exciting (B) the air-facing top surface and (C) the glass-facing back surface. (D) Schematic showing the presence of multiple different inorganic layers with varying thickness within a single film. Turquoise, purple, blue, and gray spheres represent Pb, I, N, and C atoms, respectively. Disordered atoms and hydrogen atoms omitted for clarity. (A) Adapted with permission from ref 3. Copyright 2014 John Wiley and Sons. (B, C) Adapted from ref 175. Copyright 2016 American Chemical Society.

= 3 perovskite flake shows no features below the absorption onset, identified in transmission optical measurements, so photons do not directly excite this state, instead first forming free excitons. This low-energy emission has a rise time of ca. 200 ps, suggesting the layer-edge states' population builds up more slowly than that of the photogenerated excitons. The authors attribute the mechanism of layer-edge-state formation to exciton dissociation to free carriers at the edges of the flakes, with energetic stabilization provided by a deep electronic trap state.[174] They further hypothesize that the low-energy photoluminescence of n > 1 perovskite films arises from similar exciton dissociation at grain boundaries. However, further study is required to connect the emission from films to that of exfoliated flakes.

6.2.3. Excited-State Dynamics. While carefully chosen single crystals provide a clear way to relate structure and optical properties in the n > 1 family of layered perovskites, most potential applications require thin films, thereby necessitating a deeper understanding of the role of compositional heterogeneity. Despite the potentially complex nature of this material system, general trends related to nominal n value, usually at least qualitatively follow chemical intuition such as absorption onset decreasing in energy[174] and carrier mobility[175] increasing with higher values of n. In contrast, Herz and colleagues demonstrated through optical pump–terahertz probe measurements that thin films of the nominally n = 3 member of $(C_6H_5(CH_2)_2NH_3)_2(CH_3NH_3)_{n-1}Pb_nI_{3n+1}$ have nearly double the effective mobility (11 $cm^2 \cdot V^{-1} \cdot s^{-1}$) compared to the n = 4 material (6 $cm^2 \cdot V^{-1} \cdot s^{-1}$). They attribute this surprising result to the change in film orientation with increased $C_6H_5(CH_2)_2NH_3^+$ content, corroborated by X-ray scattering. Owing to the anisotropic nature of charge transport in these layered materials, changing grain morphologies and thin film texturing leads to an anisotropic dependence on mobility not accounted for during pump–probe measurements.[175] Despite the highly local nature of terahertz-based mobility measurements, there is a large sensitivity to film processing, elegantly highlighting the difficulty of unraveling the fundamental role compositional heterogeneity plays in the n > 1 layered perovskites.

Herz and colleagues also observed that the optical properties of n > 1 films exhibit a dependence on the geometry of the excitation source. In films much thicker than the penetration depth of 3.1 eV light (<100 nm), the observed photoluminescence changes dramatically depending on whether the top or bottom of the film is excited (Figure 15B,C).[175] The bottom side of the film, which directly contacts the substrate, exhibits relatively less lower-energy photoluminescence and more higher-energy photoluminescence compared with the top side of the film. As the $C_6H_5(CH_2)_2NH_3^+$ cation is less soluble and bulkier than $CH_3NH_3^+$, during the spin-coating deposition process, lower n-values of the 2D Pb–I perovskite may precipitate first, followed by higher n-values that make up the top surface of the film,[175−177] adding a distinct spatial component to the film heterogeneity.

The combination of a distribution of n values within a given thin film (Figure 15D) coupled with the variation in E_g for those same n-valued domains enables the possibility of electronic communication between domains. Excited carriers/excitons in low n-valued domains may transfer to high n-valued domains, enhancing the observed low-energy photoluminescence. Transient absorption (TA) spectra of thin films of n > 1 layered perovskites with various different organic cations[8,9,176,177] exhibit clear photoinduced bleaching signals with maximum values at short time scales (≪1 ps). These bleach signals overlap with the excitonic peaks obtained from static absorption spectra,[9] indicating population of the different n-valued perovskite domains. However, at lower energies, comparable to those of the n = ∞ perovskite, a photoinduced bleach grows in intensity over much longer time scales (≫1 ps), suggesting slower transfer and population of the state that affords the lowest-energy photoluminescence. Recent work suggests that the organic cations can change the extent of this heterogeneity.[178]

Two proposed mechanisms for energy transfer between domains with different n values are exciton funneling, where excitons migrate from low-n (large band gap) to high-n (small band gap) regions,[8,9] and exciton ionization, where electrons and holes migrate to high and low values of n,[176,179] respectively. Both these arguments are based on the relative band offset and alignments of the different n values of the

DOI: 10.1021/acs.chemrev.8b00477
Chem. Rev. XXXX, XXX, XXX−XXX

perovskite, typically determined by ultraviolet photoelectron spectroscopy (UPS). Several different sets of UPS data support these differing mechanisms.[8,176,180] However, the exciton ionization arguments rely on significantly increased ionization energy and electron affinity[181] with increasing n. Given the simple dimensionality arguments of Umebayashi and colleagues (section 5.2.2), as well as the conflicting UPS data already present in the literature, further study is needed, such as through terahertz (THz) emission spectroscopy, to probe the proposed opposing motion of electrons and holes through thin films.[182]

Clearly, the family of $n > 1$ layered perovskites is still expanding, with great promise for applications in luminescence,[8,183] buoyed by their increased tunability, radiative efficiency, and moisture stability relative to their 3D congeners. The compositional and spatial heterogeneity of $n > 1$ perovskite films should be acknowledged. Although high-n-value regions tend to limit the photoluminescence energy of the film, they may offer certain advantages to their performance in optoelectronic applications such as improving carrier mobility, as initially suggested.[3] Recent strides in thin-film deposition have enabled the construction of efficient light-emitting diodes with both $n > 1$ layered Pb−I and Pb−Br perovskites (section 9.2) where the heterogeneity in the perovskite films is credited for improving device efficiency by funneling and concentrating the excitons to the higher-n-value regions.[8,9,184]

6.3. Rare-Earth Perovskites

The 2D perovskite $(C_4H_9NH_3)_2EuI_4$ reported by Mitzi and coworkers is the only known example of a 2D hybrid perovskite based on an f-block metal. The photoluminescence spectrum of this perovskite exhibits a single narrow resonance with an fwhm of 24 nm centered at 460 nm (Figure 16), reminiscent of

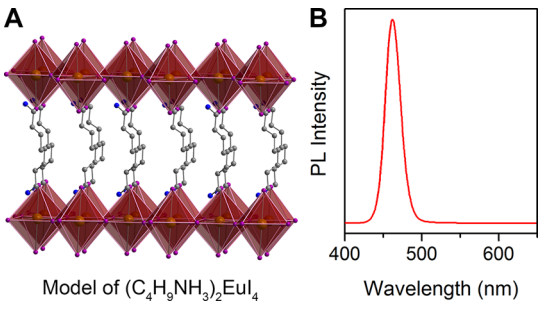

Figure 16. (A) Structural model and (B) photoluminescence of the perovskite $(BA)_2EuI_4$ (BA = butylammonium).[117] Orange, purple, blue, and gray spheres represent Eu, I, N, and C atoms, respectively. Disordered atoms and hydrogen atoms omitted for clarity. (B) Adapted from ref 117. Copyright 1997 American Chemical Society.

the excitonic emission of the Pb-based analogues.[117] This photoluminescence, however, is more similar to emission from the $4f^6 5d^1$ excited state to the $4f^7$ ground-state configuration of Eu^{2+} seen in EuI_2[185] and Eu^{2+}-doped alkali metal halides,[186] than excitonic recombination. Unlike in the lead halide perovskites, where excitonic emission blue shifts significantly with increasing quantum confinement (see section 5.2.2), the photoluminescence from this 2D Eu perovskite shows a slight red shift relative to the emission of its 3D parent perovskite $CsEuI_3$.[117] Whereas the excitons responsible for emission in 2D lead halide perovskites are strongly affected by the quantum and dielectric confinement imposed by the lattice structure (section 5.2), the strongly localized excited state in $(C_4H_9NH_3)_2EuI_4$ is relatively insensitive to its surroundings. For this reason, emission from $(C_4H_9NH_3)_2EuI_4$ is significantly more robust than that of the 2D lead halide perovskites. The more delocalized excitons in layered lead halide perovskites are susceptible to trapping at defects; therefore, excitonic photoluminescence is often quenched in low-quality samples, whereas the highly localized excitation in the Eu-based perovskite makes the emission far less dependent on sample quality.[117]

7. BROAD EMISSION

Much of the original interest in the layered lead halide perovskites stemmed from their narrow, free-excitonic photoluminescence,[19] studied since the late 1980s by Ishihara and colleagues,[49] with only occasional observations of Stokes-shifted luminescence.[152] One related example is an early report of weak, broad red photoluminescence from the 3D perovskite $CsPbCl_3$ at temperatures below ca. 200 K.[187] However, recent work has shown that broad Stokes-shifted luminescence may be a ubiquitous phenomenon in layered lead halide perovskites.[88] Most of the reports on broadband photoluminescence in the 2D perovskites implicate exciton self-trapping as the dominant emission mechanism (discussed in sections 7.1 and 7.2).[25] This is not the only mechanism for inducing broad photoluminescence: material defects and dopants (sections 7.3 and 7.6) can also broaden the emission, albeit with different operative photophysics. In this section, we also highlight several sets of perovskites based on non group 14 elements, which exhibit broad, non-free-excitonic luminescence (section 7.4).

7.1. White-Light-Emitting Perovskites

Because of the focus on understanding the narrow, free-excitonic emission (fwhm ca. 100 meV) with minimal Stokes shift (ca. 10 meV) from 2D perovskites,[88,164] white-light-emitting perovskites were not studied until 2014 by Karunadasa and colleagues.[11,89] Upon UV excitation, the inorganic layers of these perovskites emit continuously across the entire visible spectrum (spanning 400−700 nm), appearing white. This emission has a considerable Stokes shift (ca. 1 eV) and width (ca. 0.8 eV), leading to the intriguing question: how does a bulk material without obvious chromophores emit every color of visible light (section 7.2)?

7.1.1. (110) Perovskites with Corrugated Inorganic Layers. Most Pb perovskites feature flat (001) inorganic layers, and yield narrow, free-excitonic photoluminescence when excited by UV radiation (Figure 11).[88,164] However, upon UV excitation, the (110) perovskite (N-MEDA)$PbBr_4$ (N-MEDA = N^1-methylethane-1,2-diammonium) featuring corrugated inorganic layers emits broadband white light, i.e., a continuous emission from 400 to 700 nm (Figure 17).[11] This broad emission in (N-MEDA)$PbBr_4$ peaks at ca. 560 nm, with a high-energy shoulder, attributed to free-excitonic contributions,[90] at ca. 420 nm. This result was surprising, as the optical absorption spectra of this (110) perovskite and other (001) perovskites were very similar, yet their emission spectra were remarkably different (Figures 11 and 17). The emission color could be tuned through halide substitution, to afford both "warm" and "cold" white light with correlated color temperatures (CCTs) of 4669 and 6502 K, respectively. Increasing the chloride content in (N-MEDA)$PbBr_{4-x}Cl_x$ thus increased the CCT of the emission by blue-shifting the photo-

DOI: 10.1021/acs.chemrev.8b00477
Chem. Rev. XXXX, XXX, XXX−XXX

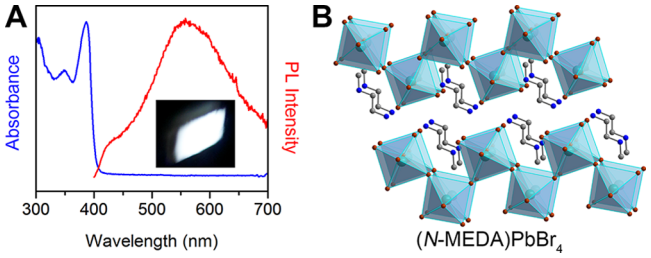

Figure 17. (A) Absorbance (blue) and photoluminescence (PL; red) and (B) crystal structure of the (110) perovskite (*N*-MEDA)-$PbBr_4$.[11,90] (inset) Photograph of (*N*-MEDA)$PbBr_4$ powder emitting white light under ultraviolet illumination. Turquoise, brown, blue, and gray spheres represent Pb, Br, N, and C atoms, respectively. Disordered atoms and hydrogen atoms omitted for clarity. (A) Adapted from ref 90. Copyright 2016 American Chemical Society. (A, inset) Adapted from ref 11. Copyright 2014 American Chemical Society.

luminescence. Chloride substitution also increased the phosphor's color-rendering index (CRI), a measure of a light source's ability to accurately reproduce illuminated colors (section 9.1), to 85. Commercial white-light sources for indoor illumination require CRI values greater than 80.[188] Chloride substitution also slightly increased the photoluminescence quantum yield (PLQE) from 0.5% in (*N*-MEDA)$PbBr_4$ to 1.5% in (*N*-MEDA)$PbBr_{2.8}Cl_{1.2}$. The second (110) white-light-emitting perovskite, (EDBE)$PbBr_4$ (EDBE = 2,2′-(ethylenedioxy)bis(ethylammonium); Figure 18A), exhibited a much higher PLQE of 9% for warm white light with a CRI of 84.[89] While chloride substitution (Figure 18B) tuned the broad photoluminescence without detriment to the PLQE, even low amounts of iodide incorporation in (EDBE)$PbBr_4$ quenched the broad component of the luminescence, consistent with (EDBE)PbI_4 showing a much narrower green emission.

Prior to the observation of white-light emission from (*N*-MEDA)$PbBr_4$ and (EDBE)$PbBr_4$, the emission of the (110) perovskite (API)$PbBr_4$ (API = 1-(3-ammoniopropyl)-1*H*-imidazol-3-ium) spanning 400−650 nm was reported as deep yellow.[189] In this study, the broad photoluminescence was attributed to a $\pi^*-\pi$ transition in the organic API^+ chromophore. However, this mechanism now seems unlikely owing to the similarity of the emission between (API)$PbBr_4$ and (110) perovskites containing simple aliphatic cations such as *N*-MEDA.[11] A recent report showed that the API^+ cation also templates a (110) Pb−Cl perovskite that emits broad white light,[190] in analogy with both the (110) Pb−Br and (001) Pb−Cl perovskites[89] (sections 7.1.1 and 7.1.2, respectively). While not strictly a (110) perovskite, *α*-(DMEN)$PbBr_4$ (DMEN = N^1,N^1-dimethylethane-1,2-diammonium), which has a larger corrugation repeat unit than a (110) perovskite (Figure 18D), was recently shown to emit cold white light at room temperature with a color rendering index of 73 (section 9.1.2; Table 5).[100]

Table 5. PLQE, CRI, and CIE Values for an Array of White-Light-Emitting Perovskites[a,b]

compound	ref	PLQE (%)	CRI	CIE (*x*, *y*)
(*N*-MEDA)$PbBr_4$	11	0.5	82	(0.36, 0.41)
(EDBE)$PbBr_4$	89	9	84	(0.39, 0.42)
(EDBE)$PbCl_4$	89	2	81	(0.33, 0.39)
α-$(DMEN)_2PbBr_4$	100	not reported	73	(0.28, 0.36)
(AEA)$PbBr_4$	88	not reported	87	(0.29, 0.34)
$(PEA)_2PbCl_4$	170	<1	84	(0.37, 0.42)
$(EA)_4Pb_3Cl_{10}$	168	not reported	66	(0.27, 0.39)
(API)$PbCl_4$	190	<1	93	(0.36, 0.37)
(MPenDA)$PbBr_4$	254	3.4	91	(0.24, 0.23)
(CyBMA)$PbBr_4$	194	1.5	not reported	(0.23, 0.29)

[a]Adapted from ref 25. Copyright 2018 American Chemical Society. [b]*N*-MEDA = N^1-methylethane-1,2-diammonium, EDBE = 2,2′-(ethylenedioxy)bis(ethylammonium), DMEN = N^1,N^1-dimethylethane-1,2-diammonium, AEA = 3-(2-ammonioethyl)anilinium, PEA = phenethylammonium, EA = ethylammonium, API = 1-(3-ammoniopropyl)-1*H*-imidazol-3-ium, MPenDA = 2-methyl-1,5-pentanediammonium, CyBMA = *cis*-1,3-bis(ammoniomethyl)-cyclohexane.

7.1.2. (001) Perovskites with Flat Inorganic Layers. The first example of a white-light-emitting (001) perovskite was (EDBE)$PbCl_4$ (Figure 18B).[89] The excitonic absorption and band gap are blue-shifted relative to the (110) perovskite (EDBE)$PbBr_4$, similar to the effects of halide substitution in (*N*-MEDA)$PbBr_{4-x}Cl_x$, and this material emits "cold" white light (section 9.1.2).[89] However, the PLQE, measured as 2%, was lower compared to (EDBE)$PbBr_4$. Boukheddaden and colleagues[191] subsequently synthesized the first white-light-emitting (001) Pb−Br perovskite $(C_6H_{11}NH_3)_2PbBr_4$, whose optical characteristics appeared very similar to those of both (EDBE)PbX_4 (X = Cl, Br) perovskites. They also observed quenching of the broad emission in $(C_6H_{11}NH_3)_2PbBr_{4-x}I_x$ with increasing iodide substitution,[192] although broad photoluminescence was observed at low temperature in $(C_6H_{11}NH_3)_2PbI_4$.[193] The highly distorted (001) perovskite (AEA)$PbBr_4$ (AEA = $^+H_3NC_6H_4(CH_2)_2NH_3^+$) emits white

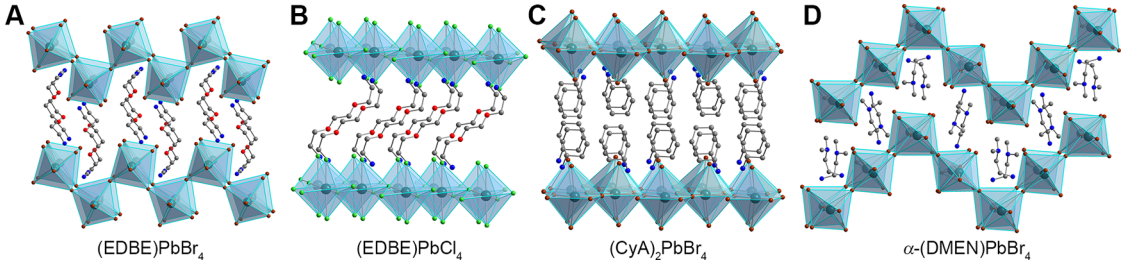

Figure 18. Crystal structures of selected white-light-emitting perovskites (A) (EDBE)$PbBr_4$ (EDBE = 2,2′-(ethylenedioxy)bis(ethylammonium),[89] (B) (EDBE)$PbCl_4$,[89] (C) $(CyA)_2PbBr_4$ (CyA = cyclohexylammonium),[76] and (D) *α*-(DMEN)$PbBr_4$ (DMEN = N^1,N^1-dimethylethane-1,2-diammonium).[100] Turquoise, brown, green, red, blue, and gray spheres represent Pb, Br, Cl, O, N, and C atoms, respectively. Disordered atoms and hydrogen atoms omitted for clarity.

DOI: 10.1021/acs.chemrev.8b00477
Chem. Rev. XXXX, XXX, XXX−XXX

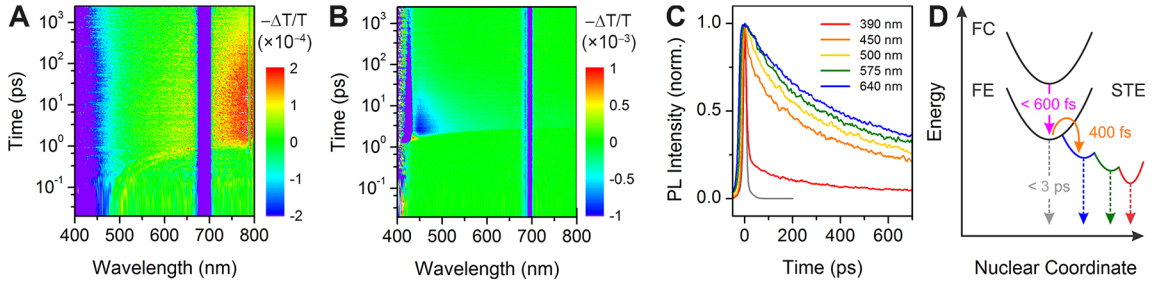

Figure 19. Transient absorbance of (A) the (110) perovskite (*N*-MEDA)$PbBr_4$ and (B) the (001) perovskite (*N*-MPDA)$PbBr_4$ upon excitation at 345 nm. Induced absorption and bleach features are shown in red and blue, respectively. The data at ca. 650−700 nm are masked owing to the laser excitation line. (C) Wavelength-dependent photoluminescence decay times for (*N*-MEDA)$PbBr_4$, with the instrument time resolution shown in gray. (D) Schematic of exciton self-trapping from the free carrier (FC) or free exciton (FE) state to a distribution of self-trapped states (STEs). Photoluminescence is shown with dotted arrows. Adapted from ref 90. Copyright 2016 American Chemical Society.

light at room temperature with a relatively high CRI of 87.[88] Further examples of white-light-emitting Pb−X (X = Br, Cl) perovskites are $(C_6H_5(CH_2)_2NH_3)_2PbCl_4$ and $(H_3NCH_2C_6H_{10}CH_2NH_3)PbBr_4$, both reported by Mathews and colleagues.[170,194] Kanatzidis and colleagues found that the $n = 3$ perovskite $(C_2H_5NH_3)_4Pb_3Cl_{10-x}Br_x$ emitted white light, where here too, the Cl:Br ratio tuned the emission color.[168] Notably, while only a few examples of (001) perovskites are white-light emitters at room temperature, Karunadasa and colleagues found that broad photoluminescence is in fact common to the entire family of (001) Pb−Br perovskites, although its appearance is highly temperature dependent (section 7.2.3).[88]

7.2. Proposed Mechanism of White-Light Emission

7.2.1. Electronic Origins of White-Light Emission. Self-trapping of free excitons is the proposed mechanism for white-light emission in layered Pb−X (X = Cl, Br) perovskites.[11,90] Following the initial proposal by Karunadasa and colleagues,[11] a number of mechanistic studies[88−90,191,192,194,195] sought to probe the origin of the broad photoluminescence in these materials. These spectroscopic, structural, and theoretical works continue to reinforce the viability of the exciton self-trapping hypothesis. Here, the exciton is trapped in a lattice deformation created through the interaction between the lattice and the exciton. Therefore, self-trapped excitons (described in sections 5.3.2 and 5.3.3) create transient, light-induced lattice deformations that can be considered as "excited-state" defects, in contrast to more permanent lattice defects such as vacancies and interstitials, which are maintained in the ground state as well. We refer to the latter as "permanent" in order to distinguish them from the transient self-trapped states, although these "permanent" defects may in some cases evolve with time, albeit much more slowly than the self-trapped states.

Mechanistic studies indicate that exciton self-trapping generates the broad Stokes-shifted emission (homogeneous emission broadening), while interaction between the self-trapped excitons and permanent lattice defects (extrinsic self-trapping; sections 5.3.2 and 5.3.3) causes heterogeneity in the excited state, further contributing to the emission width (inhomogeneous emission broadening).[89,90] The nature of the self-trapped states in these perovskites has not been experimentally identified, although the early reports invoked the possible analogy between self-trapping in Pb−Br perovskites and in $PbBr_2$.[89] In $PbBr_2$, the self-trapped species have been resolved using electron paramagnetic resonance.[154] Several computational papers have used approximations to study self-trapped species in lead halide perovskites (e.g., adding an electron/hole to the ground-state structure).[195,196] However, owing to the interrelation of the electron and hole, directly probing the self-trapped exciton though computation remains challenging, and experimental atomistic evidence of the structure of the self-trapped exciton remains a vital target for this field.

7.2.2. Mechanistic Insights. The absorbance spectra of films of the white-light-emitting (110) perovskite (*N*-MEDA)-$PbBr_4$ (Figure 17) and blue-light-emitting (001) perovskite (*N*-MPDA)$PbBr_4$ (*N*-MPDA = N^1-methylpropane-1,3-diammonium) (Figure 11) appear qualitatively similar. Both materials feature strong free-excitonic resonances and no below-exciton absorption, suggesting that similar excited states are initially populated in both materials. White-light emission from surface defect sites was discarded as a possibility as the photoluminescence quantum yield and spectral shape did not change considerably in (*N*-MEDA)$PbBr_4$ and (EDBE)$PbBr_4$ between thin films, micrometer-scale powders, or large single crystals.[11,89] Furthermore, the intensity of the observed white-light emission exhibits a linear dependence on excitation intensity. Near band-edge excitonic photoluminescence typically exhibits a linear or superlinear power dependence on excitation density, with donor−acceptor pair or carrier-trap-based recombination having a sublinear dependence.[197] While this model may not hold for highly localized excitations,[198] these results support the self-trapping hypothesis.

Cooling white-light-emitting Pb−X (X = Br, Cl) perovskites yields a significant increase in PLQE, with (EDBE)$PbBr_4$ exhibiting an estimated PLQE of ca. 85% at 105 K.[89] This increase in emission efficiency and narrowing of the broad photoluminescence with decreasing temperature are indicative of strong coupling between the electronic transition and lattice vibrations.[88,89] In (EDBE)$PbBr_4$, a fit of the temperature-dependent photoluminescence width yields the effective phonon frequency that couples to the electronic transition as 97 cm^{-1}, similar to the energy of the Pb−Br modes obtained from static Raman spectra. Although this estimate used a rough model, it implicates the inorganic layers in the emission process. Similar band shape analyses have previously been performed on the free-excitonic photoluminescence of the (001) Pb−I perovskite $(C_6H_5(CH_2)_2NH_3)_2PbI_4$,[10] and more recently for the broadened emission in the (111) perovskites such as $Cs_3Sb_2I_9$.[198]

Beyond static optical measurements, time-resolved spectroscopic experiments provided more conclusive evidence for self-

DOI: 10.1021/acs.chemrev.8b00477
Chem. Rev. XXXX, XXX, XXX−XXX

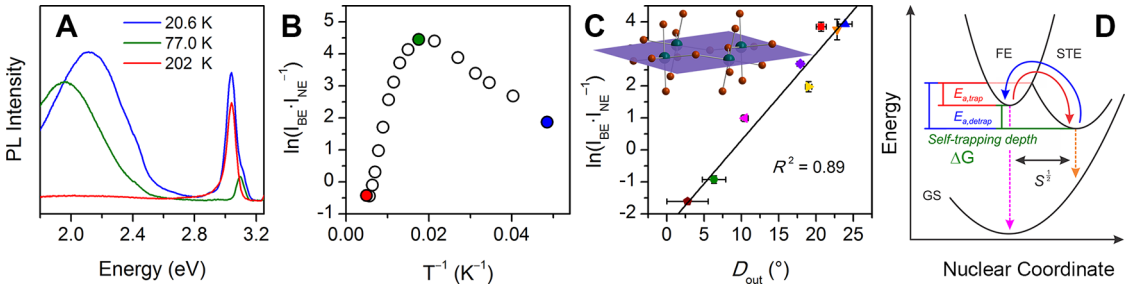

Figure 20. (A) Photoluminescence (PL) of the (001) perovskite (HIS)$PbBr_4$ (HIS = histammonium) showing both narrow (NE) and broad emission (BE). (B) Temperature-dependent ratio of integrated BE:NE intensity, $\ln(I_{BE}\cdot I_{NE}^{-1})$, for a single crystal of (HIS)$PbBr_4$. The colored symbols correspond to the PL spectra of the same colors in (A). (C) Correlation between $\ln(I_{BE}\cdot I_{NE}^{-1})$ at 80 K and out-of-plane distortion (D_{out}) for a series of (001) Pb−Br perovskites. (inset) A 2D perovskite fragment showing the plane of layer propagation. (D) Schematic of thermally activated exciton self-trapping (red arrow) and detrapping (blue arrow), where the activation energy barriers for trapping ($E_{a,trap}$) and detrapping ($E_{a,detrap}$) define the self-trapping depth (ΔG). S is the Huang−Rhys parameter that defines the distortion of the self-trapped state (STE) relative to the ground state (GS). FE is the free exciton state. PL is shown with dotted arrows. Reproduced with permission from ref 88. Copyright 2017 Royal Society of Chemistry.

trapping, as well as insight into the excited-state landscape of the (110) white-light-emitting perovskites. Using a suite of ultrafast optical measurements, Lindenberg, Karunadasa, and colleagues[90] probed the excited state of (*N*-MEDA)$PbBr_4$ across a range of time scales to understand the fate of the photogenerated carriers. In an optical pump−THz probe ultrafast spectroscopic measurement, exciting well above the band gap with 266 nm (4.66 eV) light produces free carriers that relax in <600 fs, determined by attenuation of the incident THz radiation. The THz probe is unattenuated by (*N*-MEDA)$PbBr_4$ when resonantly pumping the free-excitonic absorption at 387 nm (3.20 eV). Together, these observations are consistent with the formation of excitons on subpicosecond time scales. Transient absorbance data provide the most compelling evidence to date of self-trapping of these excitons in layered perovskites.[90] In perovskites with a narrow emission, such as the (001) perovskite $(C_4H_9NH_3)_2PbI_4$,[199] above-band-gap excitation generates a below-gap bleaching feature, indicating the filling of sub-band-gap trap states attributed to permanent lattice defects. A similar light-induced bleach is seen in the transient absorbance data for (*N*-MPDA)$PbBr_4$, which emits blue light (Figure 19B). In contrast, a broad photo-induced below-gap *absorption* spans much of the visible region in the transient absorption spectrum of (*N*-MEDA)$PbBr_4$ (Figure 19A), indicating the formation of new, transient electronic trap states upon photoexcitation, which were ascribed to exciton self-trapping.[90] Following the initial report, this transient absorption has also been observed in other white-light-emitting perovskites: (EDBE)PbX_4 (X = Br, Cl)[196] and $(PEA)_2PbCl_4$.[170]

In a pressed pellet of (*N*-MEDA)$PbBr_4$, the time-resolved photoluminescence lifetime of the white-light emission is less than 700 ps, although there is a significant wavelength dependence (Figure 19C). At the higher-energy, free-excitonic shoulder, the measured lifetime is limited by the time resolution of the experimental setup (~8 ps), with a small contribution from a very weak, longer-lived tail. Within the broad component of the emission, there is further wavelength dependence, with lower-energy states having longer emission lifetimes. This wavelength dependence of photoluminescence lifetime has also been observed in the (001) white-light-emitting perovskite $(C_6H_{11}NH_3)_2PbBr_4$,[191] and also in other systems that exhibit exciton self-trapping, such as Si nanocrystal/SiO_2 composites.[200,201] For (*N*-MEDA)$PbBr_4$, this wavelength dependence is attributed to a distribution of self-trapped sites, likely arising from extrinsic self-trapping, where permanent lattice defects modify the self-trapped sites. A similar wavelength dependence is observed for the photoluminescence rise time in (*N*-MEDA)$PbBr_4$, with the lower-energy photoluminescence rising more slowly compared to higher-energy emission. As the lower-energy photoluminescence is attributed to arise from more deeply self-trapped and distorted states, these states should take longer to form, or excitons may shuttle from lightly trapped to more deeply trapped states (Figure 19D).[90]

7.2.3. Structural Origins of White-Light Emission. Although there are scattered examples of (001) Pb−Br perovskites that emit white light at room temperature,[88,191] the vast majority exhibit narrow, free-excitonic luminescence under ambient conditions.[88] However, broad emission appears to be a general feature of 2D Pb−Br perovskites, modulated by a strong temperature dependence.[88] For example, the (001) perovskite (HIS)$PbBr_4$ (HIS = histammonium) exhibits narrow blue photoluminescence at room temperature, yet below ca. 200 K a broad, low-energy photoluminescence feature appears, which increases in intensity with further cooling. This low-temperature photoluminescence appears very similar to the white-light emission in other Pb−X (X = Br, Cl) perovskites, and it was therefore ascribed to exciton self-trapping (Figure 20A).[88] Furthermore, the ratio of integrated intensity between the broad, self-trapped (I_{BE}) and narrow, free-excitonic photoluminescence (I_{NE}) features in (HIS)$PbBr_4$, $I_{BE}\cdot I_{NE}^{-1}$, exhibits two distinct temperature-dependent regimes, similar to the (110) perovskite (*N*-MEDA)$PbBr_4$ (Figure 20B).[90] This coexistence of free and self-trapped excitonic states has also been observed in pyrene,[202−204] and a similar simplified energy diagram, wherein the free and self-trapped excitonic states are separated by an activation energy barrier, can be applied to the halide perovskites (Figure 20D). Here, the activation energy barrier for self-trapping ($E_{a,trap}$) is small and smaller than that for detrapping ($E_{a,detrap}$). As (HIS)$PbBr_4$ is cooled from room temperature, thermal energy becomes small relative to $E_{a,detrap}$, resulting in an increase in $I_{BE}\cdot I_{NE}^{-1}$. However, with further cooling, thermal energy will eventually become sufficiently small relative to $E_{a,trap}$, so excitons lack the energy to self-trap, potentially decreasing $I_{BE}\cdot I_{NE}^{-1}$, although contributions from temperature-independent effects such as tunneling to self-

DOI: 10.1021/acs.chemrev.8b00477
Chem. Rev. XXXX, XXX, XXX−XXX

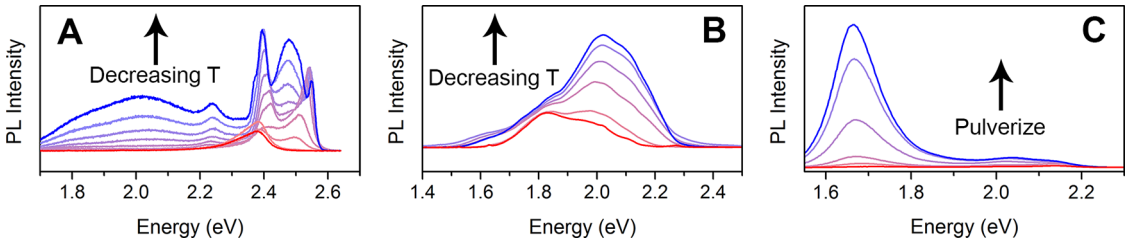

Figure 21. Temperature-dependent photoluminescence from (A) an exfoliated crystal of $(BA)_2PbI_4$ (BA = $C_4H_9NH_3^+$) and (B) from (FA)(GUA)PbI_4 (FA = $CH(NH_2)_2^+$; GUA = $C(NH_2)_3^+$). (C) Particle-size dependent photoluminescence from powders of $(MA)_2PbI_2(SCN)_2$ (MA = $CH_3NH_3^+$). (A) Adapted from ref 199. Copyright 2015 American Chemical Society. (B) Adapted from ref 101. Copyright 2018 American Chemical Society. (C) Adapted from ref 151. Copyright 2016 American Chemical Society.

trapped states can complicate this relationship.[203] The analogous temperature dependence of $I_{BE}{\cdot}I_{NE}^{-1}$ across a series of eight (001) Pb−Br perovskites implied the commonality of both the broad photoluminescence and this relationship between free and self-trapped excitonic states.

Notably, at any given temperature, the absolute value of $I_{BE}{\cdot}I_{NE}^{-1}$ varied considerably among different perovskites. Different organic cations template different structural distortions in the inorganic layers, revealed by single-crystal X-ray diffraction (SCXRD) (section 2.2.2).[62,63,72] These differences create subtle, yet important, changes in the electronic structure of the layered perovskites. Notably, the broad emission is thought to arise from sub-band-gap trap states generated from exciton self-trapping, instead of a band-edge transition. It thus need not reflect changes to the crystal/electronic structure in any systematic way. However, changes to the crystal structure can influence lattice deformability and the extent of exciton−lattice coupling.[88] Examining over 50 different structural parameters in the inorganic layers of eight (001) Pb−Br perovskites, Karunadasa and co-workers, therefore, looked for structural trends that correlated with the propensity to exhibit broad emission, quantified as $I_{BE}{\cdot}I_{NE}^{-1}$ (the ratio between the integrated intensity of the broad and narrow emissions). The tilt angle between adjacent octahedra (θ_{tilt}) may be decomposed into in-plane (θ_{in}) and out-of-plane projections (θ_{out}), where the plane is defined parallel to the inorganic layers (Figure 20C, inset). A significant positive correlation was found between $I_{BE}{\cdot}I_{NE}^{-1}$ at 80 K and the out-of-plane distortion of the inorganic sheets defined as $D_{out} = 180° - \theta_{out}$ (Figure 20C).[88] For all the other measured structural parameters, including bond lengths, bond angles, and deviations of the lead coordination sphere from octahedral symmetry (section 6.1.2), the correlations were much weaker.[88] Furthermore, the strongest correlation was observed for the largest measured value of D_{out}, rather than for the average value for crystal structures with multiple crystallographically unique Pb−(μ-Br)−Pb angles. This is consistent with exciton self-trapping, which is a highly localized phenomenon. Mitzi and co-workers have previously shown that the crystal structure reflects the band-gap energy of 2D perovskites, highlighting the correlation between θ_{tilt} and the excitonic absorption energy (and by extension the band gap).[63] Interestingly, although the broad emission is attributed to transient sub-band-gap trap states that form upon irradiation, the emission onset still shows a dependence on the bulk crystal structure.

The proposed thermally activated model for self-trapping (Figure 20D) yields a relationship between $I_{BE}{\cdot}I_{NE}^{-1}$ and the self-trapping depth (or the stabilization of the self-trapped state with respect to the free excitonic state: $\Delta G_{self\text{-}trap}$ ($=E_{a,trap} - E_{a,detrap} < 0$) given by the equation

$$\ln \frac{I_{BE}}{I_{NE}} \propto \ln \frac{k_{r,s}}{k_{r,f}} - \frac{\Delta G_{self\text{-}trap}}{k_B T}$$

where $k_{r,f}$ and $k_{r,s}$ are the radiative rate constants for free and self-trapped excitonic emission, respectively. When coupled with the structural correlation between D_{out} and $I_{BE}{\cdot}I_{NE}^{-1}$, it is apparent that increased distortion along D_{out} results in a greater propensity for self-trapping, suggesting that synthesizing (001) Pb−Br perovskites with pronounced out-of-plane distortions within the inorganic layer is a route toward new room-temperature white-light emitters.[88]

7.2.4. Structural Correlations with the Emission Width. Beyond the role of D_{out} in dictating the propensity for exciton self-trapping, other correlations between crystal structure and aspects of the broad emission have been sought. Several metrics describe deviations of a Pb−X octahedron from O_h symmetry, such as octahedral elongation (λ_{oct}), octahedral angle variance (σ_{oct}^2),[205] and bond-length distortion (Δ_{oct}).[206] De Angelis, Petrozza, and colleagues considered two perovskites and associated increased λ_{oct} and σ_{oct}^2 with photoluminescence broadening between the narrow green-light-emitting (001) perovskite $(C_4H_9NH_3)_2PbI_4$ and the slightly broader green-light-emitting (110) perovskite (EDBE)PbI_4.[207] A more recent work by Kanatzidis and colleagues considered three perovskites with corrugated inorganic layers that display broad photoluminescence and found a similar trend between increasing emission broadening and Δ_{oct}.[100] These initial studies are promising, and suggest a correlation between the local coordination environment of the lead and the emission width. However, the large variation in both structural and optical parameters even within a single family of layered perovskites means that a significant number of such materials are still required in order to articulate trends.

7.3. Broadened Emission from Lead Halide Perovskites

7.3.1. Layered Pb−I Perovskites: Emission from Defects. While all known examples of (110) Pb−Br perovskites display very broad (typically white) emission at room temperature, the same does not hold for (110) Pb−I perovskites.[89,208] For example, the (110) perovskite (EDBE)-PbI_4 (EDBE = 2,2′-(ethylenedioxy)bis(ethylammonium)) has a much narrower emission compared to the structurally analogous (EDBE)$PbBr_4$,[89] although the room-temperature emission of the (110) Pb−I perovskite is slightly broader than that of typical (001) Pb−I perovskites. Furthermore, incorporation of iodide into white-light-emitting Pb−Br 2D perovskites has been found to quench the broad emission.[89,192]

DOI: 10.1021/acs.chemrev.8b00477
Chem. Rev. XXXX, XXX, XXX−XXX

Nevertheless, there are multiple examples of broad emission from 2D Pb−I perovskites at or below room temperature, but the origin appears to differ from that of the Pb−Br perovskites.

There is substantial evidence that broad emission from Pb−I perovskites arises from traps resulting from permanent lattice defects. Using transient absorption measurements, Zhu and co-workers uncovered the presence of below-gap trap states in 3D $(CH_3NH_3)PbI_3$ films and in exfoliated crystals of the n = 1, 2, and 3 layered derivatives: $(C_4H_9NH_3)_2PbI_4$, $(C_4H_9NH_3)_2(CH_3NH_3)Pb_2I_7$, and $(C_4H_9NH_3)_2(CH_3NH_3)_2Pb_3I_{10}$.[199] Following above-gap photoexcitation at room temperature, a bleach signal appears in all four materials, significantly below the band gap, indicative of trap states in these perovskites, which can be populated by relaxation of hot carriers. This bleach signal grows in intensity from $n = \infty$ to n = 1 perovskites, leading Zhu and co-workers to suggest that the lower-n-value materials studied have a higher trap density, where the defects responsible for the traps are localized at the organic−inorganic interfaces.[199] At room temperature, no emission is observed from these midgap states, as the abundant thermal energy favors other recombination pathways. However, upon cooling below 150 K, carriers are trapped and recombine at these defects, resulting in broad photoluminescence for n = 1 $(C_4H_9NH_3)_2PbI_4$ centered at ∼2 eV (Figure 21A). Kagan and colleagues also observed similar broad photoluminescence in films of $(PEA)_2PbI_4$ (PEA = phenethylammonium) at low temperature. This broad emission has a strong dependence on film quality, supporting an origin from material defects.[135]

The n = 1 hexylammonium and dodecylammonium Pb−I perovskites also show broad, low-energy photoluminescence upon cooling below 200 K. However, unlike in the $(C_4H_9NH_3)_2(CH_3NH_3)_{n-1}Pb_nI_{3n+1}$ perovskites studied by Zhu, Deschler and co-workers remark on the absence of below-gap features in the room-temperature transient absorption spectra.[209] To explain the broad emission, the authors propose that photoexcitation creates permanent defects in the lattice. They propose that, at room temperature, there is sufficient thermal energy that these defects can be eliminated by ionic defect migration (i.e., defects migrate to grain boundaries or surfaces where they do not have the same impact on the optical properties) or defect recombination (where thermal energy permits spontaneous defect healing) mechanisms. However, as temperature decreases, these pathways are hindered by the lack of thermal energy, so the defects are trapped and mediate broad subgap emission. DFT calculations indicate that the most likely defects to be involved here are iodide interstitial and/or Frenkel defects, both of which are predicted to have relatively low formation energies and to induce deep trap states within the band gap.[209]

For the Pb−I perovskites mentioned above, broad emission does not emerge until the materials are cooled significantly below room temperature. Room-temperature broad emission has been observed, however, by Kovalenko and co-workers in the corrugated Pb−I hybrid bearing close relation to a perovskite: $(CH(NH_2)_2)(C(NH_2)_3)PbI_4$ (Figure 21B).[101] At room temperature, UV excitation induces broad red photoluminescence. Upon cooling to 78 K, this emission shows asymmetrical intensity growth, increases in width, and sharpens in places to more clearly reveal that the overall line shape is a convolution of multiple peaks. The authors propose that the shorter-lived high-energy portion of the emission arises from (near) band-edge excitons. Both defect-mediated recombination and self-trapping are suggested as possible explanations for the long-lived lower-energy emission, which is strongly affected by sample preparation method.[101]

7.3.2. An Attempt at Unifying the Mechanism of the Broad Emission from Pb−X Perovskites (X = Cl, Br, and I). Mechanistic studies show indications of transient, light-induced defects in Pb−Br perovskites that emit white light,[90] and permanent light-induced defects in Pb−I perovskites that exhibit a broad emission.[209] Some Pb−I perovskites also show indications of sub-band-gap trap states caused by material defects, even prior to illumination.[199] The dominant halide contribution to the valence band maximum means that a principal degradation pathway for halide perovskites under illumination is the evolution of halogen gas (as holes collect in primarily halide-based orbitals). Therefore, light stability is expected to increase from iodide, to bromide, to chloride perovskites. We can thus attempt to unify the separate observations for Pb−Cl, Pb−Br, and Pb−I perovskites by considering that the transient defects created through self-trapping can evolve into permanent material defects, as previously suggested.[88] This process is likely facile in iodide perovskites, and may require greater excitation fluences in bromide and chloride perovskites. This phenomenon is not new; self-trapping precedes the formation of permanent lattice defects in related materials, such as the formation of color centers (electron trapped in a halide vacancy) in alkali metal halides.[158]

7.3.3. Layered Pb−I−SCN Perovskites. The 2D perovskite $(CH_3NH_3)_2PbI_2(SCN)_2$ contains the pseudohalide ion thiocyanate (SCN^-),[122] and also exhibits room-temperature broad, low-energy photoluminescence of ambiguous origin. The intensity of this low-energy feature relative to several higher energy peaks (which are attributed to free excitonic photoluminescence) varies significantly depending on sample morphology and particle size.[151] The intensity of the higher-energy photoluminescence is much stronger in large single crystals, whereas the lower-energy photoluminescence dominates in films and grows in intensity as the crystalline material is pulverized to smaller particle size (Figure 21C). This observation suggests that the low-energy emission may arise from defects/surface sites. The energy of the lower-energy feature coincides with the emission energy of the 3D perovskite $(CH_3NH_3)PbI_3$. In fact, this 2D perovskite is very moisture sensitive and its decomposition product was identified as $(CH_3NH_3)PbI_3$.[151] Therefore, this low-energy emission may arise from an amorphous or very minor $(CH_3NH_3)PbI_3$ impurity,[151] although it does not display below-gap bleach signals in the room-temperature transient absorbance spectrum,[210] which are indicators of trap states caused by lower-band-gap impurities. Based on this and other observations, the low-energy emission has also been proposed to arise from radiative recombination of triplet excitons.[210] The low-energy emission evolves substantially with cooling and splits into multiple features, one of which is much broader than the original peak. These changes may be correlated with a structural phase transition in the material that occurs at ca. 170 K.[210]

7.4. Broadened Emission from Other Metal Halide Perovskites

7.4.1. Layered Double Perovskites. In contrast to the narrow, strong free-excitonic room-temperature emission of 2D lead perovskites, the n = 1 and 2 layered double perovskites

DOI: 10.1021/acs.chemrev.8b00477
Chem. Rev. XXXX, XXX, XXX−XXX

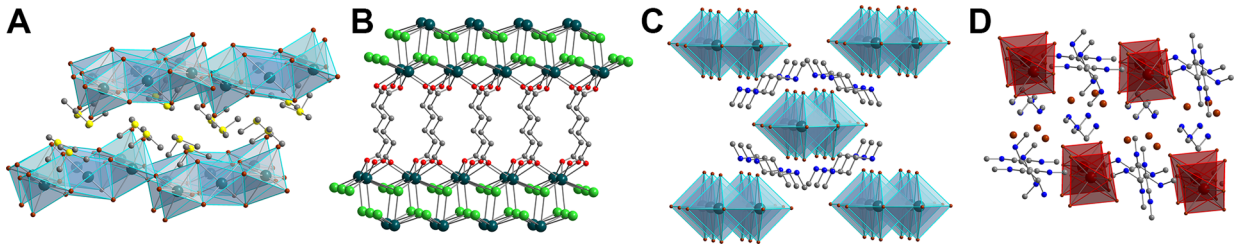

Figure 22. Crystal structures of non-perovskite metal halide hybrids featuring broad, room-temperature photoluminescence: (A) $(tms)_4Pb_3Br_{10}$ (tms = trimethylsulfonium),[227] (B) $(O_2C(CH_2)_4CO_2)Pb_2X_2$,[231] (C) (DMED)$PbBr_4$ (DMED = *N*,*N*′-dimethylethylenediammonium),[228] and (D) $(DMED)_4SnBr_6{\cdot}4Br$.[233] Turquoise, dark red, brown, light green, yellow, red, blue, and gray spheres represent Pb, Sn, Br, Cl, S, O, N, and C atoms, respectively. Disordered atoms and hydrogen atoms omitted for clarity. (A) Reprinted from ref 227. Copyright 2017 American Chemical Society.

$(C_4H_9NH_3)_4AgBiBr_8$ and $(C_4H_9NH_3)_2CsAgBiBr_7$, respectively, exhibit emission only at very low temperatures with significant broadening and increased Stokes shift compared to their Pb-based analogues. The sublinear dependence of the emission intensity on the excitation fluence in both double perovskites suggests a defect-mediated recombination pathway.[119] Most other examples of 2D double perovskites are not reported to be emissive.[108,118] Indeed, even most 3D double perovskites are not strong emitters.[211,212]

7.4.2. Layered Cd−Cl Perovskites. Broad photoluminescence has also been observed from several 2D Cd−Cl perovskites. Kamikawa and co-workers excited $(C_2H_5NH_3)_2CdCl_4$ just above the absorption onset at 5.9 eV, observing broad (fwhm ca. 0.69 eV), Stokes-shifted photoluminescence centered at 2.5 eV below ca. 50 K. They attribute this emission to exciton self-trapping.[213] In support of this assignment, Yoshinari and co-workers have shown that the exciton−phonon interaction in $(C_2H_5NH_3)_2CdCl_4$ is sufficiently strong to cause relaxation of free excitons to self-trapped states.[214] Here, the authors find that the absorption onset of $(C_2H_5NH_3)_2CdCl_4$ is well described by the Urbach rule over a wide range of temperatures (100−440 K). Based on this, they extract the exciton−phonon coupling constant (g) of the material, finding that g = 2.1.[214] This value is well above the critical value of g required for exciton self-trapping, as determined by Schreiber and Toyozawa,[215] supporting the proposal that the broad emission observed from these layered Cd−Cl materials arises from self-trapped excitons. Saparov and co-workers recently reported similar broad (fwhm ca. 0.81 eV), Stokes-shifted emission centered at 2.2 eV from the analogous perovskite $(CH_3NH_3)_2CdCl_4$.[216] However, in this case below-band-gap excitation led to room-temperature broad emission, suggesting a different emission mechanism.

7.4.3. Layered Ge−I Perovskites. Perhaps due to the instability of Ge^{2+} to oxidation,[173,217] these perovskites are still relatively unexplored, and as a result, little is known about their luminescence. In early work by Mitzi,[55] photoluminescence from $(C_4H_9NH_3)_2GeI_4$ was observed centered at 690 nm with a fwhm of ca. 180 nm at room temperature. Notably, this photoluminescence was weaker, broader, and more red-shifted than photoluminescence from the analogous Pb and Sn materials, and the intensity and peak location varied, depending on sample preparation method, suggesting the importance of defects in modulating the emissive properties.[55] Han and co-workers recently reported similarly broad emission from $(PEA)_2GeI_4$ (PEA = phenethylammonium) centered at 630 nm with a fwhm of ca. 140 nm (calculated from ref 217) and nanosecond emission lifetimes.[217]

7.4.4. Layered Mn−X Perovskites. The magnetic properties of the 2D Mn^{2+} perovskites have attracted a great deal of interest,[45,115,218] but these 2D antiferromagnets also display interesting luminescence properties. At very low temperatures (ca. 5 K), Rb_2MnCl_4 displays broad photoluminescence centered at 2 eV.[219−222] This emission is similar to that of other Mn^{2+} salts, including the n = 2 perovskite $Rb_3Mn_2Cl_7$,[219−222] and is attributed to the Laporte forbidden $^4T_1 \rightarrow {}^6A_1$ transition of Mn^{2+} ions.[220−222] With increasing temperature, exchange coupling between Mn^{2+} centers enables efficient excitation transfer between Mn sites and energy can migrate through the lattice. As a result, the intrinsic Mn^{2+} luminescence feature decreases in intensity with increasing temperature and the emission develops a longer-lived low-energy tail.[221] This decline in intensity has been attributed to excitation transfer to deep nonradiative trap states resulting from extrinsic dopants, such as Ni^{2+} or Fe^{2+}, while the tail emission may arise due to excitation transfer to Mn^{2+} sites, which are slightly perturbed by nearby impurities such as Zn^{2+}, Ca^{2+}, or Mg^{2+} and act as shallow radiative traps.[221] This thermally activated excitation transfer has also been probed by doping the Mn^{2+} lattice with luminescent rare earth ions such as Er^{3+} and Ho^{3+}. At low temperature, intrinsic Mn^{2+} emission, identical to that of the undoped material, is observed but is replaced by strong emission from rare earth ions as excitation transfer becomes more efficient at higher temperature.[220,222] It is worth noting that a similar temperature dependence of the broad, intrinsic Mn^{2+} emission has been observed in a wide array of Mn^{2+} salts including MnF_2,[223] $((CH_3)_4N)MnCl_3$,[224] and $CsMnBr_3$.[220] In all of these materials, excitation transfer is found to be a thermally activated process, though the temperature at which transfer becomes efficient varies widely. Interestingly, energy transfer in Rb_2MnCl_4 is observed even at 6 K, indicating a small activation energy in this material compared to $CsMnCl_3$, for example, where energy transfer is barely observable below 50 K.[222]

Emission from the Laporte forbidden $^4T_1 \rightarrow {}^6A_1$ transition of Mn^{2+} ions has also been observed more recently in the mixed-metal (111) perovskite $Cs_4MnSb_2Cl_{12}$. This emission, centered at 605 nm, is rapidly quenched by incorporation of Cu^{2+} ions into the lattice at the Mn^{2+} site.[127]

7.4.5. (111) Perovskites with Trivalent Metals. At room temperature, the (111) perovskites $Cs_3Sb_2I_9$ and $Rb_3Sb_2I_9$ exhibit broad photoluminescence that reaches maximum intensity at ca. 1.95 eV.[198] However, unlike the broad, highly Stokes-shifted emission observed in the Pb−X (X = Br, Cl) perovskites, this emission is narrower (ca. 300−400 meV) and has a much smaller Stokes shift (ca. <0.2 eV) at room temperature.

DOI: 10.1021/acs.chemrev.8b00477
Chem. Rev. XXXX, XXX, XXX−XXX

7.5. Broad Emission from Low-Dimensional Non-Perovskite Lattices

Beyond the relatively narrow confines of layered lead halide perovskites and their close relatives containing sheets of corner-sharing metal halide octahedra, there exists the much wider family of metal halide hybrids with edge- and face-sharing connectivity as well as lower dimensionality. Many of these materials emit broad, Stokes-shifted photoluminescence upon UV photoexcitation, although early work studied such photoluminescence only at low temperatures.[225] After the realization of perovskite lattices that emit white light under ambient conditions,[11,89] further lead halide hybrids exhibiting room-temperature broad photoluminescence followed. These include materials with 3D,[226] 2D,[227] 1D,[228−230] and 0D[227] inorganic topologies. In one family, the organic component is based on sulfonium rather than ammonium cations (Figure 22A),[227] and in another family the organic component is an anionic carboxylate (Figure 22B),[231,232] further expanding the potential phase space of these phosphors. The sulfonium hybrids display a particularly large Stokes shift of 1.7 eV, affording near-IR emission upon UV excitation. Notably, single crystals of the 1D hybrid $(H_3CNH_2(CH_2)_2NH_2CH_3)PbBr_4$ have a reported PLQE of 20%, the highest for lead halide white-light emitters (Figure 22C).[228] Expanding even further afield from lead halide perovskites offers more opportunities for realizing broad emission, with 0D Sn^{II}- and Sb^{III}-based complexes exhibiting yellow emission with PLQEs of 95 and 98%, respectively (Figure 22D).[233] Using dicarboxylates in place of amines templates cationic white-light-emitting Pb−X (X = F, Cl, Br) motifs with high chemical and thermal stability.[231,232] While the overall field of metal halide hybrids displaying broad photoluminescence remains less developed than that of perovskites, many promising avenues have recently opened for exploration.

7.6. Broad Emission from Dopants

Inclusion of emissive dopants into a host lattice is a well-explored method for obtaining broad photoluminescence. Although metal oxides and nitrides are the most well studied host lattices,[188,234] halide perovskites have also been explored for housing extrinsic emissive dopants.

7.6.1. Mn^{II} Dopants. One of the most studied extrinsic dopants in the group 14 perovskites[235−237] is Mn^{2+}. When introduced into nanocrystals of the 3D perovskite $CsPbX_3$ (X = Cl, Br), Mn^{2+} yields broad yellow-orange photoluminescence, which has been attributed to the forbidden $^4T_1 \rightarrow {}^6A_1$ d−d transition within the dopant Mn^{2+} ions (Figure 23B),[236,237] similar to the emission observed from many bulk Mn^{2+} materials (section 7.4.4). Kundu and co-workers demonstrated incorporation of Mn^{2+} at the B site of the 2D lead bromide perovskite $(C_4H_9NH_3)_2Pb_{1-x}Mn_xBr_4$.[238] Here, Mn^{2+} doping leads to nearly complete quenching of the blue excitonic photoluminescence and introduces a long-lived, broad luminescence feature at ca. 600 nm (Figure 23A). Importantly, the photoluminescence excitation (PLE) spectrum of this broad emission is very similar to the PLE spectrum of the excitonic emission feature, indicating that emission from the dopant Mn^{2+} ions arises through excitation transfer from the exciton in the Pb−Br lattice to Mn^{2+}.[238]

The 2D perovskite structure has two important effects on the emission from Mn^{2+} dopants. First, the quantum confinement imposed by the n = 1 lattice is crucial for establishing strong exchange coupling between excitons in the host material and the d-electrons of Mn^{2+}, leading to efficient energy transfer and strong emission (PLQE = 37%).[238,239] Similar PLQEs can only be achieved in 3D $CsPbX_3$ (X = Cl, Br) perovskites by nanostructuring.[236,237] Thus, the self-assembled quantum-well structure of $(C_4H_9NH_3)_2PbBr_4$ allows for efficient host-to-dopant energy transfer in a bulk material. Second, the 2D perovskite structure imparts greater stability to the broad emission, relative to 3D analogues. Exposure to conditions that essentially destroy the broad photoluminescence in Mn^{2+}-doped $CsPbCl_3$ have little effect on the emission in the 2D perovskite.[238] Thus, 2D perovskites may serve as more suitable hosts in future applications of this efficient, Stokes-shifted dopant-induced emission.

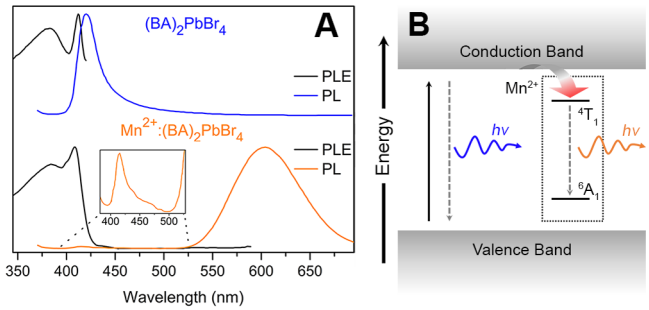

Figure 23. (A) Photoluminescence (PL) and photoluminescence excitation (PLE) spectra for the undoped perovskite $(BA)_2PbBr_4$ (BA = butylammonium) and Mn^{2+}-doped $(BA)_2PbBr_4$. (B) Simplified energy diagram for excitation transfer from the host perovskite to the Mn^{2+} dopant ions. (A) Adapted from ref 238. Copyright 2017 American Chemical Society.

7.6.2. Bi^{III} Dopants. Unlike for homovalent doping of Mn^{2+} for Pb^{2+}, where the resultant emission is similar between 3D and 2D Pb halide perovskites, the aliovalent Bi^{3+} dopant results in somewhat different photoluminescence. Song, Sun and co-workers reported that, upon doping with Bi^{3+}, the band-edge emission of the 3D perovskite $(CH_3NH_3)PbI_3$ is quenched and a new, broad (fwhm of 380 nm) luminescence feature is observed at much lower energy (ca. 1140 nm; 1.1 eV).[240] This lower-energy emission was attributed to structural defects introduced to the perovskite lattice by Bi^{3+} doping.[240,241]

In the 2D perovskite $(PEA)_2PbI_4$ (PEA = phenethylammonium), Ishihara and co-workers previously found that the intrinsic emission from free and bound excitonic states is not quenched by Bi^{3+} doping.[152] As observed in the case of $(CH_3NH_3)PbI_3$, a broad, low-energy photoluminescence feature is observed in the doped material at ca. 890 nm (ca. 1.4 eV). A new feature also appears in the absorption spectrum of Bi^{3+}-doped $(PEA)_2PbI_4$ at 2.15 eV, lower in energy than the excitonic absorption of the undoped material (2.36 eV). The authors attribute this feature to excitons bound to Bi^{3+} ions with a binding energy of 210 meV (relative to the energy of a free exciton). This feature appears in the photoluminescence excitation spectrum of the low-energy emission, suggesting that the broad luminescence arises due to Bi-bound excitons.[152] Intriguingly, the authors also present evidence that Bi^{3+} dopants introduce narrow, high-energy emission in the 2D perovskite. Under intense excitation, a photoluminescence feature is observed at 2.51 eV, higher in energy than the free excitonic emission (2.35 eV). This emission displays a superlinear dependence on laser power but shows saturation at the highest excitation intensities. Based on these

DOI: 10.1021/acs.chemrev.8b00477
Chem. Rev. XXXX, XXX, XXX−XXX

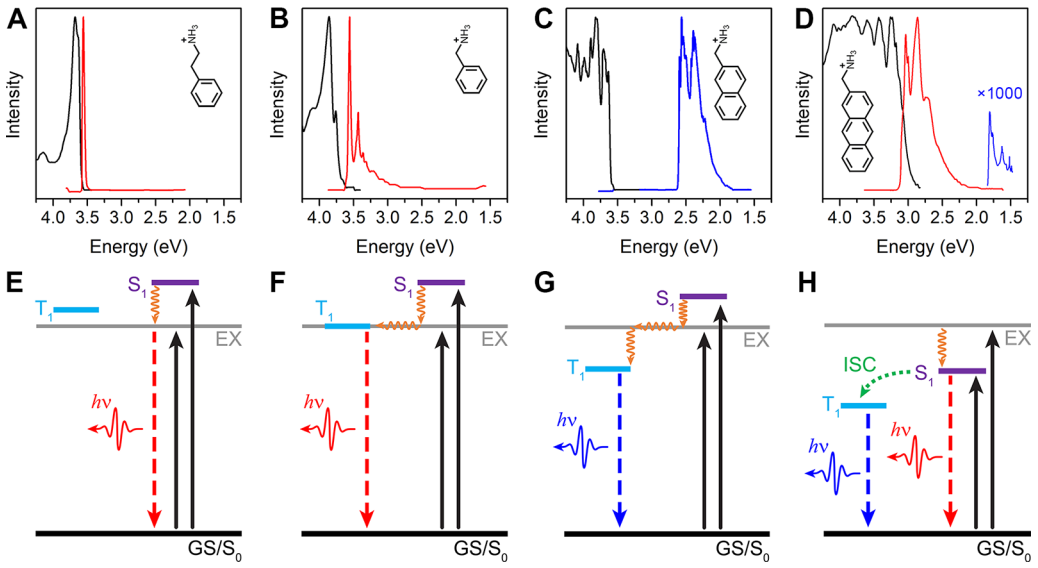

Figure 24. Low-temperature photoluminescence (red, blue) and photoluminescence excitation spectra (black) for (A) $(PEA)_2PbCl_4$ (PEA = phenethylammonium), (B) $(BZA)_2PbCl_4$ (BZA = benzylammonium), (C) $(NAPH)_2PbCl_4$ (NAPH = 2-naphthylmethylammonium), and (D) $(ANTH)_2PbCl_4$ (ANTH = 2-anthrylmethylammonium). Energy level schematics showing relaxation and recombination pathways in (E) $(PEA)_2PbCl_4$, (F) $(BZA)_2PbCl_4$, (G) $(NAPH)_2PbCl_4$, and (H) $(ANTH)_2PbCl_4$. Adapted with permission from ref 243. Copyright 1999 Elsevier.

observations, this feature is attributed to emission of biexcitons bound to Bi^{3+} sites.[152]

8. EMISSION FROM THE ORGANIC LAYER

While the diverse luminescence properties of 2D halide perovskites primarily stem from the inorganic sublattice, an even wider array of emissive materials may be accessed by coupling the luminescent properties of the inorganic sublattice to those of organic chromophores. For example, the templating effect of the inorganic sheet on the packing of the organic cations can have significant consequences, such as obviating nonradiative quenching mechanisms, while varying the energy levels of the organic and inorganic components can enable charge transfer across the organic−inorganic interface, opening several excitation and emission pathways.

A wide range of organoammonium cations containing naphthalene,[242] azobenzene,[242] anthracene,[243] pyrene,[244] thiophene derivatives,[61,245] *p*-terphenyl,[246] and other groups[125,243,247] have been incorporated into layered perovskites. While the range of organic chromophores that can be incorporated is restricted by the steric limitations of the framework, Era and Shimizu demonstrated some ability to navigate this obstacle, incorporating a bulky propylammonium-functionalized carbazole chromophore into a layered perovskite by mixing this large molecule with smaller propylammonium cations.[125]

8.1. Weak Coupling between Organic and Inorganic Layers

Incorporation of chromophores into hybrid perovskites generally leads to emission not observed in the analogous perovskite prepared with an optically inactive organic cation. In the simplest case, the chromophore-containing perovskite displays an emission profile that is simply a sum of the luminescence spectra of the individual components, indicating no interaction between excitations in the inorganic and organic sublattices. For example, Cortecchia and co-workers have shown that near-UV/blue photoluminescence can be achieved in a 2D Cu−Cl perovskite with 4,4′-(1,1′-biphenyl-4,4′-diyldioxy)dianiline in the organic layer. The emission spectrum of the hybrid perovskite is very similar to that of the HCl salt of the amine, and the photoluminescence excitation spectrum indicates that this emission arises only from the organic chromophore. As expected, no emission is observed from the Cu−Cl framework, similar to other Cu−Cl perovskites.[247]

8.2. Strong Coupling between Organic and Inorganic Layers

Strong coupling between the excited states of the organic and inorganic layers results in emissive properties that cannot be achieved with either component alone. In these cases, the energy of excitons formed in the inorganic lattice is transferred to a lower-lying empty state of a nearby chromophore, leading to emission from the organic molecule.

The emission profile of such chromophore-containing perovskites depends strongly on the excited state of the organic molecule that acts as the acceptor in the energy-transfer process. As a result, the luminescence can be tuned by controlling the energy of the chromophore's excited states relative to the excitonic band of the inorganic lattice. Wolf and co-workers have beautifully demonstrated this principle using a series of four Pb−Cl perovskites containing 2-anthrylmethyl-, 2-naphthylmethyl-, phenethyl-, and benzylammonium cations (Figure 24).[243] In the phenethylammonium perovskite, the excitonic state is lower in energy than both the singlet and triplet excited states of the chromophore (Figure 24A). With no lower-lying organic acceptor state for energy transfer, the excitons in the Pb−Cl layers radiatively recombine, leading to a typical 2D Pb−Cl perovskite emission spectrum. When anthracene is incorporated into the perovskite, the exciton's energy can be transferred to the lower-lying singlet state of the organic chromophore, resulting in strong fluorescent emission and a much weaker phosphorescence through intersystem crossing within the anthracene (Figure 24D). The singlet and triplet energy levels of naphthalene bracket the excitonic state (Figure 24C), and consequently, in the naphthalene perovskite, energy transfer occurs from the exciton to the triplet state of the organic chromophore, affording strong phosphorescence

DOI: 10.1021/acs.chemrev.8b00477
Chem. Rev. XXXX, XXX, XXX−XXX

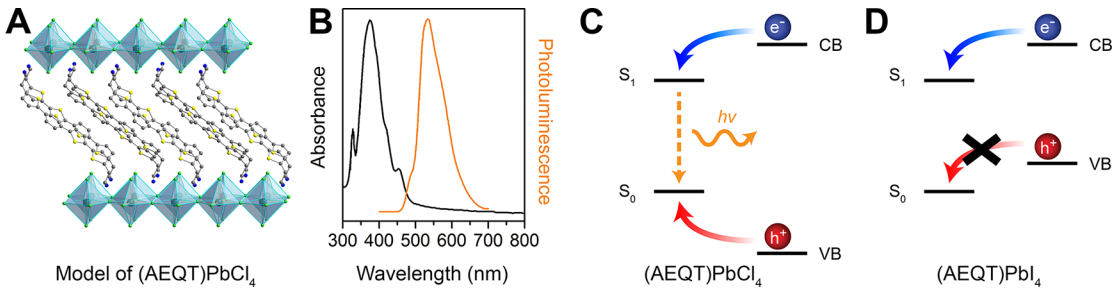

Figure 25. (A) Model of the crystal structure of $(AEQT)PbCl_4$ (AEQT = 5,5‴-bis(ethylammonium)-2,2′:5′,2″:5″,2‴-quaterthiophene). (B) Room-temperature absorbance (black) and photoluminescence (orange) spectra of a thin film of $(AEQT)PbCl_4$. Energy level schematics showing relaxation and recombination pathways in (C) $(AEQT)PbCl_4$ and (D) $(AEQT)PbI_4$. Turquoise, green, yellow, blue, and gray spheres represent Pb, Cl, S, N, and C atoms, respectively. Disordered atoms and hydrogen atoms omitted for clarity. (B–D) Adapted from ref 61. Copyright 1999 American Chemical Society.

from naphthalene. Finally, in the case of benzylamine, the exciton lies at the same energy as the triplet state of the chromophore (Figure 24B). Energy is transferred from the excitonic state to the triplet state of benzylamine but, due to the resonant interaction between the two levels, phosphorescent emission from the chromophore decays with a much shorter lifetime (30 ms) than observed in the isolated compound (6 s).[243]

8.3. Mechanism of Energy Transfer

Achieving efficient energy transfer from excitons within the inorganic lattice to the chromophores composing the organic layers should require proximity of the two components. Era and co-workers have demonstrated this by preparing Pb–Br perovskites from a series of alkylammonium-linked naphthalene molecules, varying the length of the alkyl chain in order to alter the distance of the chromophore from the Pb–Br sheets.[248] Each perovskite exhibited phosphorescence from naphthalene due to excitonic energy transfer to the triplet state, as described above. However, the perovskites formed from naphthalene derivatives with longer alkyl chains also showed excitonic emission from the Pb–Br layers, indicating that energy transfer becomes less efficient as the chromophore is moved further from the inorganic lattice.[248]

This result could be explained by either a Förster resonance energy transfer (FRET) mechanism or a Dexter charge transfer mechanism. FRET, which proceeds through nonradiative dipole–dipole coupling between a donor in an excited state and acceptor, decreases as r^{-6}, where r is the distance between donor and acceptor.[249] Dexter charge transfer involves nonradiative electron transfer from the donor to the acceptor and decreases exponentially with r.[250] Using a similar set of alkyl-linked naphthalene chromophores, Ema and co-workers demonstrated that the energy transfer rate between triplet excitons in the Pb–Br sheets and the triplet state of naphthalene has an exponential dependence on the distance of the chromophore from the inorganic sheet, pointing to a Dexter-type mechanism.[251] Thus, by controlling the distance of the chromophore from the inorganic perovskite sheets, the ratio of the broader, long-lived, phosphorescent emission to the narrow, fluorescent, excitonic emission can be varied in a predictable fashion.

8.4. Effects of the Inorganic Lattice

Although the chromophore-based photoluminescence generally arises from the organic layer, chemists can exert considerable control over this emission by tuning the templating inorganic framework.

8.4.1. Packing Effects. The packing arrangement of organic chromophores, templated by the inorganic sublattice, can have a significant impact on their emission profile. A particularly interesting case of this phenomenon was found by Wolf and co-workers in comparing the emissions of the X = Cl and Br analogues of $(pyrene\text{-}methylammonium)_2PbX_4$. The bromide perovskite exhibits strong excimeric fluorescence as a result of energy transfer from excitons in the Pb–Br sheets to the excited singlet state of pyrene, leading to excimer formation. In contrast, the chloride analogue shows only monomeric fluorescence from pyrene. This difference may result from a packing arrangement of pyrene in the bromide perovskite that is more conducive to excimer formation.[244] Several groups have also demonstrated the ability of inorganic sheets to template a highly ordered, specifically oriented arrangement of chromophores providing a pathway to enhance the emission intensity, electrical mobility, and optical nonlinearity in the resulting perovskites.[61,252]

8.4.2. Energetic Effects. Just as the excited singlet and triplet energy levels of the chromophore can be tuned to manipulate the energy-transfer dynamics from inorganic to organic states, the energetic positions of the valence and conduction bands of the inorganic lattice can similarly be varied to affect this energy transfer. As discussed in section 4.2, the valence band of 2D Pb–X perovskites consists of both lead 6s and halide p states while mostly Pb 6p states compose the conduction band (Figure 8B). The excitonic energy in 2D perovskites is thought to track similarly to the band-gap energy. Mitzi and co-workers have studied the consequences of tuning the inorganic sublattice in a series of Pb–X (X = Cl, Br, I) perovskites containing the organic chromophore 5,5‴-bis(ethylammonium)-2,2′:5′,2″:5″,2‴-quaterthiophene (AEQT).[61] Whereas $(AEQT)PbCl_4$ exhibits strong fluorescence from the thiophene chromophore due to energy transfer from the inorganic lattice (Figure 25B), $(AEQT)PbI_4$ shows very little emission from the chromophore. This different behavior could arise from the increased energy of the valence band maximum in the Pb–I perovskite, as diagramed in Figure 25C,D. According to this theory, in the Cl perovskite, both electrons and holes migrate preferentially into the LUMO and HOMO, respectively, of the thiophene molecule where they recombine radiatively (Figure 25C). However, when the VB shifts to higher energy in the iodide perovskite, holes remain trapped in the inorganic sheets, while electrons are funneled into the LUMO of the organic, separating the carriers and quenching the photoluminescence (Figure 25D).[61] Achieving such staggered energy levels, which separate electrons and

DOI: 10.1021/acs.chemrev.8b00477
Chem. Rev. XXXX, XXX, XXX–XXX

holes between the organic and inorganic layers, by changing the energy of the valence band maximum is a particularly interesting manipulation of the quantum-well-like electronic structure.

9. APPLICATIONS IN LUMINESCENCE

9.1. Phosphors

A natural application for which both the narrow and broad photoluminescence of layered group 14 perovskites can be leveraged is as phosphors.

9.1.1. Narrow Emission. Color conversion phosphors[188,234] coat blue- or UV-light-emitting diodes to yield a specific color for displays. The color of a material's luminescence can be quantified by its CIE (International Commission on Illumination) coordinates.[188,234] In layered lead halide perovskites, the narrow, free-excitonic photoluminescence[19,49,164] produces high-purity colors that can be tuned across the entire visible electromagnetic spectrum (Figure 14). This leads to a wide color gamut, which is important for backlit displays to render a large range of colors. As with many of the luminescence metrics of the layered perovskites, PLQE of bulk samples exhibits a strong dependence on structure.[172] For the blue-light-emitting Pb−Br perovskites, increased distortion of the Pb−Br lattice, as proxied by nearest-neighbor Pb−Br−Pb and Br−Pb−Br bond angles correlated with the increased quantum efficiency (22%) in $(C_6H_5(CH_2)_2NH_3)_2PbBr_4$ relative to $(C_4H_9NH_3)_2PbBr_4$ (0.36%) or $(C_6H_5CH_2NH_3)_2PbBr_4$ (3.8%).[172] Nanostructuring is a less-explored, yet highly promising route to increase quantum efficiency of these blue emitters, which are potentially attractive for wide-gamut displays. For example, the PLQE of $(C_4H_9NH_3)_2PbBr_4$ monolayers is ca. 26%.[14] Intriguingly, exfoliating crystals of $(C_6H_5(CH_2)_2NH_3)_2PbBr_4$ is reported to result in high PLQE values of ca. 79% for blue emission.[253] The massive differences in PLQE values obtained for the same perovskite composition appear to be a result of different synthetic methods. However, an understanding of how these synthetic methods modulate defects, surfaces, and recombination rates is limited, presenting an opportunity to closely study these relationships to enable the design of more efficient color-conversion phosphors. In particular, semiconducting emitters with narrow emission line widths and high PLQE values are still needed to improve on LEDs relying on III−V or organic emissive layers, especially with respect to blue-light-emitting phosphors.[253]

9.1.2. Broad Emission. The white-light-emitting perovskites have potential as single-source phosphors in solid-state lighting devices. In contrast to the narrow free-excitonic emission that affords high color purity (resolution), the broad emission (400−700 nm) yields high color rendition. The color rendering index (CRI) quantifies how accurately a light source (in this case, a material's photoluminescence) portrays a target object's color. High-CRI light sources are commercially relevant, as they are pleasing to the eye, and several applications require highly accurate color representation.[188] In order to provide high color rendition, the light source must contain all colors of the visible spectrum. Owing to their broadband emission, many of the lead halide white-light emitters exhibit CRI values above 80, a typical threshold value for commercial-quality illumination (Table 5).[188] The highest CRI reported for a layered perovskite is 93 in the (110) perovskite $(C_3N_2H_4(CH_2)_3NH_3)PbCl_4$,[190] with other high values[254] also recently reported. The emission from commercial phosphors (such as Ce^{3+}-doped yttrium aluminum garnet) used for artificial illumination is not continuous across the visible spectrum, and the color rendition is improved through the use of multiple emitters. However, a single phosphor whose emission covers the entire visible spectrum would eliminate problems associated with having multiple emitters, such as self-absorption (due to overlapping absorption and emission spectra of the various components) and changes to the emission color owing to the varying degradation rates of the different components.

Variations in spectral energy and shape of the white-light-emitting perovskites also yield different "colors" of white light, affording both warm (with more red) and cold (with more blue) white light (Figure 26). The correlated color temperature (CCT) of the emission corresponds to the temperature at which an ideal blackbody emits light of the same color; perovskite white-light emitters can be tuned to produce both warm (CCTs < 3000 K) and cold (CCTs > 5000 K) white light (Figure 26). Halide substitution provides a straightforward method to change the CCT of the emission. For example, in (*N*-MEDA)$PbBr_{4-x}Cl_x$, increasing Cl content changes the emission CIE from a yellowish white (CCT = 4669) to a bluish white (CCT = 6502).[11] The ability to easily tune the phosphor's color is an advantage for matching the CIE coordinates of current lighting sources, where the color standards have already been set (e.g., military applications).

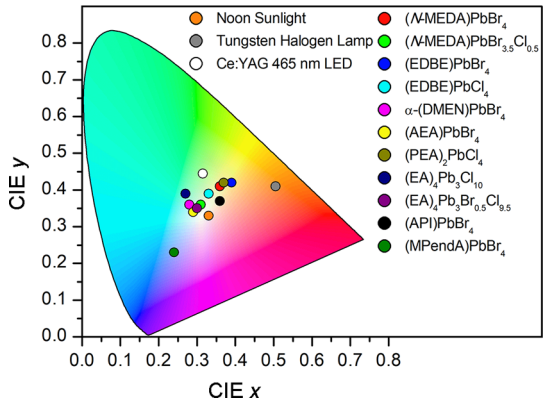

Figure 26. Chromaticity coordinate diagram[234] for white-light-emitting perovskites. See Table 5, footnote *b*, for abbreviations.

While color control is vital for potential phosphor materials, other criteria, such as stability,[188] are similarly important. The initial studies on white-light-emitting perovskites such as $(EDBE)PbBr_4$ showed promising stability, with the material showing thermal stability to over 200 °C,[89] above the typical operating temperature for light-emitting diodes.[188] Additionally, under constant UV illumination, the perovskite's emission was unchanged after 3 months under vacuum.[89] However, much more work remains to be done in assessing the stability of these materials, including incorporation into solid-state lighting assemblies under typical operating conditions and assessing performance, keeping in mind the typical thermal and photochemical decomposition pathways for organic−inorganic metal halides.[173,255]

Despite the significant progress in understanding white-light emission in perovskites,[25] challenges remain before these materials near commercial viability. While films of the 2D perovskite $(EDBE)PbBr_4$[89] and microscale crystals of the 1D

DOI: 10.1021/acs.chemrev.8b00477
Chem. Rev. XXXX, XXX, XXX−XXX

Pb−Br hybrid $(H_3CNH_2(CH_2)_2NH_2CH_3)PbBr_4$[228] exhibit PLQE values of ca. 9% for warm white light and ca. 12% for cold white light, respectively, these numbers are significantly lower than those of commercial inorganic yellow phosphors such as Ce^{3+}-doped yttrium aluminum garnet.[188] However, unlike inorganic phosphors, films of these hybrid phosphors can be inexpensively deposited from solution and they may be suited for niche luminescence applications involving large-area coatings.[25]

9.2. Light-Emitting Diodes

The attractive optoelectronic properties of the layered lead halide perovskites[20] which spurred initial interest, including broadly tunable band gaps, strong excitonic luminescence, and ease of film deposition, also motivated the early studies of their electroluminescence.[5] In light-emitting-diode (LED) applications the 2D perovskites predate their 3D congeners by over two decades.[256] While the first report of electroluminescence was from Nurmikko and co-workers in 1992, using $(C_6H_5(CH_2)_2NH_3)_2Pb_2I_7$ simply connected to a power supply with silver contacts,[4] truly engineered devices followed shortly thereafter.[5,71] These light-emitting diodes consisted of 2D Pb−I perovskite thin films spin-coated on a transparent conductive oxide substrate, followed by an electron transport layer and low work function metal. The electron transport layer also served as a hole-blocking layer, so injection of charge carriers results in the formation of excitons in the layered perovskite and subsequent electroluminescence. Despite the improved sophistication of these initial devices, bright electroluminescence was clearly observed only upon cooling below 110 K. Furthermore, extremely large applied voltages (>24 V) were required to yield luminescence.[5,71]

An alternative early approach that yielded room-temperature electroluminescence leveraged a cationic chromophore, rather than the inorganic sheets of the perovskite, as the emissive component.[6] In the perovskite (AEQT)$PbCl_4$ (AEQT = 5,5‴-bis(ethylammonium)-2,2′:5′,2″:5″,2‴-quarterthiophene), photoexcitation yields green photoluminescence rather than the expected UV excitonic emission, as a result of energy transfer from the inorganic to the organic component (section 8.4.2). Using a nearly identical[5,71] device architecture to previous studies, Mitzi and colleagues observed room-temperature electroluminescence in this perovskite with a much lower turn-on voltage of 5.5 V. The electro- and photoluminescence of the (AEQT)$PbCl_4$ perovskite matched closely with that of the AEQT·2Cl organic salt. The enhanced electroluminescence of this device relative to a purely organic analogue was attributed to several factors, including the templating influence of the inorganic layers on the packing geometry of the organic cations, the charge-carrying capacity of the inorganic component, and the increased thermal stability of the perovskite relative to typical emissive organic compounds.[6] Following a layoff of over 15 years and alongside the discovery[256] of the 3D Pb−X perovskites for tunable LED sources, the first 2D Pb−Br perovskite LEDs were developed.[257] Postsynthetic annealing of a thin film of $(C_6H_5(CH_2)_2NH_3)_2PbBr_4$ in solvent vapor resulted in narrow, room-temperature violet electroluminescence centered at 410 nm, although the external quantum efficiency (EQE) remained low, at 0.04%.[257]

Despite their efficient photoluminescence, the n = 1 perovskites present limited utility for LED applications, primarily owing to their insulating nature. In contrast, LEDs using 2D lead halide perovskites with thicker inorganic layers (n > 1) were able to navigate both the conductivity and luminescence requirements, resulting in much higher device EQEs of ca. 10%.[8,9] LEDs with n > 1 layered perovskite emitters with several different device architectures appeared nearly contemporaneously in late 2016,[7−9] just 2 years after their employment as solar-cell absorbers.[3] These early studies leveraged synthetic control over the perovskite structure and composition, with work by Huang, Wang, and colleagues demonstrating tunable electroluminescence across a wide range of the visible spectrum from ca. 500 to 800 nm using a perovskite with the nominal composition $(C_{10}H_7CH_2NH_3)_2(CH(NH_2)_2)Pb_2Br_{7-x}I_x$ (Figure 27).[9] Similarly to the photovoltaic devices using n > 1 layered perovskites,[3] part of the improved performance relative to the 3D lead halide perovskites is derived from processing advantages. When deposited by solution-based methods such as spin-coating, the n > 1 layered perovskites produce smoother films with fewer pinholes that yield shunts between transport layers.[7−9] The high efficiency of these devices was also ascribed to energy cascade or funneling mechanisms, enabled by the heterogeneity of the distribution of n values present in thin films of the n > 1 layered perovskites (section 6.2.2). It is energetically favorable for carriers or excitons generated in low n-value layers or grains to transfer to the high n-value components of the thin film. Such a transfer mechanism allows for energy concentration and hence a large local excitation density within the high n-valued components of the film. Filling of the limited number of trap states that limit radiative recombination then enhances the electroluminescence efficiency.[8]

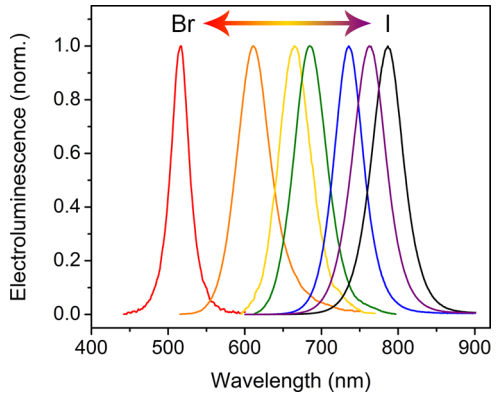

Figure 27. Color-tunable electroluminescence from light-emitting diodes containing $(C_{10}H_7CH_2NH_3)_2(CH(NH_2)_2)Pb_2Br_{7-x}I_x$. Adapted with permission from ref 9. Copyright 2016 Nature Publishing Group.

9.3. Scintillators

The luminescence properties of the 2D lead halide perovskites also make them attractive as scintillators, materials that down-convert high energy photons to lower energy photoluminescence in the UV, visible, or IR regions to enable detection of ionizing radiation. Asai and co-workers initially pointed out the ability of layered perovskites to resolve several shortcomings of some widely used scintillators.[258] For example, some applications of scintillators, such as time-of-flight positron emission tomography, require fast response times (a minimal delay between absorption and luminescence events). Inorganic scintillators are commonly plagued by slow response times on

DOI: 10.1021/acs.chemrev.8b00477
Chem. Rev. XXXX, XXX, XXX−XXX

the order of tens of nanoseconds, limiting their range of applications. The characteristically short lifetime of excitonic luminescence in 2D lead halide perovskites makes these materials uniquely suited for applications requiring a fast response time.[258] Asai and co-workers have shown that, upon irradiation with a pulsed electron beam, the luminescence decay of $(C_6H_{13}NH_3)_2PbI_4$ is well described by three components with decay times of 390 ps (28%), 3.8 ns (29%), and 16 ns (43%). Here, the fast component is attributed to free-exciton recombination whereas the slower components are attributed to excitons trapped at defects. Importantly, the decay time of 390 ps was the fastest of any scintillator known at the time, surpassing even the characteristically short lifetimes of organic scintillators.[259]

Scintillators employing undoped semiconductors commonly suffer from significant efficiency losses as the operating temperature is raised, complicating their usage since they must be cooled to cryogenic temperatures. The high exciton binding energy of the 2D lead halide perovskites means that thermal fluctuations have a significantly reduced impact on efficiency in these materials.[260,262] This effect has been well demonstrated by Shibata and co-workers, who compare the scintillation efficiencies of the 2D perovskite $(C_3H_7NH_3)_2PbBr_4$ and $(CH_3NH_3)PbBr_3$.[260] At 25 K, the efficiency of the 3D perovskite (140% relative to that of NaI:Tl) far surpasses that of the 2D material (26%) because there is insufficient thermal energy to dissociate the weakly bound excitons of $(CH_3NH_3)PbBr_3$. However, at room temperature, excitons in the 3D material are easily dissociated while those in the 2D material remain bound. As a result, the efficiency of the 2D material (6.5%) greatly exceeds that of the 3D material (0.075%) and is comparable to that of other common scintillator materials such as $Bi_4Ge_3O_{12}$ (BGO).[260]

Several other properties of 2D perovskites make them well-suited for scintillation applications. Asai and co-workers have shown that 2D perovskites are stable enough to withstand exposure to ionizing radiation at levels that would be encountered in practical applications.[258] Additionally, the presence of heavy lead atoms (and halide atoms, in the case of the iodide perovskites) allows these materials to absorb X-rays strongly, since X-ray absorption scales as Z^4 (Z = atomic number). As a result, the scintillators can be relatively thin, which helps minimize losses in efficiency and response time from self-absorption effects.[262] The small band gap of 2D halide perovskites relative to other common scintillator materials is also advantageous because the theoretical limit of a material's light yield is inversely proportional to its band gap. Furthermore, since they luminesce in the visible region, highly efficient avalanche photodiodes (quantum efficiency of 90–100%) can be used to detect the emission rather than less efficient photomultiplier tubes (quantum efficiency of 40–50%).[261,262,277]

Despite these advantages, there are several shortcomings of 2D perovskite scintillators. Because of the minimal Stokes shift of the excitonic emission, 2D perovskite scintillators suffer from self-absorption effects, which decrease their light yield and energy resolution and lead to longer-lived components of the emission.[262−264] White-light-emitting 2D perovskites such as (EDBE)$PbCl_4$ (EDBE = 2,2′-(ethylenedioxy)bis(ethylammonium)) have been proposed as a solution to minimize self-absorption. However, (EDBE)$PbCl_4$ suffers from a lower light yield and a slower response time than most 2D lead halide perovskites due to differences in the emission mechanism in this material.[262]

10. SUMMARY AND OUTLOOK

Despite their storied history, layered metal halide perovskites continue to exhibit new and surprising properties. Propelled by an incessantly expanding phase space, the photophysical properties of these materials create a host of new avenues for the scientific community to explore.

10.1. Gaining Synthetic Control over "Excited-State Defects"

Since the 2000s, researchers have exploited the structural definition of layered halide perovskites to probe how subtle changes to the crystal structure are reflected in the materials' band gaps and band dispersion.[63,172] More recent studies have probed how these structural parameters affect the thermodynamics of the electronic excited states.[88] Relating ground-state structure to excited-state energies and dynamics is a fertile ground for exploration. The a priori synthesis of lattices, with specific structural distortions, that can manipulate light in a predictable manner remains an inspiring goal in this field.

10.2. Gaining Synthetic Control over "Ground-State Defects"

The incredible diversity of layered halide perovskites is further enhanced through postsynthetic modification,[23] with small-molecule intercalation,[265,149,47] bond formation,[266,267] and ion exchange[268] as some examples of structure-preserving reactions. The effects of such postsynthetic treatments on the materials' photophysical properties[149] are much less investigated and should unearth new phenomena. Postsynthetic surface passivation or nanostructuring approaches may prove to be important for specifically enhancing luminescence, especially given the wealth of dramatic[269−271] alterations to the photoluminescence of the 3D lead halide perovskites enabled by simple treatments. Early studies[257] echo this promise in the layered perovskites, and understanding the role of surface states in defect and electronic structure is an open question. Surface chemistry may be critical to asserting further control over the luminescence of these materials, as their strong absorption coefficients mean most excitons are created near the surface of the perovskite.

10.3. Navigating the Excited State

The narrow emission observed in layered halide perovskites since the early 1990s has now yielded phosphors and LEDs with high color purity, notably blue phosphors that may fulfill a critical need in current display technology.[172,253] Indeed, there is a perovskite composition to afford most colors of visible light (Table 1). The discovery of perovskites that emit every color of visible light from a single inorganic lattice has revealed a different emission pathway.[89] While initial mechanistic,[90] structural,[88] and theoretical[195,196] studies support the exciton self-trapping hypothesis as the dominant mechanism at play, further experimental evidence is required to cement our understanding of the emission mechanism and, importantly, how to control it. Attempts at understanding the origins of the broad emission have revealed an excited-state landscape that is conducive to producing both a narrow emission and a very broad emission.[25,88] Understanding factors that tip the balance in the equilibrium between free and self-trapped excitons remains an intriguing challenge in this field.

DOI: 10.1021/acs.chemrev.8b00477
Chem. Rev. XXXX, XXX, XXX−XXX

10.4. Controlling and Using Film Heterogeneity

The number of well-characterized layered halide perovskites continues to expand, still along the first parameters elucidated: choice of metal, halide, and A-site cation.[20,21] Layered perovskites with thicker inorganic layers ($n > 1$) are increasingly both synthetically and crystallographically tractable,[3,9,52,59,109,119,168,173,272−274] adding yet another dimension of structural control. The heterogeneity in n values of films[3,175] of these perovskites provides yet another parameter to tune: e.g., to use low-n (high absorption coefficient) regions of the film to improve light absorption and high-n (low band gap) regions of the film to concentrate excitons. Developing patterns in films by tuning the spatial distribution of n could form complex heterostructures to manipulate excitons in a predictable manner.

10.5. Mixing Metals and Ligands

Recent work has driven further modifications to the layered perovskite archetype. Mixed-metal layered double perovskites yield new electronic structures,[108,127,119] and indirect-to-direct gap transitions with decreasing inorganic-layer thickness.[119] Substitution of pseudohalides, such as SCN^-, for halides can strongly affect the perovskite's photophysics,[151,210] instigating the search for other ligands to replace the halides. The recent observation of dynamic structural disorder in $(CH_3NH_3)PbI_2(SCN)_2$ gives a glimpse of the heterogeneity that may exist in the material's electronic excited state.[275] Indeed, a dynamic and flexible lattice in 2D perovskites may aid exciton self-trapping, where the free exciton can sample different lattice configurations in the excited state and become trapped at a local energy minimum.

10.6. Further Activating the Organic Layer

After the initial demonstration of charge transfer from the inorganic to the organic layers,[248] more exotic organic architectures may be designed to tune the relative energy levels of the quantum-well-like electronic structure to further drive charge separation across the organic−inorganic interface. Inclusion of highly polarizable groups in the organic layers[69,149] may even invert the dielectric profile of the layered perovskite to reduce or eliminate the dielectric confinement of the exciton, making charge separation easier. Highly conjugated aromatic systems in the organic layers have also recently been shown to improve electronic conductivity in the direction perpendicular to the plane of the inorganic sheets, attributed to a better match in energy levels between the organic and inorganic layers.[276]

10.7. Shining Brighter and for Longer

With respect to both the narrow and broad luminescence from perovskite phosphors, improving the radiative efficiencies and long-term stability of perovskite phosphors is both a materials chemistry and device engineering challenge. Technological improvements go hand in hand with more fundamental work probing the emission mechanism and gaining structural control over nonradiative decay pathways and material decomposition pathways under typical operating conditions. Such mechanistic studies on layered halide perovskites are broadly applicable to other low-dimensional lattices of similar composition.

Although the potential technological applications of the luminescent layered perovskites are many, we should not forget that much of the groundwork in this field was established decades ago through fundamental studies on their crystallography, photophysics, and structure−property relations. Fundamental studies on layered halide perovskites and related materials remain vitally important and should not take a back seat to more technologically motivated work—these materials very likely have much more to offer the exploratory investigator in the years to come.

AUTHOR INFORMATION

Corresponding Author

*E-mail: hemamala@stanford.edu.

ORCID

Matthew D. Smith: 0000-0002-4197-5176

Hemamala I. Karunadasa: 0000-0003-4949-8068

Author Contributions

†M.D.S. and B.A.C.: These authors contributed equally.

Notes

The authors declare no competing financial interest.

Biographies

Matthew D. Smith received his B.S. in chemistry from Haverford College working with Profs. Alexander Norquist and Joshua Schrier on structure−property relationships in amine-templated metal oxides. As a Ph.D. student at Stanford University working with Prof. Hemamala Karunadasa, his interests include excitons in dimensionally confined systems with unusual photoluminescence properties.

Bridget A. Connor received her B.S. in chemistry from the California Institute of Technology working with Prof. Jonas Peters on small molecule activation by first-row transition metal complexes. As a Ph.D. student at Stanford University working with Prof. Hemamala Karunadasa, her interests include exploring the properties of novel two-dimensional double perovskites.

Hemamala I. Karunadasa is an assistant professor in chemistry at Stanford University. Her group synthesizes functional materials using techniques from both molecular and solid-state chemistry. She received her A.B. from Princeton University studying geometrically frustrated magnets with Prof. Robert Cava and her Ph.D. from University of California, Berkeley, with Prof. Jeffrey Long synthesizing molecules with large magnetic anisotropy. She studied molecular electrocatalysts during her postdoctoral research with Profs. Christopher Chang and Jeffrey Long at UC Berkeley and the Lawrence Berkeley National Laboratory and with Prof. Harry Gray at the California Institute of Technology.

ACKNOWLEDGMENTS

We are grateful for support from the National Science Foundation (NSF) CAREER award (DMR-1351538), the Department of Energy, Laboratory Directed Research and Development program at SLAC National Accelerator Laboratory (DE-AC02-76SF00515), the Alfred P. Sloan fellowship, and Stanford University. M.D.S. is supported by a graduate fellowship from the Center for Molecular Analysis and Design (CMAD) at Stanford University, and B.A.C. is supported by an NSF graduate fellowship (DGE-114747).

REFERENCES

(1) Topsøe, H. Krystallographisch-Chemische Untersuchungen Homologer Verbindungen. *Z. Kristallogr. - Cryst. Mater.* **1884**, *8*, 246.

(2) Desjardins, S. R.; Penfield, K. W.; Cohen, S. L.; Musselman, R. L.; Solomon, E. I. Detailed Absorption, Reflectance, and UV Photoelectron Spectroscopic and Theoretical Studies of the Charge-

DOI: 10.1021/acs.chemrev.8b00477
Chem. Rev. XXXX, XXX, XXX−XXX

Transfer Transitions of $CuCl_4^{2-}$: Correlation of the Square-Planar and the Tetrahedral Limits. *J. Am. Chem. Soc.* **1983**, *105*, 4590−4603.
(3) Smith, I. C.; Hoke, E. T.; Solis-Ibarra, D.; McGehee, M. D.; Karunadasa, H. I. A Layered Hybrid Perovskite Solar-Cell Absorber with Enhanced Moisture Stability. *Angew. Chem., Int. Ed.* **2014**, *53*, 11232−11235.
(4) Hong, X.; Ishihara, T.; Nurmikko, A. V. Photoconductivity and Electroluminescence in Lead Iodide Based Natural Quantum Well Structures. *Solid State Commun.* **1992**, *84*, 657−661.
(5) Era, M.; Morimoto, S.; Tsutsui, T.; Saito, S. Organic−Inorganic Heterostructure Electroluminescent Device Using a Layered Perovskite Semiconductor $(C_6H_5C_2H_4NH_3)_2PbI_4$. *Appl. Phys. Lett.* **1994**, *65*, 676−678.
(6) Chondroudis, K.; Mitzi, D. B. Electroluminescence From an Organic−Inorganic Perovskite Incorporating a Quaterthiophene Dye within Lead Halide Perovskite Layers. *Chem. Mater.* **1999**, *11*, 3028−3030.
(7) Byun, J.; Cho, H.; Wolf, C.; Jang, M.; Sadhanala, A.; Friend, R. H.; Yang, H.; Lee, T.-W. Efficient Visible Quasi-2D Perovskite Light-Emitting Diodes. *Adv. Mater.* **2016**, *28*, 7515−7520.
(8) Yuan, M.; Quan, L. N.; Comin, R.; Walters, G.; Sabatini, R.; Voznyy, O.; Hoogland, S.; Zhao, Y.; Beauregard, E. M.; Kanjanaboos, P.; et al. Perovskite Energy Funnels for Efficient Light-Emitting Diodes. *Nat. Nanotechnol.* **2016**, *11*, 872−877.
(9) Wang, N.; Cheng, L.; Ge, R.; Zhang, S.; Miao, Y.; Zou, W.; Yi, C.; Sun, Y.; Cao, Y.; Yang, R.; et al. Perovskite Light-Emitting Diodes Based on Solution-Processed Self-Organized Multiple Quantum Wells. *Nat. Photonics* **2016**, *10*, 699−704.
(10) Gauthron, K.; Lauret, J.-S.; Doyennette, L.; Lanty, G.; Al Choueiry, A.; Zhang, S. J.; Brehier, A.; Largeau, L.; Mauguin, O.; Bloch, J.; et al. Optical Spectroscopy of Two-Dimensional Layered $(C_6H_5C_2H_4\text{-}NH_3)_2\text{-}PbI_4$ Perovskite. *Opt. Express* **2010**, *18*, 5912−5919.
(11) Dohner, E. R.; Hoke, E. T.; Karunadasa, H. I. Self-Assembly of Broadband White-Light Emitters. *J. Am. Chem. Soc.* **2014**, *136*, 1718−1721.
(12) Kojima, A.; Teshima, K.; Shirai, Y.; Miyasaka, T. Organometal Halide Perovskites as Visible-Light Sensitizers for Photovoltaic Cells. *J. Am. Chem. Soc.* **2009**, *131*, 6050−6051.
(13) Lee, M. M.; Teuscher, J.; Miyasaka, T.; Murakami, T. N.; Snaith, H. J. Efficient Hybrid Solar Cells Based on Meso-Superstructured Organometal Halide Perovskites. *Science* **2012**, *338*, 643−647.
(14) Dou, L.; Wong, A. B.; Yu, Y.; Lai, M.; Kornienko, N.; Eaton, S. W.; Fu, A.; Bischak, C. G.; Ma, J.; Ding, T.; et al. Atomically Thin Two-Dimensional Organic−Inorganic Hybrid Perovskites. *Science* **2015**, *349*, 1518−1521.
(15) Yaffe, O.; Chernikov, A.; Norman, Z. M.; Zhong, Y.; Velauthapillai, A.; van der Zande, A.; Owen, J. S.; Heinz, T. F. Excitons in Ultrathin Organic−Inorganic Perovskite Crystals. *Phys. Rev. B: Condens. Matter Mater. Phys.* **2015**, *92*, No. 045414.
(16) Wells, H. L. On Caesium-Mercuric Halides. *Am. J. Sci.* **1892**, *s3-44*, 221−236.
(17) Wells, H. L. On the Caesium- and the Potassium-Lead Halides. *Am. J. Sci.* **1893**, *s3-45*, 121−134.
(18) Arend, H.; Huber, W.; Mischgofsky, F. H.; Richter-Van Leeuwen, G. K. Layer Perovskites of the $(C_nH_{2n+1}NH_3)_2MX_4$ and $NH_3(CH_2)_mNH_3MX_4$ Families with M = Cd, Cu, Fe, Mn OR Pd and X = Cl OR Br: Importance, Solubilities and Simple Growth Techniques. *J. Cryst. Growth* **1978**, *43*, 213−223.
(19) Ishihara, T. Optical Properties of PbI-Based Perovskite Structures. *J. Lumin.* **1994**, *60−61*, 269−274.
(20) Mitzi, D. B. Synthesis, Structure, and Properties of Organic-Inorganic Perovskites and Related Materials. *Prog. Inorg. Chem.* **2007**, *48*, 1−121.
(21) Saparov, B.; Mitzi, D. B. Organic−Inorganic Perovskites: Structural Versatility for Functional Materials Design. *Chem. Rev.* **2016**, *116*, 4558−4596.
(22) Pedesseau, L.; Sapori, D.; Traore, B.; Robles, R.; Fang, H.-H.; Loi, M. A.; Tsai, H.; Nie, W.; Blancon, J.-C.; Neukirch, A.; et al. Advances and Promises of Layered Halide Hybrid Perovskite Semiconductors. *ACS Nano* **2016**, *10*, 9776−9786.
(23) Smith, I. C.; Smith, M. D.; Jaffe, A.; Lin, Y.; Karunadasa, H. I. Between the Sheets: Postsynthetic Transformations in Hybrid Perovskites. *Chem. Mater.* **2017**, *29*, 1868−1884.
(24) Jaffe, A.; Lin, Y.; Karunadasa, H. I. Halide Perovskites under Pressure: Accessing New Properties through Lattice Compression. *ACS Energy Lett.* **2017**, *2*, 1549−1555.
(25) Smith, M. D.; Karunadasa, H. I. White-Light Emission from Layered Halide Perovskites. *Acc. Chem. Res.* **2018**, *51*, 619−627.
(26) Smith, M. D.; Crace, E. J.; Jaffe, A.; Karunadasa, H. I. The Diversity of Layered Halide Perovskites. *Annu. Rev. Mater. Res.* **2018**, *48*, 111−136.
(27) van Arkel, A. E. Kristalstructuur van Magnesiumfluoride en Andere Verbindingen van Hetzelfde Kristaltype. *Physica* **1925**, *5*, 162−171.
(28) Natta, G.; Passerini, L. Isomorfismo, Polimorfismo e Morfotropia. - I. Composti del Tipo ABX_3. *Gazz. Chim. Ital.* **1928**, *58*, 472−484.
(29) Wells, H. L. Some Complex Chlorides Containing Gold. *Am. J. Sci.* **1922**, *s5-3*, 315−326.
(30) Elliott, N.; Pauling, L. The Crystal Structure of Cesium Aurous Auric Chloride, $Cs_2AuAuCl_6$, and Cesium Argentous Auric Chloride, $Cs_2AgAuCl_6$. *J. Am. Chem. Soc.* **1938**, *60*, 1846−1851.
(31) Cross, W.; Hillebrand, W. F. Contributions to the Mineralogy of the Rocky Mountains. *U.S. Geol. Surv. Bull.* **1885**, No. 20, 1−115.
(32) Náray-Szabó, I.; Sigmond, G. A Kryolith-Káliumkryolith-Rendszer Olvadási Görbéje. *Mathematikai és Természettudományi Értesíto* **1941**, *60*, 364−371.
(33) Frondel, C. New Data on Elpasolite and Hagemannite. *Am. Mineral.* **1948**, *33*, 84−87.
(34) Møller, C. K. A Phase Transition in Caesium Plumbochloride. *Nature* **1957**, *180*, 981−982.
(35) Møller, C. K. Crystal Structure and Photoconductivity of Caesium Plumbohalides. *Nature* **1958**, *182*, 1436−1436.
(36) Beal, R. E.; Slotcavage, D. J.; Leijtens, T.; Bowring, A. R.; Belisle, R. A.; Nguyen, W. H.; Burkhard, G. F.; Hoke, E. T.; McGehee, M. D. Cesium Lead Halide Perovskites with Improved Stability for Tandem Solar Cells. *J. Phys. Chem. Lett.* **2016**, *7*, 746−751.
(37) Weber, D. $CH_3NH_3PbX_3$, ein Pb(II)-System mit Kubischer Perowskitstruktur. *Z. Naturforsch., B: J. Chem. Sci.* **1978**, *33b*, 1443−1445.
(38) von Fedorow, E. XVII. Allgemeinste Krystallisationsgesetze und die Darauf Fussende Eindeutige Aufstellung der Krystalle. *Z. Kristallogr. - Cryst. Mater.* **1904**, *38*, 321−490.
(39) Röntgen, W. C. On a New Kind of Rays. *Science* **1896**, *3*, 227−231.
(40) Willett, R. D. Crystal Structure of $(NH_4)_2CuCl_4$. *J. Chem. Phys.* **1964**, *41*, 2243−2244.
(41) Willett, R. D.; Liles, O. L.; Michelson, C. Electronic Absorption Spectra of Monomeric Copper(II) Chloride Species and the Electron Spin Resonance Spectrum of the Square-Planar $CuCl_4^{2-}$ Ion. *Inorg. Chem.* **1967**, *6*, 1885−1889.
(42) Bellitto, C.; Day, P. Bis(monoalkylammonium) Tetrachlorochromates(II): A New Series of Two-Dimensional Ionic Ferromagnets. *J. Chem. Soc., Chem. Commun.* **1976**, *0*, 870−871.
(43) Day, P. New Transparent Ferromagnets. *Acc. Chem. Res.* **1979**, *12*, 236−243.
(44) de Jongh, L. J.; Botterman, A. C.; de Boer, F. R.; Miedema, A. R. Transition Temperature of the Two-Dimensional Heisenberg Ferromagnet with S = 1/2. *J. Appl. Phys.* **1969**, *40*, 1363−1365.
(45) de Jongh, L. J.; Miedema, A. R. Experiments on Simple Magnetic Model Systems. *Adv. Phys.* **1974**, *23*, 1−260.
(46) Payen de la Garanderie, H. Complexes Luminescents du Chlorure de Manganèse avec les Amines. *C. R. Hebd. Seances Acad. Sci.* **1962**, *254*, 2739.

DOI: 10.1021/acs.chemrev.8b00477
Chem. Rev. XXXX, XXX, XXX−XXX

(47) Dolzhenko, Y. I.; Inabe, T.; Maruyama, Y. In Situ X-Ray Observation on the Intercalation of Weak Interaction Molecules into Perovskite-Type Layered Crystals $(C_9H_{19}NH_3)_2PbI_4$ and $(C_{10}H_{21}NH_3)_2CdCl_4$. *Bull. Chem. Soc. Jpn.* **1986**, *59*, 563−567.
(48) Nagapetyan, S. S.; Dolzhenko, Y. I.; Arakelova, E. R.; Koshkin, V. M.; Struchkov, Y. T.; Shklover, V. E. Synthesis, Structure and Properties of Normal-Nonylammonium Tetraiodoplumbate(III). *Zh. Neorg. Khim.* **1988**, *33*, 2806−2812.
(49) Ishihara, T.; Takahashi, J.; Goto, T. Exciton State in Two-Dimensional Perovskite Semiconductor $(C_{10}H_{21}NH_3)_2PbI_4$. *Solid State Commun.* **1989**, *69*, 933−936.
(50) Papavassiliou, G. C.; Patsis, A. P.; Lagouvardos, D. J.; Koutselas, I. B. Spectroscopic Studies of $(C_{10}H_{21}NH_3)_2PbI_4$, $(CH_3NH_3)(C_{10}H_{21}NH_3)_2Pb_2I_7$, $(CH_3NH_3)PbI_3$, and Similar Compounds. *Synth. Met.* **1993**, *57*, 3889−3894.
(51) Papavassiliou, G. C.; Koutselas, J. B.; Lagouvardos, D. J. Preparation and Characterization of $(C_6H_5CH_2CH_2NH_3)_2SnI_4$ and $(C_6H_5CH_2CH_2NH_3)_2SnBr_4$. *Z. Naturforsch., B: J. Chem. Sci.* **1993**, *48*, 1013−1014.
(52) Mitzi, D. B.; Feild, C. A.; Harrison, W. T. A.; Guloy, A. M. Conducting Tin Halides with a Layered Organic-Based Perovskite Structure. *Nature* **1994**, *369*, 467−469.
(53) Papavassiliou, G. C.; Koutselas, I. B.; Terzis, A.; Whangbo, M. H. Structural and Electronic Properties of the Natural Quantum-Well System $(C_6H_5CH_2CH_2NH_3)_2SnI_4$. *Solid State Commun.* **1994**, *91*, 695−698.
(54) Papavassiliou, G. C.; Koutselas, I. B. Structural, Optical and Related Properties of Some Natural Three- and Lower-Dimensional Semiconductor Systems. *Synth. Met.* **1995**, *71*, 1713−1714.
(55) Mitzi, D. B. Synthesis, Crystal Structure, and Optical and Thermal Properties of $(C_4H_9NH_3)_2MI_4$ (M = Ge, Sn, Pb). *Chem. Mater.* **1996**, *8*, 791−800.
(56) Kitazawa, N. Compositional Modulation of Two-Dimensional Layered Perovskite $(RNH_3)_2Pb(Cl, Br, I)_4$ and Its Optical Properties. *Jpn. J. Appl. Phys., Part 1* **1996**, *35*, 6202−6207.
(57) Kitazawa, N. Excitons in Two-Dimensional Layered Perovskite Compounds: $(C_6H_5C_2H_4NH_3)_2Pb(Br,I)_4$ and $(C_6H_5C_2H_4NH_3)_2Pb(Cl,Br)_4$. *Mater. Sci. Eng., B* **1997**, *49*, 233−238.
(58) Calabrese, J.; Jones, N. L.; Harlow, R. L.; Herron, N.; Thorn, D. L.; Wang, Y. Preparation and Characterization of Layered Lead Halide Compounds. *J. Am. Chem. Soc.* **1991**, *113*, 2328−2330.
(59) Mitzi, D. B.; Wang, S.; Feild, C. A.; Chess, C. A.; Guloy, A. M. Conducting Layered Organic−Inorganic Halides Containing ⟨110⟩-Oriented Perovskite Sheets. *Science* **1995**, *267*, 1473−1476.
(60) Mitzi, D. B.; Dimitrakopoulos, C. D.; Kosbar, L. L. Structurally Tailored Organic−Inorganic Perovskites: Optical Properties and Solution-Processed Channel Materials for Thin-Film Transistors. *Chem. Mater.* **2001**, *13*, 3728−3740.
(61) Mitzi, D. B.; Chondroudis, K.; Kagan, C. R. Design, Structure, and Optical Properties of Organic−Inorganic Perovskites Containing an Oligothiophene Chromophore. *Inorg. Chem.* **1999**, *38*, 6246−6256.
(62) Mitzi, D. B. Templating and Structural Engineering in Organic−Inorganic Perovskites. *J. Chem. Soc., Dalton Trans.* **2001**, *0*, 1−12.
(63) Knutson, J. L.; Martin, J. D.; Mitzi, D. B. Tuning the Band Gap in Hybrid Tin Iodide Perovskite Semiconductors Using Structural Templating. *Inorg. Chem.* **2005**, *44*, 4699−4705.
(64) Koutselas, I. B.; Ducasse, L.; Papavassiliou, G. C. Electronic Properties of Three- and Low-Dimensional Semiconducting Materials with Pb Halide and Sn Halide Units. *J. Phys.: Condens. Matter* **1996**, *8*, 1217.
(65) Mousdis, G. A.; Gionis, V.; Papavassiliou, G. C.; Raptopoulou, C. P.; Terzis, A. Preparation, Structure and Optical Properties of $[CH_3SC(=NH_2)NH_2]_3PbI_5$, $[CH_3SC(=NH_2)NH_2]_4Pb_2Br_8$ and $[CH_3SC(=NH_2)NH_2]_3PbCl_5\bullet CH_3SC(=NH_2)NH_2Cl$. *J. Mater. Chem.* **1998**, *8*, 2259−2262.
(66) Papavassiliou, G. C.; Mousdis, G. A.; Koutselas, I. B. Some New Organic−Inorganic Hybrid Semiconductors Based on Metal Halide Units: Structural, Optical and Related Properties. *Adv. Mater. Opt. Electron.* **1999**, *9*, 265−271.
(67) Mousdis, G. A.; Papavassiliou, G. C.; Raptopoulou, C. P.; Terzis, A. Preparation and Characterization of $[H_3N(CH_2)_6NH_3]PbI_4$ and Similar Compounds with a Layered Perovskite Structure. *J. Mater. Chem.* **2000**, *10*, 515−518.
(68) Ishihara, T.; Takahashi, J.; Goto, T. Optical Properties Due to Electronic Transitions in Two-Dimensional Semiconductors $(C_nH_{2n+1}NH_3)_2PbI_4$. *Phys. Rev. B: Condens. Matter Mater. Phys.* **1990**, *42*, 11099−11107.
(69) Hong, X.; Ishihara, T.; Nurmikko, A. V. Dielectric Confinement Effect on Excitons in PbI_4-Based Layered Semiconductors. *Phys. Rev. B: Condens. Matter Mater. Phys.* **1992**, *45*, 6961−6964.
(70) Muljarov, E. A.; Tikhodeev, S. G.; Gippius, N. A.; Ishihara, T. Excitons in Self-Organized Semiconductor/Insulator Superlattices: PbI-Based Perovskite Compounds. *Phys. Rev. B: Condens. Matter Mater. Phys.* **1995**, *51*, 14370−14378.
(71) Hattori, T.; Taira, T.; Era, M.; Tsutsui, T.; Saito, S. Highly Efficient Electroluminescence from a Heterostructure Device Combined with Emissive Layered-Perovskite and an Electron-Transporting Organic Compound. *Chem. Phys. Lett.* **1996**, *254*, 103−108.
(72) Xu, Z.; Mitzi, D. B.; Dimitrakopoulos, C. D.; Maxcy, K. R. Semiconducting Perovskites $(2\text{-}XC_6H_4C_2H_4NH_3)_2SnI_4$ (X = F, Cl, Br): Steric Interaction between the Organic and Inorganic Layers. *Inorg. Chem.* **2003**, *42*, 2031−2039.
(73) Billing, D. G.; Lemmerer, A. Inorganic−Organic Hybrid Materials Incorporating Primary Cyclic Ammonium Cations: The Lead Iodide Series. *CrystEngComm* **2007**, *9*, 236−244.
(74) Billing, D. G.; Lemmerer, A. Synthesis, Characterization and Phase Transitions in the Inorganic−Organic Layered Perovskite-Type Hybrids $[(C_nH_{2n+1}NH_3)_2PbI_4]$, *n* = 4, 5 and 6. *Acta Crystallogr., Sect. B: Struct. Sci.* **2007**, *63*, 735−747.
(75) Billing, D. G.; Lemmerer, A. Synthesis, Characterization and Phase Transitions of the Inorganic−Organic Layered Perovskite-Type Hybrids $[(C_nH_{2n+1}NH_3)_2PbI_4]$ (*n* = 12, 14, 16 and 18). *New J. Chem.* **2008**, *32*, 1736−1746.
(76) Billing, D. G.; Lemmerer, A. Inorganic−Organic Hybrid Materials Incorporating Primary Cyclic Ammonium Cations: The Lead Bromide and Chloride Series. *CrystEngComm* **2009**, *11*, 1549−1562.
(77) Lemmerer, A.; Billing, D. G. Effect of Heteroatoms in the Inorganic−Organic Layered Perovskite-Type Hybrids $[(ZC_nH_{2n}NH_3)_2PbI_4]$, *n* = 2, 3, 4, 5, 6; Z = OH, Br and I; and $[(H_3NC_2H_4S_2C_2H_4NH_3)PbI_4]$. *CrystEngComm* **2010**, *12*, 1290−1301.
(78) Lemmerer, A.; Billing, D. G. Synthesis, Characterization and Phase Transitions of the Inorganic−Organic Layered Perovskite-Type Hybrids $(C_nH_{2n+1}NH_3)_2PbI_4$, *n* = 7, 8, 9 and 10. *Dalton Trans.* **2012**, *41*, 1146−1157.
(79) Lemmerer, A.; Billing, D. G. Lead Halide Inorganic−Organic Hybrids Incorporating Diammonium Cations. *CrystEngComm* **2012**, *14*, 1954−1966.
(80) Mercier, N.; Poiroux, S.; Riou, A.; Batail, P. Unique Hydrogen Bonding Correlating with a Reduced Band Gap and Phase Transition in the Hybrid Perovskites $(HO(CH_2)_2NH_3)_2PbX_4$ (X = I, Br). *Inorg. Chem.* **2004**, *43*, 8361−8366.
(81) Mercier, N.; Riou, A. An Organic−Inorganic Hybrid Perovskite Containing Copper Paddle-Wheel Clusters Linking Perovskite Layers: $[Cu(O_2C\text{-}(CH_2)_3\text{-}NH_3)_2]PbBr_4$. *Chem. Commun.* **2004**, 844−845.
(82) Sourisseau, S.; Louvain, N.; Bi, W.; Mercier, N.; Rondeau, D.; Boucher, F.; Buzaré, J.-Y.; Legein, C. Reduced Band Gap Hybrid Perovskites Resulting from Combined Hydrogen and Halogen Bonding at the Organic−Inorganic Interface. *Chem. Mater.* **2007**, *19*, 600−607.
(83) Sourisseau, S.; Louvain, N.; Bi, W.; Mercier, N.; Rondeau, D.; Buzaré, J.-Y.; Legein, C. Hybrid Perovskite Resulting from the Solid-State Reaction between the Organic Cations and Perovskite Layers of $\alpha 1\text{-}(Br\text{-}(CH_2)_2\text{-}NH_3)_2PbI_4$. *Inorg. Chem.* **2007**, *46*, 6148−6154.

DOI: 10.1021/acs.chemrev.8b00477
Chem. Rev. XXXX, XXX, XXX−XXX

(84) Louvain, N.; Bi, W.; Mercier, N.; Buzaré, J.-Y.; Legein, C.; Corbel, G. $Pb_nI_{4n+2}^{(2n+2)-}$ Ribbons (n = 3, 5) as Dimensional Reductions of 2D Perovskite Layers in Cystamine Cation Based Hybrids, also Incorporating Iodine Molecules or Reversible Guest Water Molecules. *Dalton Trans.* **2007**, *0*, 965−970.
(85) Mercier, N.; Louvain, N.; Bi, W. Structural Diversity and Retro-Crystal Engineering Analysis of Iodometalate Hybrids. *CrystEngComm* **2009**, *11*, 720−734.
(86) Stoumpos, C. C.; Cao, D. H.; Clark, D. J.; Young, J.; Rondinelli, J. M.; Jang, J. I.; Hupp, J. T.; Kanatzidis, M. G. Ruddlesden−Popper Hybrid Lead Iodide Perovskite 2D Homologous Semiconductors. *Chem. Mater.* **2016**, *28*, 2852−2867.
(87) Tsai, H.; Nie, W.; Blancon, J.-C.; Stoumpos, C. C.; Asadpour, R.; Harutyunyan, B.; Neukirch, A. J.; Verduzco, R.; Crochet, J. J.; Tretiak, S.; et al. High-Efficiency Two-Dimensional Ruddlesden−Popper Perovskite Solar Cells. *Nature* **2016**, *536*, 312−316.
(88) Smith, M. D.; Jaffe, A.; Dohner, E. R.; Lindenberg, A. M.; Karunadasa, H. I. Structural Origins of Broadband Emission from Layered Pb−Br Hybrid Perovskites. *Chem. Sci.* **2017**, *8*, 4497−4504.
(89) Dohner, E. R.; Jaffe, A.; Bradshaw, L. R.; Karunadasa, H. I. Intrinsic White-Light Emission from Layered Hybrid Perovskites. *J. Am. Chem. Soc.* **2014**, *136*, 13154−13157.
(90) Hu, T.; Smith, M. D.; Dohner, E. R.; Sher, M.-J.; Wu, X.; Trinh, M. T.; Fisher, A.; Corbett, J.; Zhu, X.-Y.; Karunadasa, H. I.; et al. Mechanism for Broadband White-Light Emission from Two-Dimensional (110) Hybrid Perovskites. *J. Phys. Chem. Lett.* **2016**, *7*, 2258−2263.
(91) Glazer, A. M. The Classification of Tilted Octahedra in Perovskites. *Acta Crystallogr., Sect. B: Struct. Crystallogr. Cryst. Chem.* **1972**, *28*, 3384−3392.
(92) Lufaso, M. W.; Woodward, P. M. Jahn-Teller Distortions, Cation Ordering and Octahedral Tilting in Perovskites. *Acta Crystallogr., Sect. B: Struct. Sci.* **2004**, *60*, 10−20.
(93) Yamada, K.; Funabiki, S.; Horimoto, H.; Matsui, T.; Okuda, T.; Ichiba, S. Structural Phase Transitions of the Polymorphs of $CsSnI_3$ by Means of Rietveld Analysis of the X-Ray Diffraction. *Chem. Lett.* **1991**, *20*, 801−804.
(94) Weber, D. $CH_3NH_3SnBr_xI_{3-x}$ (x = 0−3), ein Sn(II)-System mit kubischer Perowskitstruktur. *Z. Naturforsch., B: J. Chem. Sci.* **1978**, *33*, 862−865.
(95) Christensen, A. N.; Rasmussen, S. E. A Ferroelectric Chloride of Perowskite Type. Crystal Structures of $CsGeCl_3$. *Acta Chem. Scand.* **1965**, *19*, 421−428.
(96) Mitzi, D. B.; Liang, K. Synthesis, Resistivity, and Thermal Properties of the Cubic Perovskite $NH_2CH=NH_2SnI_3$ and Related Systems. *J. Solid State Chem.* **1997**, *134*, 376−381.
(97) Kieslich, G.; Sun, S.; Cheetham, A. K. Solid-State Principles Applied to Organic−Inorganic Perovskites: New Tricks for an Old Dog. *Chem. Sci.* **2014**, *5*, 4712−4715.
(98) Kallel, A.; Bats, J. W. Tris(trimethylammonium) Nonachlorodiantimonate(III), $[NH(CH_3)_3]_3[Sb_2Cl_9]$. *Acta Crystallogr., Sect. C: Cryst. Struct. Commun.* **1985**, *41*, 1022−1024.
(99) Guan, J.; Tang, Z.; Guloy, A. M. α-$[NH_3(CH_2)_5NH_3]SnI_4$: A New Layered Perovskite Structure. *Chem. Commun.* **1999**, 1833−1834.
(100) Mao, L.; Wu, Y.; Stoumpos, C. C.; Wasielewski, M. R.; Kanatzidis, M. G. White-Light Emission and Structural Distortion in New Corrugated Two-Dimensional Lead Bromide Perovskites. *J. Am. Chem. Soc.* **2017**, *139*, 5210−5215.
(101) Nazarenko, O.; Kotyrba, M. R.; Yakunin, S.; Aebli, M.; Rainò, G.; Benin, B. M.; Wörle, M.; Kovalenko, M. V. Guanidinium-Formamidinium Lead Iodide: A Layered Perovskite-Related Compound with Red Luminescence at Room Temperature. *J. Am. Chem. Soc.* **2018**, *140*, 3850−3853.
(102) Mostafa, M. F.; Abdel-Kader, M. M.; Arafat, S. S.; Kandeel, E. M. Thermochromic Phase Transitions in Two Aromatic Tetrachlorocuprates. *Phys. Scr.* **1991**, *43*, 627−629.
(103) Pan, X.; Wu, G.; Wang, M.; Chen, H. Partially Reversible Photochromic Behavior of Organic−Inorganic Perovskites with Copper(II) Chloride. *J. Zhejiang Univ., Sci., A* **2009**, *10*, 710−715.
(104) Thomson, R. I.; Rawson, J. M.; Goeta, A.; Probert, M. R.; Coome, J. A.; Hoang, T. K. A.; Carpenter, M. A. Elastic Coupling and Anelastic Relaxation Associated with Multiple Phase Transitions in *para*-Chloroanilinium Tetrachlorocuprate, $[p\text{-}ClC_6H_4NH_3]_2CuCl_4$. *Mater. Chem. Phys.* **2013**, *139*, 34−46.
(105) Lermer, C.; Birkhold, S. T.; Moudrakovski, I. L.; Mayer, P.; Schoop, L. M.; Schmidt-Mende, L.; Lotsch, B. V. Toward Fluorinated Spacers for MAPI-Derived Hybrid Perovskites: Synthesis, Characterization, and Phase Transitions of $(FC_2H_4NH_3)_2PbCl_4$. *Chem. Mater.* **2016**, *28*, 6560−6566.
(106) Xu, Z.; Mitzi, D. B.; Medeiros, D. R. $[(CH_3)_3NCH_2CH_2NH_3]SnI_4$: A Layered Perovskite with Quaternary/Primary Ammonium Dications and Short Interlayer Iodine-Iodine Contacts. *Inorg. Chem.* **2003**, *42*, 1400−1402.
(107) Du, K.; Tu, Q.; Zhang, X.; Han, Q.; Liu, J.; Zauscher, S.; Mitzi, D. B. Two-Dimensional Lead(II) Halide-Based Hybrid Perovskites Templated by Acene Alkylamines: Crystal Structures, Optical Properties, and Piezoelectricity. *Inorg. Chem.* **2017**, *56*, 9291−9302.
(108) Vargas, B.; Ramos, E.; Pérez-Gutiérrez, E.; Alonso, J. C.; Solis-Ibarra, D. A Direct Bandgap Copper-Antimony Halide Perovskite. *J. Am. Chem. Soc.* **2017**, *139*, 9116−9119.
(109) Stoumpos, C. C.; Soe, C. M. M.; Tsai, H.; Nie, W.; Blancon, J.-C.; Cao, D. H.; Liu, F.; Traoré, B.; Katan, C.; Even, J.; et al. High Members of the 2D Ruddlesden-Popper Halide Perovskites: Synthesis, Optical Properties, and Solar Cells of $(CH_3(CH_2)_3NH_3)_2(CH_3NH_3)_4Pb_5I_{16}$. *Chem.* **2017**, *2*, 427−440.
(110) Balz, D.; Plieth, K. Die Struktur des Kaliumnickelfluorids, K_2NiF_4. *Z. Elektrochem.* **1955**, *59*, 545−551.
(111) Lazarini, F. Caesium Enneabromodibismuthate(III). *Acta Crystallogr., Sect. B: Struct. Crystallogr. Cryst. Chem.* **1977**, *33*, 2961−2964.
(112) Goodyear, J.; Ali, E. M.; Sutherland, H. H. Trirubidium Heptachlorodimanganate. *Acta Crystallogr., Sect. B: Struct. Crystallogr. Cryst. Chem.* **1978**, *34*, 2617−2618.
(113) Mitzi, D. B. Organic−Inorganic Perovskites Containing Trivalent Metal Halide Layers: The Templating Influence of the Organic Cation Layer. *Inorg. Chem.* **2000**, *39*, 6107−6113.
(114) Jaffe, A.; Karunadasa, H. I. Lithium Cycling in a Self-Assembled Copper Chloride-Polyether Hybrid Electrode. *Inorg. Chem.* **2014**, *53*, 6494−6496.
(115) Arend, H.; Tichy, K.; Baberschke, K.; Rys, F. Chloride Perovskite Layer Compounds of $[NH_3\text{-}(CH_2)_n\text{-}NH_3]MnCl_4$ Formula. *Solid State Commun.* **1976**, *18*, 999−1003.
(116) Han, J.; Nishihara, S.; Inoue, K.; Kurmoo, M. On the Nature of the Structural and Magnetic Phase Transitions in the Layered Perovskite-Like $(CH_3NH_3)_2[Fe^{II}Cl_4]$. *Inorg. Chem.* **2014**, *53*, 2068−2075.
(117) Mitzi, D. B.; Liang, K. Preparation and Properties of $(C_4H_9NH_3)_2EuI_4$: A Luminescent Organic−Inorganic Perovskite with a Divalent Rare-Earth Metal Halide Framework. *Chem. Mater.* **1997**, *9*, 2990−2995.
(118) Castro-Castro, L. M.; Guloy, A. M. Organic-Based Layered Perovskites of Mixed-Valent Gold(I)/Gold(III) Iodides. *Angew. Chem., Int. Ed.* **2003**, *42*, 2771−2774.
(119) Connor, B. A.; Leppert, L.; Smith, M. D.; Neaton, J. B.; Karunadasa, H. I. Layered Halide Double Perovskites: Dimensional Reduction of $Cs_2AgBiBr_6$. *J. Am. Chem. Soc.* **2018**, *140*, 5235−5240.
(120) Kitazawa, N. Optical Absorption and Photoluminescence Properties of Pb(I, Br)-Based Two-Dimensional Layered Perovskite. *Jpn. J. Appl. Phys., Part 1* **1997**, *36* (36), 2272−2276.
(121) Xiao, Z.; Du, K.; Meng, W.; Wang, J.; Mitzi, D. B.; Yan, Y. Intrinsic Instability of $Cs_2In(I)M(III)X_6$ (M = Bi, Sb; X = Halogen) Double Perovskites: A Combined Density Functional Theory and Experimental Study. *J. Am. Chem. Soc.* **2017**, *139*, 6054−6057.

DOI: 10.1021/acs.chemrev.8b00477
Chem. Rev. XXXX, XXX, XXX−XXX

(122) Daub, M.; Hillebrecht, H. Synthesis, Single-Crystal Structure and Characterization of $(CH_3NH_3)_2Pb(SCN)_2I_2$. *Angew. Chem., Int. Ed.* **2015**, *54*, 11016−11017.
(123) Wang, K.; Wu, C.; Yang, D.; Jiang, Y.; Priya, S. Quasi-Two-Dimensional Halide Perovskite Single Crystal Photodetector. *ACS Nano* **2018**, *12*, 4919−4929.
(124) Mitzi, D. B. Thin-Film Deposition of Organic−Inorganic Hybrid Materials. *Chem. Mater.* **2001**, *13*, 3283−3298.
(125) Era, M.; Shimizu, A. Incorporation of Bulky Chromophore into PbBr-Based Layered Perovskite Organic/Inorganic Superlattice by Mixing of Chromophore-Linked Ammonium and Alkyl Ammonium Molecules. *Mol. Cryst. Liq. Cryst. Sci. Technol., Sect. A* **2001**, *371*, 199−202.
(126) Xu, Z.; Mitzi, D. B. SnI_4^{2-}-Based Hybrid Perovskites Templated by Multiple Organic Cations: Combining Organic Functionalities through Noncovalent Interactions. *Chem. Mater.* **2003**, *15*, 3632−3637.
(127) Vargas, B.; Torres-Cadena, R.; Rodríguez-Hernández, J.; Gembicky, M.; Xie, H.; Jiménez-Mier, J.; Liu, Y.-S.; Menéndez-Proupin, E.; Dunbar, K. R.; Lopez, N.; et al. Optical, Electronic and Magnetic Engineering of ⟨111⟩ Layered Halide Perovskites. *Chem. Mater.* **2018**, *30*, 5315−5321.
(128) Polyakov, A. O.; Arkenbout, A. H.; Baas, J.; Blake, G. R.; Meetsma, A.; Caretta, A.; van Loosdrecht, P. H. M.; Palstra, T. T. M. Coexisting Ferromagnetic and Ferroelectric Order in a $CuCl_4$-Based Organic−Inorganic Hybrid. *Chem. Mater.* **2012**, *24*, 133−139.
(129) Moritomo, Y.; Tokura, Y. Pressure-Induced Disappearance of the In-Plane Lattice Distortion in Layered Cupric Chloride: $(C_2H_5NH_3)_2CuCl_4$. *J. Chem. Phys.* **1994**, *101*, 1763−1766.
(130) Jaffe, A.; Lin, Y.; Mao, W. L.; Karunadasa, H. I. Pressure-Induced Conductivity and Yellow-to-Black Piezochromism in a Layered Cu-Cl Hybrid Perovskite. *J. Am. Chem. Soc.* **2015**, *137*, 1673−1678.
(131) Gupta, S.; Pandey, T.; Singh, A. K. Suppression of Jahn−Teller Distortions and Origin of Piezochromism and Thermochromism in Cu−Cl Hybrid Perovskite. *Inorg. Chem.* **2016**, *55*, 6817−6824.
(132) Desjardins, S. R.; Wilcox, D. E.; Musselman, R. L.; Solomon, E. I. Polarized, Single-Crystal, Electronic Spectral Studies of Hexachlorodicuprate(2-): Excited-State Effects of Binuclear Interaction. *Inorg. Chem.* **1987**, *26*, 288−300.
(133) Valiente, R.; Rodríguez, F. Electron-Phonon Coupling in Charge-Transfer and Crystal-Field States of Jahn-Teller $CuCl_6^{4-}$ Systems. *Phys. Rev. B: Condens. Matter Mater. Phys.* **1999**, *60*, 9423−9429.
(134) Umebayashi, T.; Asai, K.; Kondo, T.; Nakao, A. Electronic Structures of Lead Iodide Based Low-Dimensional Crystals. *Phys. Rev. B: Condens. Matter Mater. Phys.* **2003**, *67*, 155405.
(135) Straus, D. B.; Hurtado Parra, S.; Iotov, N.; Gebhardt, J.; Rappe, A. M.; Subotnik, J. E.; Kikkawa, J. M.; Kagan, C. R. Direct Observation of Electron−Phonon Coupling and Slow Vibrational Relaxation in Organic−Inorganic Hybrid Perovskites. *J. Am. Chem. Soc.* **2016**, *138*, 13798−13801.
(136) Ni, L.; Huynh, U.; Cheminal, A.; Thomas, T. H.; Shivanna, R.; Hinrichsen, T. F.; Ahmad, S.; Sadhanala, A.; Rao, A. Real-Time Observation of Exciton−Phonon Coupling Dynamics in Self-Assembled Hybrid Perovskite Quantum Wells. *ACS Nano* **2017**, *11*, 10834−10843.
(137) Du, M. H. Efficient Carrier Transport in Halide Perovskites: Theoretical Perspectives. *J. Mater. Chem. A* **2014**, *2*, 9091−9098.
(138) Yin, W.-J.; Yang, J.-H.; Kang, J.; Yan, Y.; Wei, S.-H. Halide Perovskite Materials for Solar Cells: a Theoretical Review. *J. Mater. Chem. A* **2015**, *3*, 8926−8942.
(139) Green, M. A.; Jiang, Y.; Soufiani, A. M.; Ho-Baillie, A. Optical Properties of Photovoltaic Organic−Inorganic Lead Halide Perovskites. *J. Phys. Chem. Lett.* **2015**, *6*, 4774−4785.
(140) Even, J.; Pedesseau, L.; Katan, C. Understanding Quantum Confinement of Charge Carriers in Layered 2D Hybrid Perovskites. *ChemPhysChem* **2014**, *15*, 3733−3741.
(141) Frenkel, J. On the Transformation of Light into Heat in Solids. I. *Phys. Rev.* **1931**, *37*, 17−44.
(142) Toyozawa, Y. In *Optical Processes in Solids*; Cambridge University Press: Cambridge, U.K., 2003; pp 113−148.
(143) Adachi, S. In *Physical Properties of III-V Semiconductor Compounds*; Wiley-VCH Verlag GmbH & Co. KGaA: 2005; pp 135−192.
(144) Lin, Q.; Armin, A.; Nagiri, R. C. R.; Burn, P. L.; Meredith, P. Electro-Optics of Perovskite Solar Cells. *Nat. Photonics* **2015**, *9*, 106−112.
(145) Shinada, M.; Sugano, S. Interband Optical Transitions in Extremely Anisotropic Semiconductors. I. Bound and Unbound Exciton Absorption. *J. Phys. Soc. Jpn.* **1966**, *21*, 1936−1946.
(146) Keldysh, L. V. Coulomb Interaction in Thin Films of Semiconductors and Semimetals. *Pis'ma Zh. Eksp. Teor. Fiz.* **1979**, *29*, 716−719.
(147) Hanamura, E.; Nagaosa, N.; Kumagai, M.; Takagahara, T. Quantum Wells with Enhanced Exciton Effects and Optical Non-Linearity. *Mater. Sci. Eng., B* **1988**, *1*, 255−258.
(148) Tran Thoai, D. B.; Zimmermann, R.; Grundmann, M.; Bimberg, D. Image Charges in Semiconductor Quantum Wells: Effect on Exciton Binding Energy. *Phys. Rev. B: Condens. Matter Mater. Phys.* **1990**, *42*, 5906−5909.
(149) Smith, M. D.; Pedesseau, L.; Kepenekian, M.; Smith, I. C.; Katan, C.; Even, J.; Karunadasa, H. I. Decreasing the Electronic Confinement in Layered Perovskites through Intercalation. *Chem. Sci.* **2017**, *8*, 1960−1968.
(150) Takagi, H.; Kunugita, H.; Ema, K. Influence of the Image Charge Effect on Excitonic Energy Structure in Organic−Inorganic Multiple Quantum Well Crystals. *Phys. Rev. B: Condens. Matter Mater. Phys.* **2013**, *87*, 125421.
(151) Umeyama, D.; Lin, Y.; Karunadasa, H. I. Red-to-Black Piezochromism in a Compressible Pb−I−SCN Layered Perovskite. *Chem. Mater.* **2016**, *28*, 3241−3244.
(152) Fujisawa, J.; Ishihara, T. Excitons and Biexcitons Bound to a Positive Ion in a Bismuth-Doped Inorganic−Organic Layered Lead Iodide Semiconductor. *Phys. Rev. B: Condens. Matter Mater. Phys.* **2004**, *70*, 205330.
(153) Song, K. S.; Williams, R. T. *Self-Trapped Excitons*, 2nd ed.; Springer: Berlin, Germany, 1996; Vol. *105*.
(154) Iwanaga, M.; Azuma, J.; Shirai, M.; Tanaka, K.; Hayashi, T. Self-Trapped Electrons and Holes in $PbBr_2$ Crystals. *Phys. Rev. B: Condens. Matter Mater. Phys.* **2002**, *65*, 214306.
(155) Fujita, M.; Itoh, M.; Bokumoto, Y.; Nakagawa, H.; Alov, D. L.; Kitaura, M. Optical Spectra and Electronic Structures of Lead Halides. *Phys. Rev. B: Condens. Matter Mater. Phys.* **2000**, *61*, 15731−15737.
(156) Iwanaga, M.; Hayashi, T. Exciton-Relaxation Dynamics in Lead Halides. *J. Lumin.* **2003**, *102*−*103*, 663−668.
(157) Nakahara, J.; Kobayashi, K. Edge Emissions and Broad Band Emissions in Thallous Halides. *J. Phys. Soc. Jpn.* **1976**, *40*, 180−188.
(158) Tokizaki, T.; Makimura, T.; Akiyama, H.; Nakamura, A.; Tanimura, K.; Itoh, N. Femtosecond Cascade-Excitation Spectroscopy for Nonradiative Deexcitation and Lattice Relaxation of the Self-Trapped Exciton in NaCl. *Phys. Rev. Lett.* **1991**, *67*, 2701−2704.
(159) Solomon, E. I. Electronic Absorption Spectroscopy—Vibronic Coupling and Band Shape Analysis. *Comments Inorg. Chem.* **1984**, *3*, 300−318.
(160) Ishihara, T.; Hong, X.; Ding, J.; Nurmikko, A. V. Dielectric Confinement Effect for Exciton and Biexciton States in PbI_4-Based Two-Dimensional Semiconductor Structures. *Surf. Sci.* **1992**, *267*, 323−326.
(161) Wood, D. L.; Tauc, J. Weak Absorption Tails in Amorphous Semiconductors. *Phys. Rev. B: Solid State* **1972**, *5*, 3144−3151.
(162) Dolgonos, A.; Mason, T. O.; Poeppelmeier, K. R. Direct Optical Band Gap Measurement in Polycrystalline Semiconductors: A Critical Look at the Tauc Method. *J. Solid State Chem.* **2016**, *240*, 43−48.
(163) Papavassiliou, G. C.; Koutselas, I. B.; Lagouvardos, D. J.; Kapoutsis, J.; Terzis, A.; Papaioannou, G. J. Optical and Related

DOI: 10.1021/acs.chemrev.8b00477
Chem. Rev. XXXX, XXX, XXX−XXX

Properties of Some Natural Three and Lower Dimensional Semiconductor Systems. *Mol. Cryst. Liq. Cryst. Sci. Technol., Sect. A* **1994**, *253*, 103−112.
(164) Tanaka, K.; Takahashi, T.; Kondo, T.; Umeda, K.; Ema, K.; Umebayashi, T.; Asai, K.; Uchida, K.; Miura, N. Electronic and Excitonic Structures of Inorganic−Organic Perovskite-Type Quantum-Well Crystal $(C_4H_9NH_3)_2PbBr_4$. *Jpn. J. Appl. Phys., Part 1* **2005**, *44* (44), 5923−5932.
(165) Ishihara, T.; Hirasawa, M.; Goto, T. Optical Properties and Electronic Structures of Self-Organized Quantum Well $(C_nH_{2n+1}NH_3)_2PbX_4$ (X= I, Br, Cl). *Jpn. J. Appl. Phys.* **1995**, *34*, 71.
(166) Lanty, G.; Jemli, K.; Wei, Y.; Leymarie, J.; Even, J.; Lauret, J. S.; Deleporte, E. Room-Temperature Optical Tunability and Inhomogeneous Broadening in 2D-Layered Organic−Inorganic Perovskite Pseudobinary Alloys. *J. Phys. Chem. Lett.* **2014**, *5*, 3958−3963.
(167) Lanzetta, L.; Marin-Beloqui, J. M.; Sanchez-Molina, I.; Ding, D.; Haque, S. A. Two-Dimensional Organic Tin Halide Perovskites with Tunable Visible Emission and Their Use in Light-Emitting Devices. *ACS Energy Lett.* **2017**, *2*, 1662−1668.
(168) Mao, L.; Wu, Y.; Stoumpos, C. C.; Traore, B.; Katan, C.; Even, J.; Wasielewski, M. R.; Kanatzidis, M. G. Tunable White-Light Emission in Single-Cation-Templated Three-Layered 2D Perovskites $(CH_3CH_2NH_3)_4Pb_3Br_{10-x}Cl_x$. *J. Am. Chem. Soc.* **2017**, *139*, 11956−11963.
(169) Cai, P.; Wang, X.; Seo, H. J.; Yan, X. Bluish-White-Light-Emitting Diodes Based on Two-Dimensional Lead Halide Perovskite $(C_6H_5C_2H_4NH_3)_2PbCl_2Br_2$. *Appl. Phys. Lett.* **2018**, *112*, 153901.
(170) Thirumal, K.; Chong, W. K.; Xie, W.; Ganguly, R.; Muduli, S. K.; Sherburne, M.; Asta, M.; Mhaisalkar, S.; Sum, T. C.; Soo, H. S.; et al. Morphology-Independent Stable White-Light Emission from Self-Assembled Two-Dimensional Perovskites Driven by Strong Exciton−Phonon Coupling to the Organic Framework. *Chem. Mater.* **2017**, *29*, 3947−3953.
(171) Pradeesh, K.; Nageswara Rao, K.; Vijaya Prakash, G. Synthesis, Structural, Thermal and Optical Studies of Inorganic−Organic Hybrid Semiconductors, R-PbI_4. *J. Appl. Phys.* **2013**, *113*, No. 083523.
(172) Kawano, N.; Koshimizu, M.; Sun, Y.; Yahaba, N.; Fujimoto, Y.; Yanagida, T.; Asai, K. Effects of Organic Moieties on Luminescence Properties of Organic−Inorganic Layered Perovskite-Type Compounds. *J. Phys. Chem. C* **2014**, *118*, 9101−9106.
(173) Slavney, A. H.; Smaha, R. W.; Smith, I. C.; Jaffe, A.; Umeyama, D.; Karunadasa, H. I. Chemical Approaches to Addressing the Instability and Toxicity of Lead−Halide Perovskite Absorbers. *Inorg. Chem.* **2017**, *56*, 46−55.
(174) Blancon, J. C.; Tsai, H.; Nie, W.; Stoumpos, C. C.; Pedesseau, L.; Katan, C.; Kepenekian, M.; Soe, C. M. M.; Appavoo, K.; Sfeir, M. Y.; et al. Extremely Efficient Internal Exciton Dissociation through Edge States in Layered 2D Perovskites. *Science* **2017**, *355*, 1288−1291.
(175) Milot, R. L.; Sutton, R. J.; Eperon, G. E.; Haghighirad, A. A.; Martinez Hardigree, J.; Miranda, L.; Snaith, H. J.; Johnston, M. B.; Herz, L. M. Charge-Carrier Dynamics in 2D Hybrid Metal−Halide Perovskites. *Nano Lett.* **2016**, *16*, 7001−7007.
(176) Liu, J.; Leng, J.; Wu, K.; Zhang, J.; Jin, S. Observation of Internal Photoinduced Electron and Hole Separation in Hybrid Two-Dimentional Perovskite Films. *J. Am. Chem. Soc.* **2017**, *139*, 1432−1435.
(177) Shang, Q.; Wang, Y.; Zhong, Y.; Mi, Y.; Qin, L.; Zhao, Y.; Qiu, X.; Liu, X.; Zhang, Q. Unveiling Structurally Engineered Carrier Dynamics in Hybrid Quasi-Two-Dimensional Perovskite Thin Films Toward Controllable Emission. *J. Phys. Chem. Lett.* **2017**, *8*, 4431−4438.
(178) Proppe, A. H.; Quintero-Bermudez, R.; Tan, H.; Voznyy, O.; Kelley, S. O.; Sargent, E. H. Synthetic Control over Quantum Well Width Distribution and Carrier Migration in Low-Dimensional Perovskite Photovoltaics. *J. Am. Chem. Soc.* **2018**, *140*, 2890−2896.
(179) Gwo, S.; Lin, M.-H.; He, C.-L.; Chen, H.-Y.; Teranishi, T. Bottom-Up Assembly of Colloidal Gold and Silver Nanostructures for Designable Plasmonic Structures and Metamaterials. *Langmuir* **2012**, *28*, 8902−8908.
(180) Cao, D. H.; Stoumpos, C. C.; Farha, O. K.; Hupp, J. T.; Kanatzidis, M. G. 2D Homologous Perovskites as Light-Absorbing Materials for Solar Cell Applications. *J. Am. Chem. Soc.* **2015**, *137*, 7843−7850.
(181) Kahn, A. Fermi Level, Work Function and Vacuum Level. *Mater. Horiz.* **2016**, *3*, 7−10.
(182) Guzelturk, B.; Belisle, R. A.; Smith, M. D.; Bruening, K.; Prasanna, R.; Yuan, Y.; Gopalan, V.; Tassone, C. J.; Karunadasa, H. I.; McGehee, M. D.; et al. Terahertz Emission from Hybrid Perovskites Driven by Ultrafast Charge Separation and Strong Electron−Phonon Coupling. *Adv. Mater.* **2018**, *30*, 1704737.
(183) Tsai, H.; Nie, W.; Blancon, J. C.; Stoumpos, C. C.; Soe, C. M. M.; Yoo, J.; Crochet, J.; Tretiak, S.; Even, J.; Sadhanala, A.; et al. Stable Light-Emitting Diodes Using Phase-Pure Ruddlesden−Popper Layered Perovskites. *Adv. Mater.* **2018**, *30*, 1704217.
(184) Wang, Q.; Ren, J.; Peng, X.-F.; Ji, X.-X.; Yang, X.-H. Efficient Sky-Blue Perovskite Light-Emitting Devices Based on Ethylammonium Bromide Induced Layered Perovskites. *ACS Appl. Mater. Interfaces* **2017**, *9*, 29901−29906.
(185) Wang, L.; Wang, S.; Zhao, X.; Sun, J. Stability, Structure and Fluorescence Spectra of High-Pressure-Treated Eu^{2+} Iodides. *J. Alloys Compd.* **1995**, *225*, 174−177.
(186) Hernandez, A. J.; Lopez, F. J.; Murrieta, S. H.; Rubio, O. J. Optical Absorption, Emission, and Excitation Spectra of Eu^{2+} in the Alkali Halides. *J. Phys. Soc. Jpn.* **1981**, *50*, 225−229.
(187) Hayashi, T.; Kobayashi, T.; Iwanaga, M.; Watanabe, M. Exciton Dynamics Related with Phase Transitions in $CsPbCl_3$ Single Crystals. *J. Lumin.* **2001**, *94*−*95*, 255−259.
(188) Silver, J.; Withnall, R. In *Luminescent Materials and Applications*; Kitai, A., Ed.; John Wiley & Sons: Chichester, U.K., 2008; pp 75−109. DOI: 10.1002/9780470985687.ch3.
(189) Li, Y. Y.; Lin, C. K.; Zheng, G. L.; Cheng, Z. Y.; You, H.; Wang, W. D.; Lin, J. Novel ⟨110⟩-Oriented Organic−Inorganic Perovskite Compound Stabilized by *N*-(3-aminopropyl)imidazole with Improved Optical Properties. *Chem. Mater.* **2006**, *18*, 3463−3469.
(190) Wu, Z.; Ji, C.; Sun, Z.; Wang, S.; Zhao, S.; Zhang, W.; Li, L.; Luo, J. Broadband White-Light Emission with a High Color Rendering Index in a Two-Dimensional Organic−Inorganic Hybrid Perovskite. *J. Mater. Chem. C* **2018**, *6*, 1171−1175.
(191) Yangui, A.; Garrot, D.; Lauret, J. S.; Lusson, A.; Bouchez, G.; Deleporte, E.; Pillet, S.; Bendeif, E. E.; Castro, M.; Triki, S.; et al. Optical Investigation of Broadband White-Light Emission in Self-Assembled Organic−Inorganic Perovskite $(C_6H_{11}NH_3)_2PbBr_4$. *J. Phys. Chem. C* **2015**, *119*, 23638−23647.
(192) Yangui, A.; Pillet, S.; Lusson, A.; Bendeif, E.-E.; Triki, S.; Abid, Y.; Boukheddaden, K. Control of the White-Light Emission in the Mixed Two-Dimensional Hybrid Perovskites $(C_6H_{11}NH_3)_2[PbBr_{4-x}I_x]$. *J. Alloys Compd.* **2017**, *699*, 1122−1133.
(193) Yangui, A.; Pillet, S.; Mlayah, A.; Lusson, A.; Bouchez, G.; Triki, S.; Abid, Y.; Boukheddaden, K. Structural Phase Transiton Causing Anomalous Photoluminescence Behavior in Perovskite $(C_6H_{11}NH_3)_2[PbI_4]$. *J. Chem. Phys.* **2015**, *143*, 224201.
(194) Neogi, I.; Bruno, A.; Bahulayan, D.; Goh, T. W.; Ghosh, B.; Ganguly, R.; Cortecchia, D.; Sum, T. C.; Soci, C.; Mathews, N.; et al. Broadband-Emitting 2D Hybrid Organic−Inorganic Perovskite Based on Cyclohexane-Bis(methylamonium) Cation. *ChemSusChem* **2017**, *10*, 3765−3772.
(195) Yin, J.; Li, H.; Cortecchia, D.; Soci, C.; Brédas, J.-L. Excitonic and Polaronic Properties of 2D Hybrid Organic−Inorganic Perovskites. *ACS Energy Lett.* **2017**, *2*, 417−423.
(196) Cortecchia, D.; Yin, J.; Bruno, A.; Lo, S.-Z. A.; Gurzadyan, G. G.; Mhaisalkar, S.; Brédas, J.-L.; Soci, C. Polaron Self-Localization in White-Light Emitting Hybrid Perovskites. *J. Mater. Chem. C* **2017**, *5*, 2771−2780.

DOI: 10.1021/acs.chemrev.8b00477
Chem. Rev. XXXX, XXX, XXX−XXX

(197) Schmidt, T.; Lischka, K.; Zulehner, W. Excitation-Power Dependence of the Near-Band-Edge Photoluminescence of Semiconductors. *Phys. Rev. B: Condens. Matter Mater. Phys.* **1992**, *45*, 8989−8994.
(198) McCall, K. M.; Stoumpos, C. C.; Kostina, S. S.; Kanatzidis, M. G.; Wessels, B. W. Strong Electron−Phonon Coupling and Self-Trapped Excitons in the Defect Halide Perovskites $A_3M_2I_9$ (A = Cs, Rb; M = Bi, Sb). *Chem. Mater.* **2017**, *29*, 4129−4145.
(199) Wu, X.; Trinh, M. T.; Niesner, D.; Zhu, H.; Norman, Z.; Owen, J. S.; Yaffe, O.; Kudisch, B. J.; Zhu, X.-Y. Trap States in Lead Iodide Perovskites. *J. Am. Chem. Soc.* **2015**, *137*, 2089−2096.
(200) Vial, J. C.; Bsiesy, A.; Gaspard, F.; Hérino, R.; Ligeon, M.; Muller, F.; Romestain, R.; Macfarlane, R. M. Mechanisms of Visible-Light Emission from Electro-Oxidized Porous Silicon. *Phys. Rev. B: Condens. Matter Mater. Phys.* **1992**, *45*, 14171−14176.
(201) Kobitski, A. Y.; Zhuravlev, K. S.; Wagner, H. P.; Zahn, D. R. T. Self-Trapped Exciton Recombination in Silicon Nanocrystals. *Phys. Rev. B: Condens. Matter Mater. Phys.* **2001**, *63*, 115423.
(202) Matsui, A.; Nishimura, H. Luminescence of Free and Self Trapped Excitons in Pyrene. *J. Phys. Soc. Jpn.* **1980**, *49*, 657−663.
(203) Matsui, A.; Mizuno, K.; Tamai, N.; Yamazaki, I. Transient Free-Exciton Luminescence and Exciton-Lattice Interaction in Pyrene Crystals. *Chem. Phys.* **1987**, *113*, 111−117.
(204) Matsui, A. H.; Nakamura, T.; Nakatani, S.; Ohno, T.; Mizuno, K. Direct Self-Trapping Path of Excitons in Pyrene Crystals. *Synth. Met.* **1994**, *64*, 177−183.
(205) Robinson, K.; Gibbs, G. V.; Ribbe, P. H. Quadratic Elongation: A Quantitative Measure of Distortion in Coordination Polyhedra. *Science* **1971**, *172*, 567−570.
(206) Ertl, A.; Hughes, J. M.; Pertlik, F.; Foit, F. F. J.; Wright, S. E.; Brandstätter, F.; Marler, B. Polyhedron Distortions in Tourmaline. *Can. Mineral.* **2002**, *40*, 153−162.
(207) Cortecchia, D.; Neutzner, S.; Srimath Kandada, A. R.; Mosconi, E.; Meggiolaro, D.; De Angelis, F.; Soci, C.; Petrozza, A. Broadband Emission in Two-Dimensional Hybrid Perovskites: The Role of Structural Deformation. *J. Am. Chem. Soc.* **2017**, *139*, 39−42.
(208) Daub, M.; Haber, C.; Hillebrecht, H. Synthesis, Crystal Structures, Optical Properties and Phase Transitions of the Layered Guanidinium-Based Hybrid Perovskites $(C(NH_2)_3)_2MI_4$; *M* = Sn, Pb. *Eur. J. Inorg. Chem.* **2017**, *2017*, 1120−1126.
(209) Booker, E. P.; Thomas, T. H.; Quarti, C.; Stanton, M. R.; Dashwood, C. D.; Gillett, A. J.; Richter, J. M.; Pearson, A. J.; Davis, N. J. L. K.; Sirringhaus, H.; et al. Formation of Long-Lived Color Centers for Broadband Visible Light Emission in Low-Dimensional Layered Perovskites. *J. Am. Chem. Soc.* **2017**, *139*, 18632−18639.
(210) Younts, R.; Duan, H.-S.; Gautam, B.; Saparov, B.; Liu, J.; Mongin, C.; Castellano, F. N.; Mitzi, D. B.; Gundogdu, K. Efficient Generation of Long-Lived Triplet Excitons in 2D Hybrid Perovskite. *Adv. Mater.* **2017**, *29*, 1604278.
(211) Slavney, A. H.; Hu, T.; Lindenberg, A. M.; Karunadasa, H. I. A Bismuth-Halide Double Perovskite with Long Carrier Recombination Lifetime for Photovoltaic Applications. *J. Am. Chem. Soc.* **2016**, *138*, 2138−2141.
(212) Hoye, R. L. Z.; Eyre, L.; Wei, F.; Brivio, F.; Sadhanala, A.; Sun, S.; Li, W.; Zhang, K. H. L.; MacManus-Driscoll, J. L.; Bristowe, P. D.; et al. Fundamental Carrier Lifetime Exceeding 1 μs in $Cs_2AgBiBr_6$ Double Perovskite. *Adv. Mater. Interfaces* **2018**, *5*, 1800464.
(213) Ohnishi, A.; Yamada, T.; Yoshinari, T.; Akimoto, I.; Kan'no, K.; Kamikawa, T. Emission Spectra and Decay Characteristics in Photo-Stimulated $(C_nH_{2n+1}NH_3)_2CdCl_4$: *n* = 1, 2, 3. *J. Electron Spectrosc. Relat. Phenom.* **1996**, *79*, 163−166.
(214) Ohnishi, A.; Tanaka, K.; Yoshinari, T. Exciton Self-Trapping in Two-Dimensional System of $(C_2H_5NH_3)_2CdCl_4$ Single Crystal. *J. Phys. Soc. Jpn.* **1999**, *68*, 288−290.
(215) Schreiber, M.; Toyozawa, Y. Numerical Experiments on the Absorption Lineshape of the Exciton under Lattice Vibrations. III. The Urbach Rule. *J. Phys. Soc. Jpn.* **1982**, *51*, 1544−1550.
(216) Roccanova, R.; Ming, W.; Whiteside, V. R.; McGuire, M. A.; Sellers, I. R.; Du, M.-H.; Saparov, B. Synthesis, Crystal and Electronic Structures, and Optical Properties of $(CH_3NH_3)_2CdX_4$ (X = Cl, Br, I). *Inorg. Chem.* **2017**, *56*, 13878−13888.
(217) Cheng, P.; Wu, T.; Zhang, J.; Li, Y.; Liu, J.; Jiang, L.; Mao, X.; Lu, R.-F.; Deng, W.-Q.; Han, K. $(C_6H_5C_2H_4NH_3)_2GeI_4$: A Layered Two-Dimensional Perovskite with Potential for Photovoltaic Applications. *J. Phys. Chem. Lett.* **2017**, *8*, 4402−4406.
(218) Epstein, A.; Gurewitz, E.; Makovsky, J.; Shaked, H. Magnetic Structure and Two-Dimensional Behavior of Rb_2MnCl_4 and Cs_2MnCl_4. *Phys. Rev. B: Solid State* **1970**, *2*, 3703−3706.
(219) Kestigian, M.; Holloway, W. W. J. The Preparation, Single-Crystal-Growth, and Fluorescence Studies of Divalent Manganese Chlorides of Rubidium and Cesium. *Phys. Status Solidi A* **1971**, *6*, K19−K22.
(220) McPherson, G. L.; Devaney, K. O.; Willard, S. C.; Francis, A. H. Energy Transfer in One-, Two-, and Three-Dimensionally Coupled Salts of Divalent Manganese. *Chem. Phys. Lett.* **1979**, *68*, 9−12.
(221) Kambli, U.; Gudel, H. U.; Briat, B. Optical Absorption and Luminescence Studies of the 2D Antiferromagnets Rb_2MnCl_4 and $Rb_3Mn_2Cl_7$. *J. Phys. C: Solid State Phys.* **1984**, *17*, 3113−3122.
(222) Kambli, U.; Guedel, H. U. Transfer of Electronic Excitation Energy in the Antiferromagnets Rubidium Trichloromanganate(II), Cesium Trichloromanganate(II), Cesium Tribromomanganate(II), and Rubidium Tetrachloromanganate(II). *Inorg. Chem.* **1984**, *23*, 3479−3486.
(223) Wilson, B. A.; Yen, W. M.; Hegarty, J.; Imbusch, G. F. Luminescence from Pure MnF_2 and from MnF_2 Doped with Eu^{3+} and Er^{3+}. *Phys. Rev. B: Condens. Matter Mater. Phys.* **1979**, *19*, 4238−4250.
(224) Yamamoto, H.; McClure, D. S.; Marzzacco, C.; Waldman, M. Energy Migration in a Nearly One-Dimensional Compound, Tetramethyl Ammonium Manganese Chloride (TMMC). *Chem. Phys.* **1977**, *22*, 79−87.
(225) Azuma, J.; Tanaka, K.; Kan'no, K. Two Types of Self-Trapped Excitons in a Quasi-One-Dimensional Crystal Piperidinium Tribromoplumbate. *J. Phys. Soc. Jpn.* **2002**, *71*, 971−977.
(226) Wang, G.-E.; Xu, G.; Wang, M.-S.; Cai, L.-Z.; Li, W.-H.; Guo, G.-C. Semiconductive 3-D Haloplumbate Framework Hybrids with High Color Rendering Index White-Light Emission. *Chem. Sci.* **2015**, *6*, 7222−7226.
(227) Smith, M. D.; Watson, B. L.; Dauskardt, R. H.; Karunadasa, H. I. Broadband Emission with a Massive Stokes Shift from Sulfonium Pb−Br Hybrids. *Chem. Mater.* **2017**, *29*, 7083−7087.
(228) Yuan, Z.; Zhou, C.; Tian, Y.; Shu, Y.; Messier, J.; Wang, J. C.; van de Burgt, L. J.; Kountouriotis, K.; Xin, Y.; Holt, E.; et al. One-Dimensional Organic Lead Halide Perovskites with Efficient Bluish White-Light Emission. *Nat. Commun.* **2017**, *8*, 14051.
(229) Wu, Z.; Li, L.; Ji, C.; Lin, G.; Wang, S.; Shen, Y.; Sun, Z.; Zhao, S.; Luo, J. Broad-Band-Emissive Organic−Inorganic Hybrid Semiconducting Nanowires Based on an ABX_3-Type Chain Compound. *Inorg. Chem.* **2017**, *56*, 8776−8781.
(230) Lin, H.; Zhou, C.; Tian, Y.; Besara, T.; Neu, J.; Siegrist, T.; Zhou, Y.; Bullock, J.; Schanze, K. S.; Ming, W.; et al. Bulk Assembly of Organic Metal Halide Nanotubes. *Chem. Sci.* **2017**, *8*, 8400−8404.
(231) Zhuang, Z.; Peng, C.; Zhang, G.; Yang, H.; Yin, J.; Fei, H. Intrinsic Broadband White-Light Emission from Ultrastable, Cationic Lead Halide Layered Materials. *Angew. Chem., Int. Ed.* **2017**, *56*, 14411−14416.
(232) Peng, C.; Zhuang, Z.; Yang, H.; Zhang, G.; Fei, H. Ultrastable, Cationic Three-Dimensional Lead Bromide Frameworks that Intrinsically Emit Broadband White-Light. *Chem. Sci.* **2018**, *9*, 1627−1633.
(233) Zhou, C.; Lin, H.; Tian, Y.; Yuan, Z.; Clark, R.; Chen, B.; van de Burgt, L. J.; Wang, J. C.; Zhou, Y.; Hanson, K.; et al. Luminescent Zero-Dimensional Organic Metal Halide Hybrids with Near-Unity Quantum Efficiency. *Chem. Sci.* **2018**, *9*, 586−593.
(234) Ye, S.; Xiao, F.; Pan, Y. X.; Ma, Y. Y.; Zhang, Q. Y. Phosphors in Phosphor-Converted White Light-Emitting Diodes: Recent Advances in Materials. *Mater. Sci. Eng., R* **2010**, *71*, 1−34.
(235) Cape, J. A.; White, R. L.; Feigelson, R. S. EPR Study of the Structure of $CsPbCl_3$. *J. Appl. Phys.* **1969**, *40*, 5001−5005.

DOI: 10.1021/acs.chemrev.8b00477
Chem. Rev. XXXX, XXX, XXX−XXX

(236) Liu, W.; Lin, Q.; Li, H.; Wu, K.; Robel, I.; Pietryga, J. M.; Klimov, V. I. Mn^{2+}-Doped Lead Halide Perovskite Nanocrystals with Dual-Color Emission Controlled by Halide Content. *J. Am. Chem. Soc.* **2016**, *138*, 14954−14961.
(237) Parobek, D.; Roman, B. J.; Dong, Y.; Jin, H.; Lee, E.; Sheldon, M.; Son, D. H. Exciton-to-Dopant Energy Transfer in Mn-Doped Cesium Lead Halide Perovskite Nanocrystals. *Nano Lett.* **2016**, *16*, 7376−7380.
(238) Biswas, A.; Bakthavatsalam, R.; Kundu, J. Efficient Exciton to Dopant Energy Transfer in Mn^{2+}-Doped $(C_4H_9NH_3)_2PbBr_4$ Two-Dimensional (2D) Layered Perovskites. *Chem. Mater.* **2017**, *29*, 7816−7825.
(239) Viswanatha, R.; Pietryga, J. M.; Klimov, V. I.; Crooker, S. A. Spin-Polarized Mn^{2+} Emission from Mn-Doped Colloidal Nanocrystals. *Phys. Rev. Lett.* **2011**, *107*, No. 067402.
(240) Zhou, Y.; Yong, Z.-J.; Zhang, K.-C.; Liu, B.-M.; Wang, Z.-W.; Hou, J.-S.; Fang, Y.-Z.; Zhou, Y.; Sun, H.-T.; Song, B. Ultrabroad Photoluminescence and Electroluminescence at New Wavelengths from Doped Organometal Halide Perovskites. *J. Phys. Chem. Lett.* **2016**, *7*, 2735−2741.
(241) Zhou, Y.; Yong, Z.-J.; Zhang, W.; Ma, J.-P.; Sadhanala, A.; Chen, Y.-M.; Liu, B.-M.; Zhou, Y.; Song, B.; Sun, H.-T. Ultra-Broadband Optical Amplification at Telecommunication Wavelengths Achieved by Bismuth-Activated Lead Iodide Perovskites. *J. Mater. Chem. C* **2017**, *5*, 2591−2596.
(242) Era, M.; Maeda, K.; Tsutsui, T. PbBr-Based Layered Perovskite Containing Chromophore-Linked Ammonium Molecule as an Organic Layer. *Chem. Lett.* **1997**, *26*, 1235−1236.
(243) Braun, M.; Tuffentsammer, W.; Wachtel, H.; Wolf, H. C. Tailoring of Energy Levels in Lead Chloride Based Layered Perovskites and Energy Transfer between the Organic and Inorganic Planes. *Chem. Phys. Lett.* **1999**, *303*, 157−164.
(244) Braun, M.; Tuffentsammer, W.; Wachtel, H.; Wolf, H. C. Pyrene as Emitting Chromophore in Organic−Inorganic Lead Halide-Based Layered Perovskites with Different Halides. *Chem. Phys. Lett.* **1999**, *307*, 373−378.
(245) Zhu, X.-H.; Mercier, N.; Frère, P.; Blanchard, P.; Roncali, J.; Allain, M.; Pasquier, C.; Riou, A. Effect of Mono- versus Di-Ammonium Cation of 2,2'-Bithiophene Derivatives on the Structure of Organic−Inorganic Hybrid Materials Based on Iodo Metallates. *Inorg. Chem.* **2003**, *42*, 5330−5339.
(246) Sakai, K.-i.; Sonoyama, T.; Tsuzuki, T.; Ichikawa, M.; Taniguchi, Y. Lead Halide-Based Layered Perovskites Incorporated with a *p*-Terphenyl Laser Dye. *Chem. Lett.* **2005**, *34*, 212−213.
(247) Cortecchia, D.; Soci, C.; Cametti, M.; Petrozza, A.; Martí-Rujas, J. Crystal Engineering of a Two-Dimensional Lead-Free Perovskite with Functional Organic Cations by Second-Sphere Coordination. *ChemPlusChem* **2017**, *82*, 681−685.
(248) Era, M.; Maeda, K.; Tsutsui, T. Enhanced Phosphorescence from Naphthalene-Chromophore Incorporated into Lead Bromide-Based Layered Perovskite Having Organic−Inorganic Superlattice Structure. *Chem. Phys. Lett.* **1998**, *296*, 417−420.
(249) Förster, T. Zwischenmolekulare Energiewanderung und Fluoreszenz. *Ann. Phys.* **1948**, *437*, 55−75.
(250) Dexter, D. L. A Theory of Sensitized Luminescence in Solids. *J. Chem. Phys.* **1953**, *21*, 836−850.
(251) Ema, K.; Inomata, M.; Kato, Y.; Kunugita, H.; Era, M. Nearly Perfect Triplet-Triplet Energy Transfer from Wannier Excitons to Naphthalene in Organic−Inorganic Hybrid Quantum-Well Materials. *Phys. Rev. Lett.* **2008**, *100*, 257401.
(252) Era, M.; Miyake, K.; Yoshida, Y.; Yase, K. Orientation of Azobenzene Chromophore Incorporated into Metal Halide-Based Layered Perovskite Having Organic−Inorganic Superlattice Structure. *Thin Solid Films* **2001**, *393*, 24−27.
(253) Gong, X.; Voznyy, O.; Jain, A.; Liu, W.; Sabatini, R.; Piontkowski, Z.; Walters, G.; Bappi, G.; Nokhrin, S.; Bushuyev, O.; et al. Electron−Phonon Interaction in Efficient Perovskite Blue Emitters. *Nat. Mater.* **2018**, *17*, 550−556.
(254) Wang, S.; Yao, Y.; Kong, J.; Zhao, S.; Sun, Z.; Wu, Z.; Li, L.; Luo, J. Highly Efficient White-Light Emission in a Polar Two-Dimensional Hybrid Perovskite. *Chem. Commun.* **2018**, *54*, 4053−4056.
(255) Fang, H. H.; Yang, J.; Tao, S.; Adjokatse, S.; Kamminga, M. E.; Ye, J.; Blake, G. R.; Even, J.; Loi, M. A. Unravelling Light-Induced Degradation of Layered Perovskite Crystals and Design of Efficient Encapsulation for Improved Photostability. *Adv. Funct. Mater.* **2018**, *28*, 1800305.
(256) Tan, Z.-K.; Moghaddam, R. S.; Lai, M. L.; Docampo, P.; Higler, R.; Deschler, F.; Price, M.; Sadhanala, A.; Pazos, L. M.; Credgington, D.; et al. Bright Light-Emitting Diodes Based on Organometal Halide Perovskite. *Nat. Nanotechnol.* **2014**, *9*, 687−692.
(257) Liang, D.; Peng, Y.; Fu, Y.; Shearer, M. J.; Zhang, J.; Zhai, J.; Zhang, Y.; Hamers, R. J.; Andrew, T. L.; Jin, S. Color-Pure Violet-Light-Emitting Diodes Based on Layered Lead Halide Perovskite Nanoplates. *ACS Nano* **2016**, *10*, 6897−6904.
(258) Shibuya, K.; Koshimizu, M.; Takeoka, Y.; Asai, K. Scintillation Properties of $(C_6H_{13}NH_3)_2PbI_4$: Exciton Luminescence of an Organic/Inorganic Multiple Quantum Well Structure Compound Induced by 2.0 MeV Protons. *Nucl. Instrum. Methods Phys. Res., Sect. B* **2002**, *194*, 207−212.
(259) Shibuya, K.; Koshimizu, M.; Murakami, H.; Muroya, Y.; Katsumura, Y.; Asai, K. Development of Ultra-Fast Semiconducting Scintillators Using Quantum Confinement Effect. *Jpn. J. Appl. Phys.* **2004**, *43*, L1333.
(260) Shibuya, K.; Koshimizu, M.; Asai, K.; Shibata, H. Quantum Confinement for Large Light Output from Pure Semiconducting Scintillators. *Appl. Phys. Lett.* **2004**, *84*, 4370−4372.
(261) Birowosuto, M. D.; Dorenbos, P.; van Eijk, C. W. E.; Krämer, K. W.; Güdel, H. U. High-Light-Output Scintillator for Photodiode Readout: $LuI_3:Ce^{3+}$. *J. Appl. Phys.* **2006**, *99*, 123520.
(262) Birowosuto, M. D.; Cortecchia, D.; Drozdowski, W.; Brylew, K.; Lachmanski, W.; Bruno, A.; Soci, C. X-ray Scintillation in Lead Halide Perovskite Crystals. *Sci. Rep.* **2016**, *6*, 37254.
(263) van Eijk, C. W. E.; de Haas, J. T. M.; Rodnyi, P. A.; Khodyuk, I. V.; Shibuya, K.; Nishikido, F.; Koshimizu, M. *IEEE Nucl. Sci. Symp. Conf. Rec.* **2008**, 3525−3528.
(264) Kawano, N.; Koshimizu, M.; Okada, G.; Fujimoto, Y.; Kawaguchi, N.; Yanagida, T.; Asai, K. Scintillating Organic−Inorganic Layered Perovskite-Type Compounds and the Gamma-Ray Detection Capabilities. *Sci. Rep.* **2017**, *7*, 14754.
(265) Mitzi, D. B.; Medeiros, D. R.; Malenfant, P. R. Intercalated Organic−Inorganic Perovskites Stabilized by Fluoroaryl-Aryl Interactions. *Inorg. Chem.* **2002**, *41*, 2134−2145.
(266) Tieke, B.; Chapuis, G. Solid-State Polymerization of Butadienes. Crystal Structure and Solution Properties of a Stereoregular Amphoteric 1,4-*trans*-Polybutadiene. *J. Polym. Sci., Polym. Chem. Ed.* **1984**, *22*, 2895−2921.
(267) Solis-Ibarra, D.; Karunadasa, H. I. Reversible and Irreversible Chemisorption in Nonporous-Crystalline Hybrids. *Angew. Chem., Int. Ed.* **2014**, *53*, 1039−1042.
(268) Solis-Ibarra, D.; Smith, I. C.; Karunadasa, H. I. Post-Synthetic Halide Conversion and Selective Halogen Capture in Hybrid Perovskites. *Chem. Sci.* **2015**, *6*, 4054−4059.
(269) Abate, A.; Saliba, M.; Hollman, D. J.; Stranks, S. D.; Wojciechowski, K.; Avolio, R.; Grancini, G.; Petrozza, A.; Snaith, H. J. Supramolecular Halogen Bond Passivation of Organic−Inorganic Halide Perovskite Solar Cells. *Nano Lett.* **2014**, *14*, 3247−3254.
(270) de Quilettes, D. W.; Vorpahl, S. M.; Stranks, S. D.; Nagaoka, H.; Eperon, G. E.; Ziffer, M. E.; Snaith, H. J.; Ginger, D. S. Impact of Microstructure on Local Carrier Lifetime in Perovskite Solar Cells. *Science* **2015**, *348*, 683−686.
(271) deQuilettes, D. W.; Koch, S.; Burke, S.; Paranji, R. K.; Shropshire, A. J.; Ziffer, M. E.; Ginger, D. S. Photoluminescence Lifetimes Exceeding 8 μs and Quantum Yields Exceeding 30% in Hybrid Perovskite Thin Films by Ligand Passivation. *ACS Energy Lett.* **2016**, *1*, 438−444.

DOI: 10.1021/acs.chemrev.8b00477
Chem. Rev. XXXX, XXX, XXX−XXX

(272) Mao, L.; Ke, W.; Pedesseau, L.; Wu, Y.; Katan, C.; Even, J.; Wasielewski, M. R.; Stoumpos, C. C.; Kanatzidis, M. G. Hybrid Dion–Jacobson 2D Lead Iodide Perovskites. *J. Am. Chem. Soc.* **2018**, *140*, 3775–3783.
(273) Li, L.; Sun, Z.; Wang, P.; Hu, W.; Wang, S.; Ji, C.; Hong, M.; Luo, J. Tailored Engineering of an Unusual $(C_4H_9NH_3)_2(CH_3NH_3)_2Pb_3Br_{10}$ Two-Dimensional Multilayered Perovskite Ferroelectric for a High-Performance Photodetector. *Angew. Chem., Int. Ed.* **2017**, *56*, 12150–12154.
(274) Nazarenko, O.; Kotyrba, M. R.; Wörle, M.; Cuervo-Reyes, E.; Yakunin, S.; Kovalenko, M. V. Luminescent and Photoconductive Layered Lead Halide Perovskite Compounds Comprising Mixtures of Cesium and Guanidinium Cations. *Inorg. Chem.* **2017**, *56*, 11552–11564.
(275) Nishida, J.; Breen, J. P.; Lindquist, K. P.; Umeyama, D.; Karunadasa, H. I.; Fayer, M. D. Dynamically Disordered Lattice in a Layered Pb-I-SCN Perovskite Thin Film Probed by 2D IR Spectroscopy. *J. Am. Chem. Soc.* **2018**, *140*, 9882–9890.
(276) Passarelli, J. V.; Fairfield, D. J.; Sather, N. A.; Hendricks, M. P.; Sai, H.; Stern, C. L.; Stupp, S. I. Enhanced Out-of-Plane Conductivity and Photovoltaic Performance in n = 1 Layered Perovskites through Organic Cation Design. *J. Am. Chem. Soc.* **2018**, *140*, 7313–7323.
(277) Nikl, M. Scintillation detectors for X-rays. *Meas. Sci. Technol.* **2006**, *17*, R37–R54.

DOI: 10.1021/acs.chemrev.8b00477
Chem. Rev. XXXX, XXX, XXX–XXX